Use of Permanent Magnets to Improve the Seismic Behavior of Light-Framed Structures

Hardik Patel

Thesis submitted to the Faculty of the Virginia Polytechnic Institute and State University in partial fulfillment of the requirements for the degree of

Master of Science
In
Civil Engineering

Approved:

____

Dr. Finley A. Charney
Committee Chairman

____

Dr. Raymond H. Plaut
Committee Member

____

Dr. Carin L. Roberts-Wollmann
Committee Member

May 12, 2005
Blacksburg, Virginia

Keywords: Permanent magnets, Friction dampers, Passive energy dissipation devices, Light frame structures, Wood shear walls, Sliding walls, Slip resistance

Use of Permanent Magnets to Improve the Seismic Behavior of Light-Framed Structures

Hardik Patel

Committee Chairman and Advisor: Dr. Finley A. Charney

ABSTRACT

Light-framed wood structures generally have satisfied the life safety objective of the current seismic design approach. The main source of energy dissipation in such structures is the inelastic behavior of the connectors connecting framing and sheathing elements. Wood framed structures when subjected to strong ground excitations experience structural and non-structural damage which may incur large repair/replacement costs or may even render the structure out of service. Thus, it is very important to apply techniques to mitigate the seismic response of the light-framed structures and avoid large monetary losses.

It is proposed to use commercially available permanent magnets, incorporated in the form of passive friction dampers, to dissipate a part of input energy induced due to strong ground motions, thereby reducing the inelastic energy dissipation demand of the lateral load resisting system. The force of attraction between the permanent magnet and ferromagnetic material like steel was utilized to produce the required friction resistance. A sliding wall configuration consisting of flexible permanent magnets and steel plates sandwiched between the plywood sheets was analyzed for its effectiveness in mitigating the response of a two story wood shear wall structure. The structural analysis program

SAP2000 was used to perform nonlinear dynamic analysis of the finite element models generated using the meshing algorithms incorporated into 'WoodFrameMesh'. Nonlinear link elements available in SAP2000 were used to model the friction between the flexible magnet sheet and the steel plate. The effects of various modeling parameters on the solution of the nonlinear analysis were studied so as to arrive at appropriate values to represent the friction problem. Also the friction damped structure was analyzed to study its forced and free vibration characteristics. Further, the responses of the friction damped structure and the undamped structure were compared when subjected to different ground accelerations. The response of the friction damped structure was also compared to that of the structure in which the proposed friction dampers were replaced by normal shear walls. A huge reduction in the response of the friction damped structure was observed when compared to the response of the undamped structure. The friction damped structure was also analyzed for different values of modal damping ratios. Over all about 60-80% of the input energy was dissipated by friction damping in all the cases. The slip resistance of a flexible permanent magnet sheet was also verified in the laboratory. Above all the magnetic properties of commercially available permanent magnets and the effects of strong permanent magnets on human health were also studied.

Dedication

I dedicate this thesis to:

My parents

And

All the lives lost in Earthquakes

Acknowledgements

I would like to thank my advisor, Dr. Finley A. Charney, for his invaluable support, guidance and patience over the past one year. I respect his thorough knowledge in the field of Seismic design and supplemental damping systems which helped me to understand these subjects easily. I am thankful to my committee members Dr. Raymond H. Plaut and Dr. Carin L. Roberts-Wollmann for their help and support in reviewing my thesis.

I would also like to thank Brett Farmer and Dennis Huffman for their technical assistance at the Virginia Tech Structures Lab. Special thanks to Arnold Magnetic Technologies for supplying the required magnetic material for testing. My sincere appreciation goes to my colleagues: Anantha, David Martin, Hari, John Ryan, Rakesh and Yasser, and friends: Abhi, Anant, Harshit and Nasir at Virginia Tech for their co-operation and advice in difficult times.

I am grateful to my parents for their love and support throughout my life. Finally, I am thankful to all the people who directly or indirectly have helped me to finish my graduate studies.

Table of Contents

List of Figures

List of Tables

Chapter 1

Introduction

1.1 General

The performance of structures during seismic loading depends on the capacity of the structure to dissipate energy over a large number of deformation reversals. Due to economic reasons, structures are conventionally designed for lower force than required for elastic behavior. However, the lateral load resisting system is detailed so as to achieve ductile behavior when subjected to earthquake loading, which aids dissipation of the induced vibration energy. Inelastic hysteretic behavior of the lateral load resisting system causes both structural and non-structural damage. Regardless of the damage being reparable or irreparable, the design is a "success" if no life is lost. Considering the huge monetary impact due to permanent damage and loss of functionality caused by inelastic behavior of the structure, it is desirable to dissipate part of the input energy by specially designed energy dissipating devices. The use of such devices reduces damage to the lateral load resisting system. Reduction in *ductility demand*[1] of the structural system is achieved as most of the input energy is dissipated by the energy dissipation devices. Installation of such devices also mitigates interstory drift, reducing the non-structural damage.

[1] The requirement on the design of the lateral load resisting structural system to deform beyond the elastic limit is defined as ductility demand [Chopra, 2002].

1.2 Response of Wood Frame Structures to Seismic Excitation

Most wood frame structures accomplish the life safety objective of the design when subjected to moderate or strong ground motion. However, they experience both structural and non-structural damage while dissipating the induced energy. The primary sources of such dissipation in wood frame structures are inelastic behavior of framing-to-sheathing connections, excessive deformation of framing elements, and damage to non-structural components such as gypsum board sheathing [Dutil and Symans, 2004]. Such severe damage may result in costly repairs or replacements of the damaged components, thus causing "economic failure" of the structure [Dinehart and Lewicki, 2001]. The 1994, Northridge earthquake proved to be one of the costliest disasters in U.S. history, causing a direct loss of $25 billion and estimated total loss of about $40 billion [Tierney, 1997]. This event caused severe damage to wood frame structures, for instance 60,000 residential wood structures in Los Angeles County experienced severe damage due to this quake [Holmes and Somers, 1995]. It was found that approximately half of the total estimated loss, that is $20 billion, was due to the damage to wood frame structures [CUREE, 1999].

The above facts demonstrate a clear need for additional energy dissipation sources in wood frame structures, and hence, it is worth the time and effort required to develop innovative techniques of energy dissipation in such structures. Energy dissipation devices for light-frame structures should be capable of dissipating an appreciable amount of induced earthquake energy, thus minimizing energy dissipation demand on structural components. Such devices should curb the displacement response of the structure so as to minimize non-structural damage. The main aim of this research is to investigate the use of permanent magnets in a passive energy dissipation device to improve the seismic behavior of light-frame structures.

1.3 Permanent Magnets and Energy Dissipation

The essence behind the proposed use of permanent magnets to dissipate vibration induced energy in a structure is to utilize the high slip resistance between a permanent magnet and a ferromagnetic material such as steel. The force of attraction between unlike poles of permanent magnets as well as between a magnet and ferromagnetic material enhances the frictional resistance between the contact surfaces. Such high friction resistance can be utilized as a potential source of energy dissipation in structures. The main aim of such a passive friction damper is to reduce the motion of the building "by braking rather than breaking" [Pall and Marsh, 1982].

The slip resistance created by commonly available flexible permanent magnets (e.g. refrigerator/sign magnet) is good enough that it can be utilized to dissipate energy through friction between the contact surface of the magnet and steel plate installed in light-frame (wood frame) structures. Rare earth magnets are strong enough to be utilized for concrete or steel structures provided the handling problems are addressed and economic feasibility is checked. Devices with self centering properties can be designed using rare earth magnets, which will be a favorable aspect.

This research focuses on utilizing flexible permanent magnets induced in a sliding/overlapping shear wall configuration installed in a typical two-story light-frame wood structure. The above mentioned sliding wall configuration will be discussed in detail in *Chapter 2*. Undoubtedly, there are many more applications of such flexible permanent magnets or permanent magnets in general, as energy dissipating or vibration control mechanisms.

1.4 Scope

The energy dissipation capacity of the proposed passive friction damper using permanent magnets was evaluated. A preliminary study to find the influence of a strong static magnetic field, induced by permanent magnets, on humans was carried out. The magnetic properties of different type of commercially available permanent magnet material were studied to confirm the feasibility of magnetic friction dampers for light-frame structures.

A thorough analytical investigation of the behavior of a typical wood frame structure with the proposed device was performed. Efforts were made to model the slip problem and to develop the finite element models of wood frame shear wall structure with friction devices using the structural analysis package, SAP2000[2] and WoodFrameMesh[3]. Nonlinear link elements were used to emulate the friction problem, and the Fast Nonlinear Analysis approach available in SAP2000 was used to evaluate the behavior. The responses of the friction damped structure to the El Centro and Northridge ground motions were compared with those of the structure without any passive energy devices, and the benefits of inducing such device were studied. Finally, the slip resistance of the ferrite flexible magnet was verified by tests performed in the Virginia Tech Structures Laboratory.

1.5 Thesis Organization

Chapter 2 discusses the basic concepts and presents a theoretical background on passive energy dissipation devices. A detailed configuration of the proposed friction damper is also presented.

Chapter 3 deals with commercially produced permanent magnets and their properties. Various formulae to calculate magnetic flux density for different shapes of permanent magnets are discussed as it is required to have an understanding of the flux induced by a particular type of permanent magnet so as to anticipate its effects on day to day human life.

[2] Structural analysis package developed by Computers and Structures, Inc., Berkeley, CA.

[3] Developed at Virginia Tech by Dr. Finley A. Charney and Rakesh Pathak. The program has capabilities to generate simplified finite element models of wood frame shear wall structures especially for lateral load analysis [Pathak, 2004].

Chapter 4 discusses the findings of a preliminary investigation of the effects of strong static magnetic fields on humans.

Chapter 5 presents the development of a finite element model of a two story wood frame structure with friction dampers. Also the effects of various modeling parameters and different loading conditions are discussed. Finally, the effectiveness of the proposed device subjected to ground excitations is evaluated by comparing the responses of the structure with and without friction dampers.

Chapter 6 presents the experimental investigation which was performed to verify the slip resistance of the flexible ferrite magnets.

Finally, in Chapter 7, general conclusions are drawn followed by suggestions for future work.

Chapter 2

Passive Energy Dissipation Devices

2.1 General

Energy dissipating devices are categorized as Passive, Semi-active or Active control systems. A passive energy dissipation system does not require external power to produce controlling forces to curb the excitations, and its performance depends on the response of the structure in which it is installed. Active control systems require an external source of power for their operation. Such devices produce controlling action by modifying the dynamic behavior of the structure depending on the feedback from the sensors measuring the response of the structure. Semi-active systems utilize the advantages of both passive and active control systems thus, requiring minimal amount of external power for their operation. Passive energy dissipation systems are more commonly used because they are relatively cheaper and simpler to implement, in addition to not requiring external power to operate.

Passive energy dissipation devices can broadly be classified as viscous fluid dampers, viscoelastic, metallic, friction and other special devices [Charney, 2005]. The metallic yielding (internal friction) and friction (dry friction) dampers can also be categorized as hysteretic dampers in which force and displacement are related to each other. Such devices are also called displacement dependent dampers [Constantinou et al, 1998] since their behavior depends solely on the relative lateral displacement of the story in which they are installed. The behavior of viscoelastic and viscous dampers are dependent on the loading frequency. The force in the dampers is proportional to the velocity experienced by the device and hence, they are referred to as velocity dependent passive energy devices.

2.2 Fluid Viscous Dampers

A viscous damper utilizes properties of viscous fluid to mitigate the seismic disturbances induced in a structure. They operate on the principle of flow of a viscous liquid like silicon oil through an orifice in a typical piston cylinder assembly as shown in Figure 2.1. Constantinou and Symans (1992) successfully checked the application of such piston cylinder fluid viscous dampers for seismic hazard mitigation. The behavior of such dampers is dependent on the frequency of applied force and temperature of the fluid. The flow of the viscous liquid through the orifice is altered with velocity of the piston in such a way that the pressure difference across the piston generates force in the damper proportional to $|\dot{u}|^{\alpha}$ where, $\dot{u}$ is the velocity experienced by the damper and the parameter α varies from 0.2 to 2 [Charney, 2005]. For α = 1 the viscous force linearly varies with velocity and a damper with such property is called linear fluid viscous damper. The force displacement relationship for a linear viscous damper is elliptical as shown in Figure 2.2.

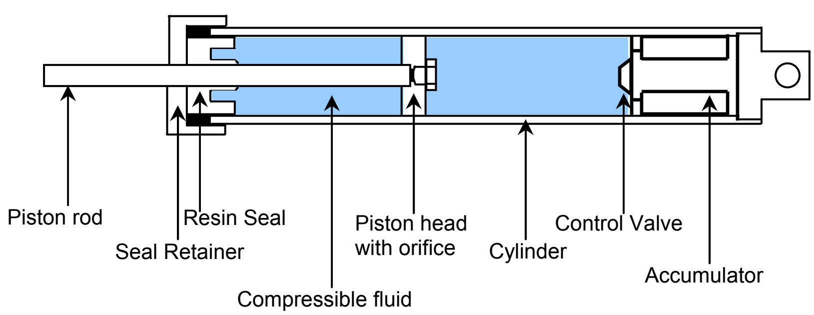

Figure 2.1: Fluid viscous damper [Constantinou and Symans, 1992]

Unlike other passive devices, fluid dampers have very low or no added stiffness and hence, do not alter the frequency of vibration of the structure. Also the damping viscous force is in phase with velocity and out of phase with elastic forces for linear viscous dampers, thus reducing the force demand in structural components. Both base shear and displacement response of the structure may be controlled equally by using linear viscous dampers.

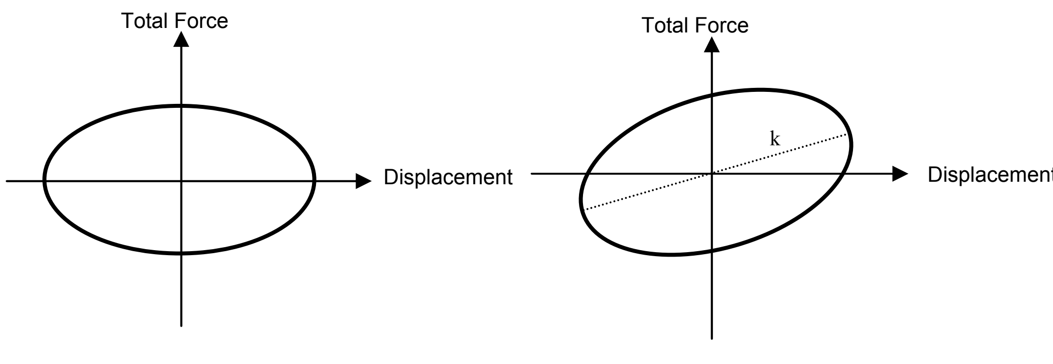

(a) Fluid viscous dampers **(b) Viscoelastic dampers**

Figure 2.2: Force displacement relationship for a linear viscous damper

The viscous damping wall system, as shown in Figure 2.3, developed by Sumitomo construction company, Japan, consists of a casing filled with viscous fluid attached to the lower floor and a steel plate, immersed in the fluid, attached to the top floor of a story, thus utilizing relative velocity of the story to generate viscous damping force. Added damping of 20% to 35% was monitored for viscous damping wall system installed in a 78m high SUT building in Japan [Miyazaki and Mitsusaka, 1992]. Arima et al. (1988) observed a reduction of response for a typical four story steel frame by 66% to 80%.

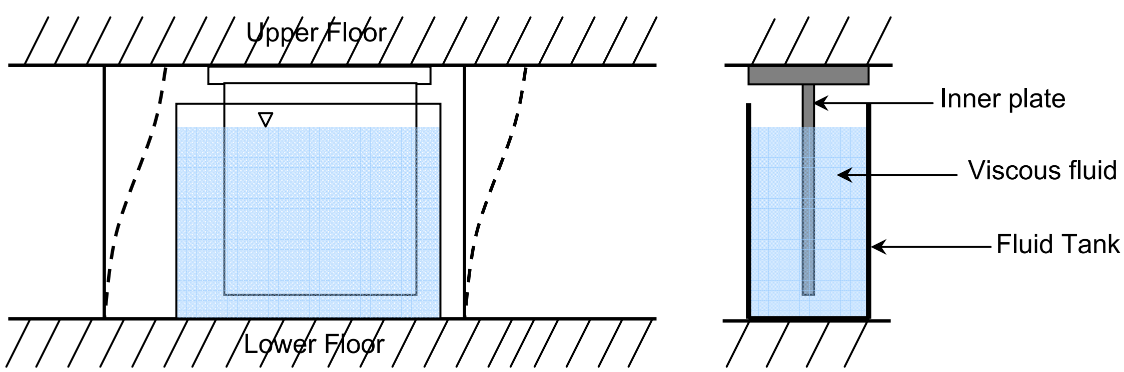

Figure 2.3: Viscous damping wall system

2.3 Viscoelastic Dampers

Viscoelastic (VE) dampers dissipate energy by axial strains and shear deformations in elastomers like rubber. The behavior of VE dampers is very similar to viscous fluid dampers except they always have inherent material stiffness. As shown in Figure 2.3 (b) the force displacement relation for VE dampers is an ellipse with inclined major axis, which represents inherent stiffness (k) of the VE material. Mahmoodi (1969) proposed the use of viscoelastic shear damper in reducing the dynamic response of the structure. A typical VE damper consists of a viscoelastic material sandwiched between steel plates as shown in Figure 2.4. VE dampers are sensitive to temperature and loading frequency. They are very simple and inexpensive.

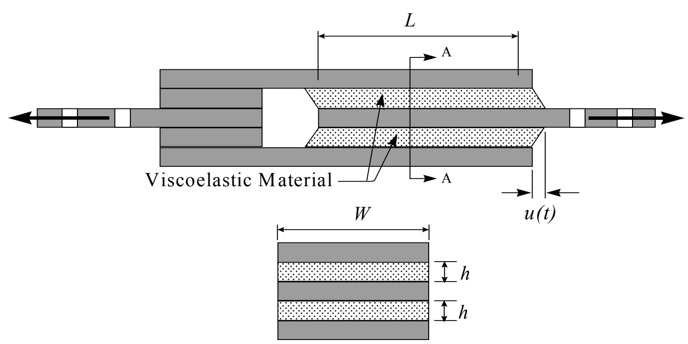

Figure 2.4: Typical viscoelastic damper [Charney, 2005]

Chang et al., (1993) showed the effectiveness of VE dampers in a steel frame by conducting shake table tests on a scaled frame. They also concluded that although less efficient at high temperatures, viscoelastic dampers improve the response of the structure. Viscoelastic dampers have been used successfully in specially designed beam column connections. As shown in Figure 2.5 the connection consists of two symmetrically placed single toothed devices with elastomeric pads. Because a shear pin or shear tab is used to transfer the shear, the devices are subjected only to axial force causing axial deformation in the elastomeric pads thereby dissipating energy. A reduction in response by 30% - 60%

was observed for viscoelastic dampers used in connections of a braced frame [Hsu and Fafitis, 1992].

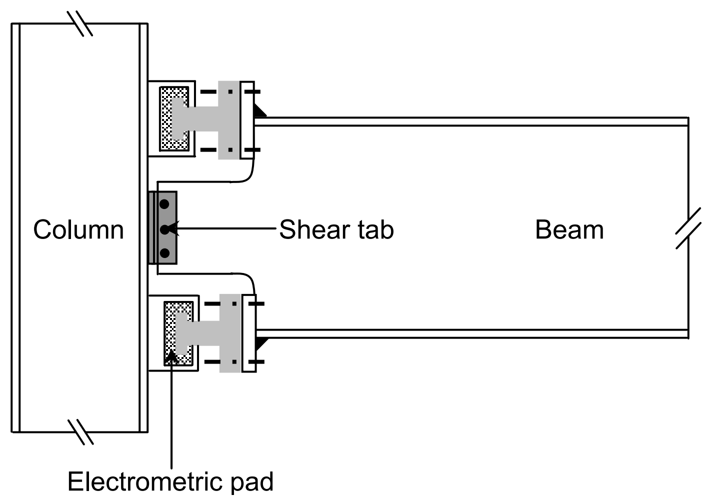

Figure 2.5: VE dampers configured in beam – column connection [Hsu and Fafitis, 1992]

2.4 Metallic Yielding Dampers

Metallic yielding dampers are designed as steel “fuses” [Charney, 2005] which undergo inelastic deformations, thereby diverting the over load (inelastic hysteretic energy dissipation demand) from the members of lateral load resisting frame and preventing it from sustaining any structural damage. Metallic yielding devices consist of a sacrificial metallic mass in the form of plates capable of undergoing inelastic deformations when subjected to extreme lateral loading. They are generally incorporated in the bracing system of frames and are also called Added Damping and Stiffness (ADAS) devices. ADAS devices have stable hysteretic loops and high resistance to fatigue. Researchers all over the globe have proposed different configurations of ADAS devices. ‘X’ shaped ADAS devices were developed by Bechtel power corporation [NISTIR 5923, 1996]. Experimental and analytical study on X-ADAS was carried out by Whittaker et al. (1991). Cyclic loading tests were performed on X-ADAS by Bergman and Goel (1987). Triangular shaped ADAS (TADAS) devices as shown in Figure 2.6 were originally introduced in New Zealand and were successfully used by Kelly and Skinner (1980) for piping systems in nuclear power plants. TADAS were also implemented in buildings later using design guidelines for seismic resistant TADAS frames proposed by Tsai et al., (1993). A typical TADAS assembly consists of the triangular plates embedded in to a common slotted base plate. Connection between the bracing system and the TADAS device is achieved using pins through slotted side plates welded to the bracing system. The triangular plates undergo uniform yielding throughout its volume when subjected to high lateral loads.

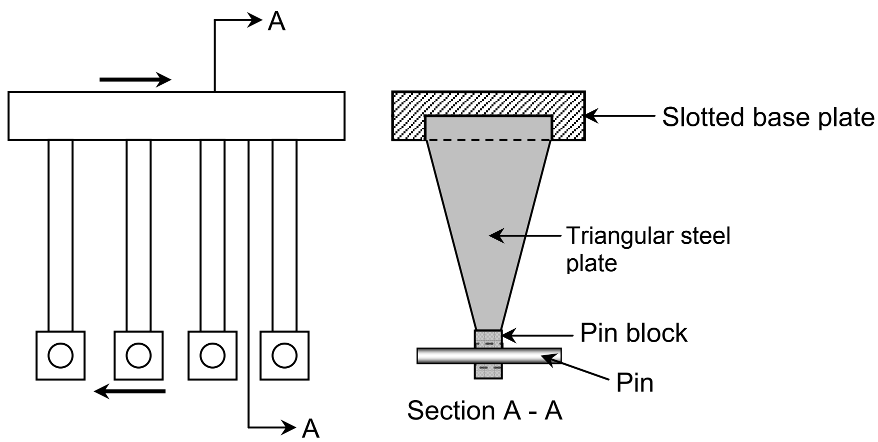

Figure 2.6: TADAS [Tsai et al., 1993]

Metallic yielding dampers consisting of a lead core and steel rings were developed in Japan by Sakurai et al. (1992). Metallic yielding devices dissipate a reasonable amount of energy and a decrease in displacement response is achieved. However, the added stiffness may cause an increase in base shear response. Such devices furnish an advantage of easy replacement in case of damage after an extreme load event.

Pinelli et al. (1993) proposed advanced energy dissipating cladding connections which utilized tapered connectors made from square tubes, Figure 2.7. These connectors are very similar to the 'X' shaped ADAS devices. Such devices minimize the damage in connection anchors as the deformations are concentrated in the connector body. Energy dissipation is achieved by plastic deformation of the 'X' shaped connector body. An analytical study conducted by Pinelli et al. also showed that about 60-70% of the input energy was dissipated by the connectors for different ground motions.

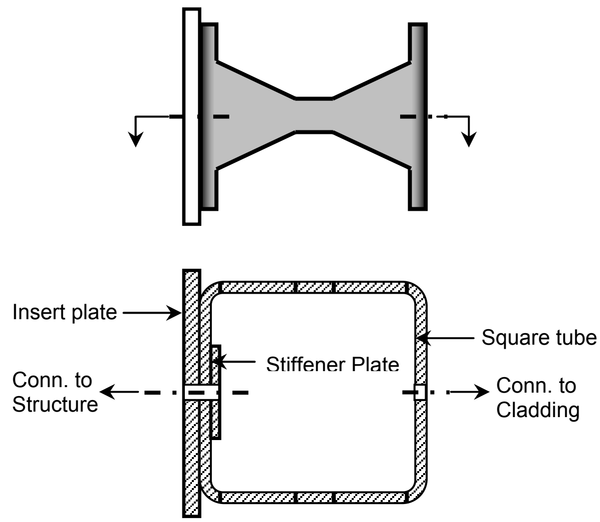

Figure 2.7: Tapered cladding connector [Pinelli et al., 1993]

2.5 Friction Dampers

Friction dampers are based on the principle of Coulomb damping. Such devices utilize the frictional resistance developed between the contact surfaces to dissipate energy in the form of heat. Behavior of friction dampers is independent of loading frequency, while it is a function of the normal/clamping force and coefficient of friction between the contact surfaces. The hysteretic loop for friction dampers is generally rectangular as shown in Figure 2.8, representing idealized elastic perfectly plastic behavior with high initial stiffness. The slip load of the friction damper can be thought of as a fictitious yielding strength (F_y) and high initial stiffness as device stiffness before slip.

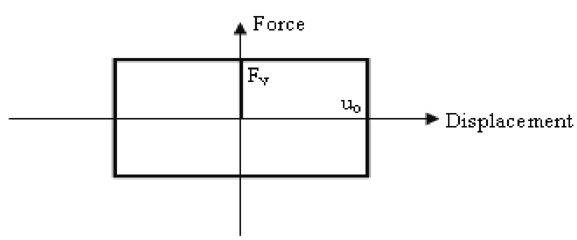

Figure 2.8: Hysteresis loop – friction dampers

2.5.1 Coulomb Damping

The Coulomb friction force ‘f’ can be expressed as $f = \mu N$ where μ is the coefficient of friction between the slip surfaces and ‘N’ is the normal force. The equation of motion governing coulomb damped free vibration of a single degree of freedom system is:

$$m\ddot{u} + ku \pm f = 0 \qquad 2.1$$

where m is the mass of the system, k represents the lateral stiffness and f is the Coulomb friction force. $\ddot{u}$ and u are the relative acceleration and displacement experienced by the dynamic degree of freedom. The direction of friction force f will always oppose the motion of the system. Free vibration decay of a coulomb damped structure is linear and the amplitude for each successive cycle is given by equation 2.2.

$$u_{i+1} = u_i - 4u_f \qquad 2.2$$

where $u_f = f / k$. Unlike viscously damped system, the fundamental time period of a coulomb damped system is same as its undamped counterpart [Chopra, 2002].

The equation of motion for forced vibration of a coulomb damped single degree of freedom system is as follows:

$$m\ddot{u} + ku \pm f = p(t) \qquad 2.3$$

where $p(t)$ is the harmonic forcing function. Coulomb damped structures, when loaded at the resonant frequency, show unbounded response, unlike viscously damped systems. The presence of a friction force does not constrain the response, mainly because energy dissipated due to friction in each cycle is less than the input energy thus, resulting in an unbalance which adds up in subsequent cycles causing an increase in the response. An approximate solution for displacement amplitude (u_o) for coulomb damped forced vibration is given by [Chopra, 2002]:

$$\frac{u_o}{(u_{st})_o} = \frac{\left\{1-[(4/\pi)(f/p_o)]^2\right\}^{1/2}}{1-(\omega/\omega_n)^2} \qquad \text{.....................................2.4}$$

where u_o is the displacement amplitude, $(u_{st})_o = p_o/k$ is referred as static deformation, p_o is the amplitude of applied cyclic force, k is the lateral stiffness of the system, f is the friction force, ω is the forcing frequency and ω_n is the natural frequency of the system.

2.5.2 Friction Dampers Applied to Structures

A large number of configurations of passive energy devices based on the principle of friction have been proposed by researchers. Pall and Marsh (1982) were the first to propose the use of friction damped braced frames to mitigate seismic hazard. As shown in Figure 2.9 brake lining pads as sliding surfaces were introduced at the intersection of tension only 'X' shaped braces. The configuration of the links formed at the intersection of the two braces was such that slip can be achieved in both the braces simultaneously. Aiken et al. (1988) verified effectiveness of such a configuration by comparing it with a moment resisting frame. Cherry and Filiatrault (1993) developed a method to find optimum slip force for the Pall friction dampers. They also performed an analytical and experimental investigation to verify the effectiveness of these dampers. Grigorian et al. (1993) checked the effectiveness of slotted bolted connections with friction surface and found that more than 85 % of the input energy was dissipated by such connections.

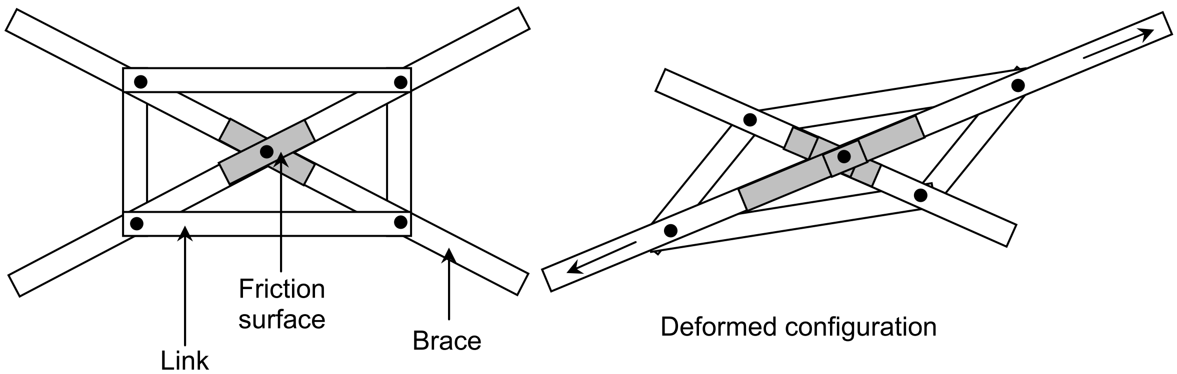

Figure 2.9: Pall friction dampers [Pall and Marsh, 1982]

Energy dissipating restraint (EDR) based on the principle of passive friction was successfully evaluated by Nims et al. (1993). The EDR is a self centering friction damper and the force induced in the damper is proportional to its displacement, Figure 2.10. The device consists of steel wedges, friction wedges, a spring, steel cylinder, piston and friction stops. The frictional resistance, proportional to the spring force, is achieved by special arrangement of steel and bronze friction wedges which produces the required normal force against the cylinder wall. Friction stops are provided to control slip in the device.

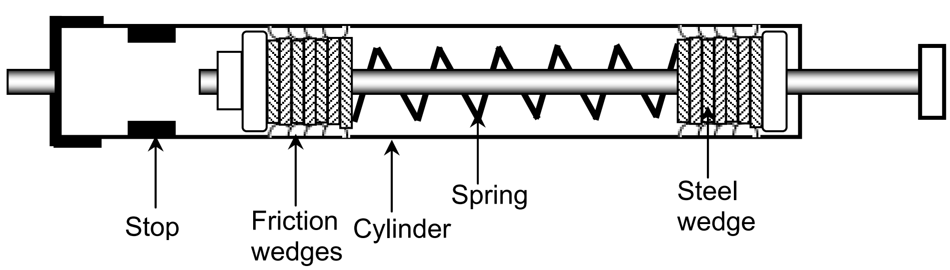

Figure 2.10: Energy dissipating restraint [Nims et al., 1993]

A friction wall damper for reinforced concrete structures was proposed by Cho and Kwon (2004). It consists of ‘U’ and ‘T’ shaped steel sections and sandwiched Teflon® sliders, Figure 2.11. An oil jack loading system can be used to apply a normal force on the assembly. Friction resistance can easily be varied in accordance to the anticipated earthquake loading by adjusting the normal force. Such a configuration eliminates connection problems faced in retrofitting the structure. Analytical testing of the structure with such walls was done to show the efficiency of such friction devices.

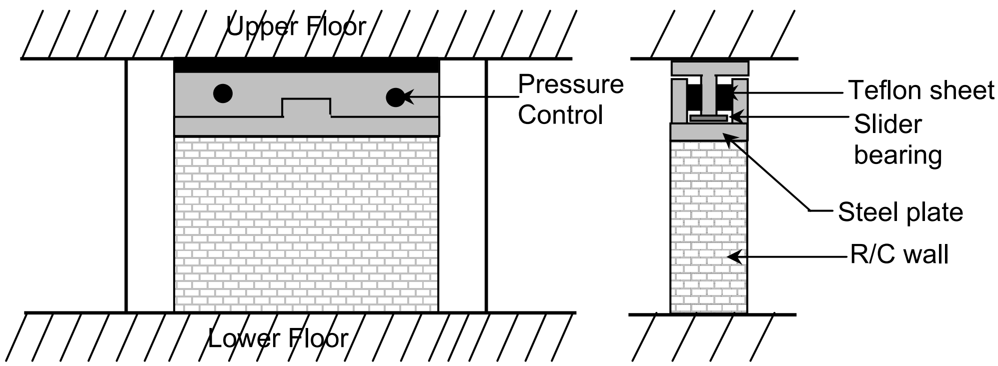

Figure 2.11: Friction wall damper for reinforced concrete structures [Cho and Kwon, 2004]

Friction dampers can be fabricated with ease using readily available materials. Such dampers being displacement dependent should be placed in that portion of the structure where maximum relative motion is expected. Friction dampers generally have a high amount of inherent stiffness causing an improved displacement response but may increase the force demand of the structural components to which it is attached.

2.6 Passive Dissipation Devices in Wood Frame Structures

Though wood structures have high inherent damping capacity, past experiences have revealed huge economic losses due to structural and non-structural damage in wood frame structures. Several successful attempts have been made to implement passive energy devices in light frame wood structures. A slotted friction device located in corners of a shear wall panel was proposed by Filiatrault (1990). Analytical studies of a single degree of freedom model with such a mechanism showed an appreciable dissipation of induced earthquake energy, thus controlling the damage in wood framed structures.

The use of Viscoelastic (VE) solids to improve the seismic behavior of wood frame structures was first proposed by Dinehart and Shenton (1998). Cyclic testing of VE dampers consisting of a VE material bonded with wood instead of conventional steel plates was carried out by Dinehart and Lewicki (2001), Figure 2.12. The tests conducted proved the equivalence of these dampers with VE dampers using steel plates. Also, it was observed that bonding between wood and viscoelastic material was intact at test frequencies of 0.1 Hz and 0.5 Hz and strains of 10% and 50%.

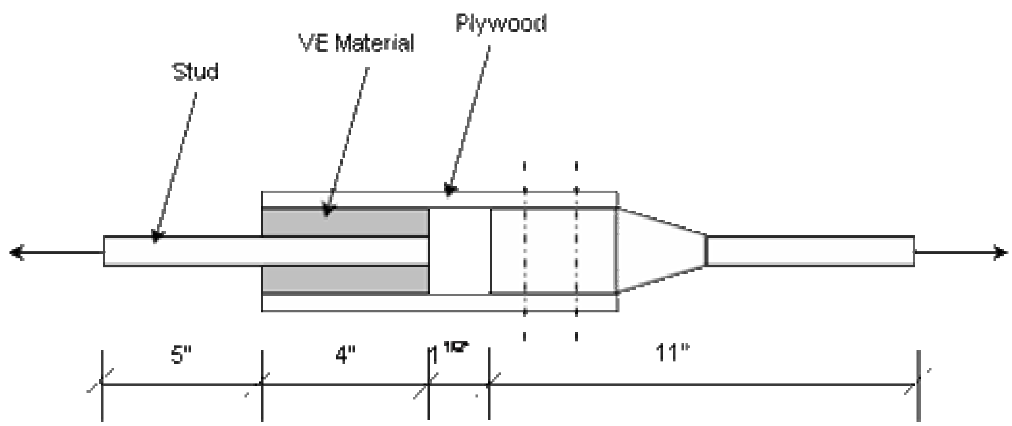

Figure 2.12: VE wood damper [Dinehart and Lewicki, 2001]

Dinehart and Shenton (1998) also utilized VE dampers in a brace configuration and showed improvement in behavior of the wood frame shear walls. Dinehart et al. (2004) placed a thin VE sheet (0.005 in. thick) between the framing and sheathing to improve the behavior of the connection, thereby dissipating energy due to viscoelastic action, Figure 2.13. Full scale testing of typical shear walls also revealed improvement of the response which was similar to the VE brace dampers in the shear wall initially tested by Dinehart and Shenton (1998). Energy dissipation capacity of wood shear walls increased by 26% for displacement ranging from 0.5-1.25 in.

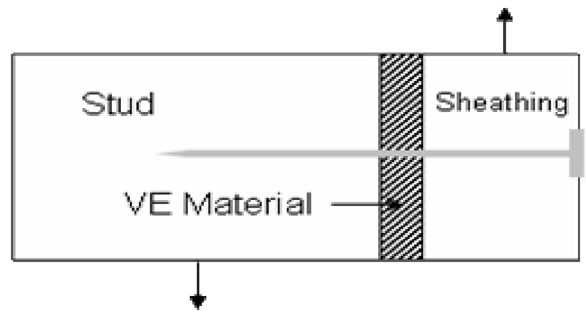

Figure 2.13: Viscoelastic sheet in framing sheathing connection [Dinehart and Lewicki, 2001]

Higgins (2001) proposed a bracing system for wood frame structures which had sliding anchors at one of its ends dissipating energy by friction. Experimental investigation of such a device showed improvement in damping characteristics of the frame and elimination of pinching behavior of wood frame shear walls. Symans et al. (2001) proposed the use of fluid viscous dampers in wood frame structures. An improvement in the behavior was demonstrated by both analytical and experimental testing. It was concluded that viscous fluid dampers with damping constant C = 100 lb-s/in. and C = 500 lb-s/in. increased the damping of fundamental mode from 2% critical to 5.7% and 20.4% critical respectively [Symans et al., 2004]. Such fluid dampers can be easily incorporated in conventional wood shear walls with minimal or no alterations as shown in Figure 2.14.

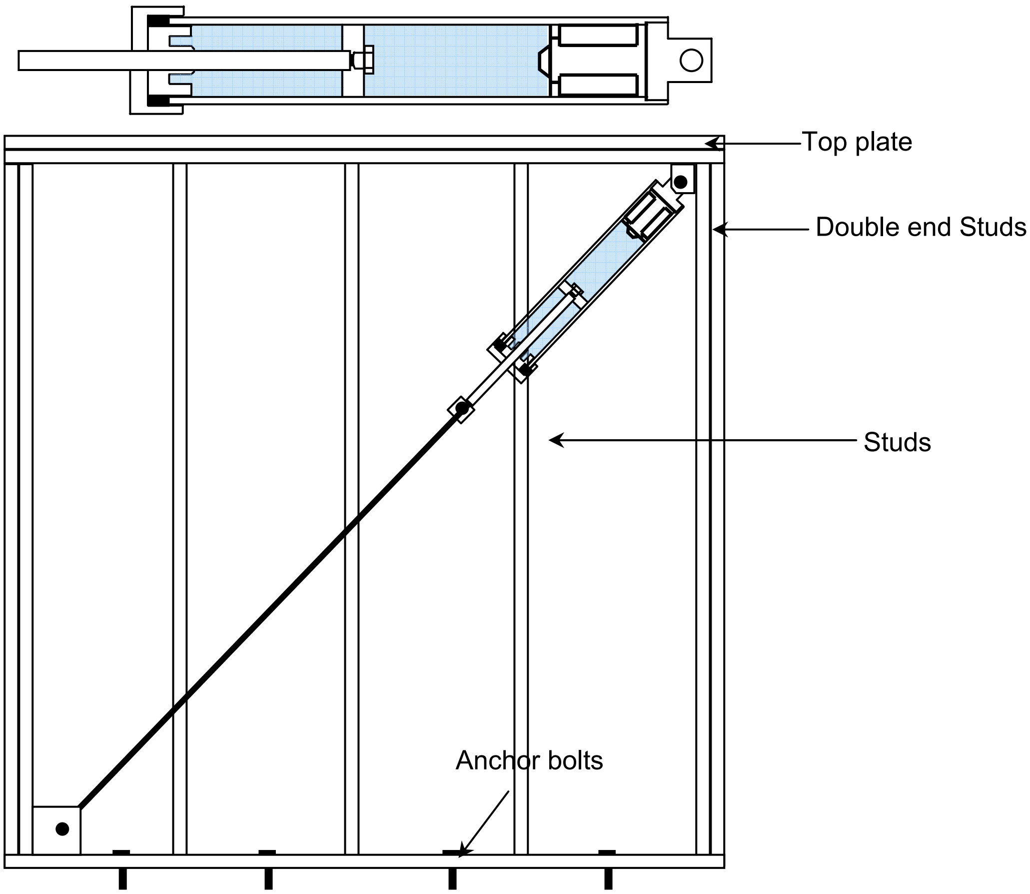

Figure 2.14: Fluid viscous damper for wood frame structures [Symans et al., 2001]

2.7 Lateral Load Resisting System in Wood Frame Structures

The dead load in a wood frame structure is resisted by the frame elements (vertical studs and horizontal beams) where as the lateral load induced by wind or earthquake is primarily resisted by shear walls. A shear wall consists of sheathing panels effectively connected to the vertical frame elements by nails or glue. Glued wood frames, being stiffer than their nailed counterparts, attract more shear and dissipate less energy as compared to nailed shear walls. In case of earthquake loading the horizontal force from the diaphragm is transferred to the top plate which transfers the shear to the sheathing elements via the framing elements and nailed or glued connections. As shown in Figure

2.15 (a) the end studs are typically designed stronger than the inner ones as high tension force is induced in the exterior chords. The engineered design approach considers the shear wall as a deep cantilever beam in the vertical direction to estimate the demand in the framing members. Uplift in the shear wall should be prevented by using hold–down devices placed in bottom corners, connected to the vertical end stud and anchored in the foundation. Anchor bolts are installed at a regular distance to facilitate efficient shear transfer from the shear wall to the foundation. Shear walls generally deform in the racked configuration, where the frame undergoes shear deformation and the sheathing panels undergoes rigid body rotations under minor loading events, Figure 2.15 (b). The behavior of shear walls in resisting lateral loads largely depends on the framing-sheathing connections. The hysteretic behavior of the connectors is the prime source of energy dissipation in wood frame structures. A number of force deformation models for framing-sheathing connectors have been proposed on the basis of cyclic tests performed on shear walls. Plywood sheets, having very low inherent damping capacity, are also used as primary lateral load resisting system in wood structures.

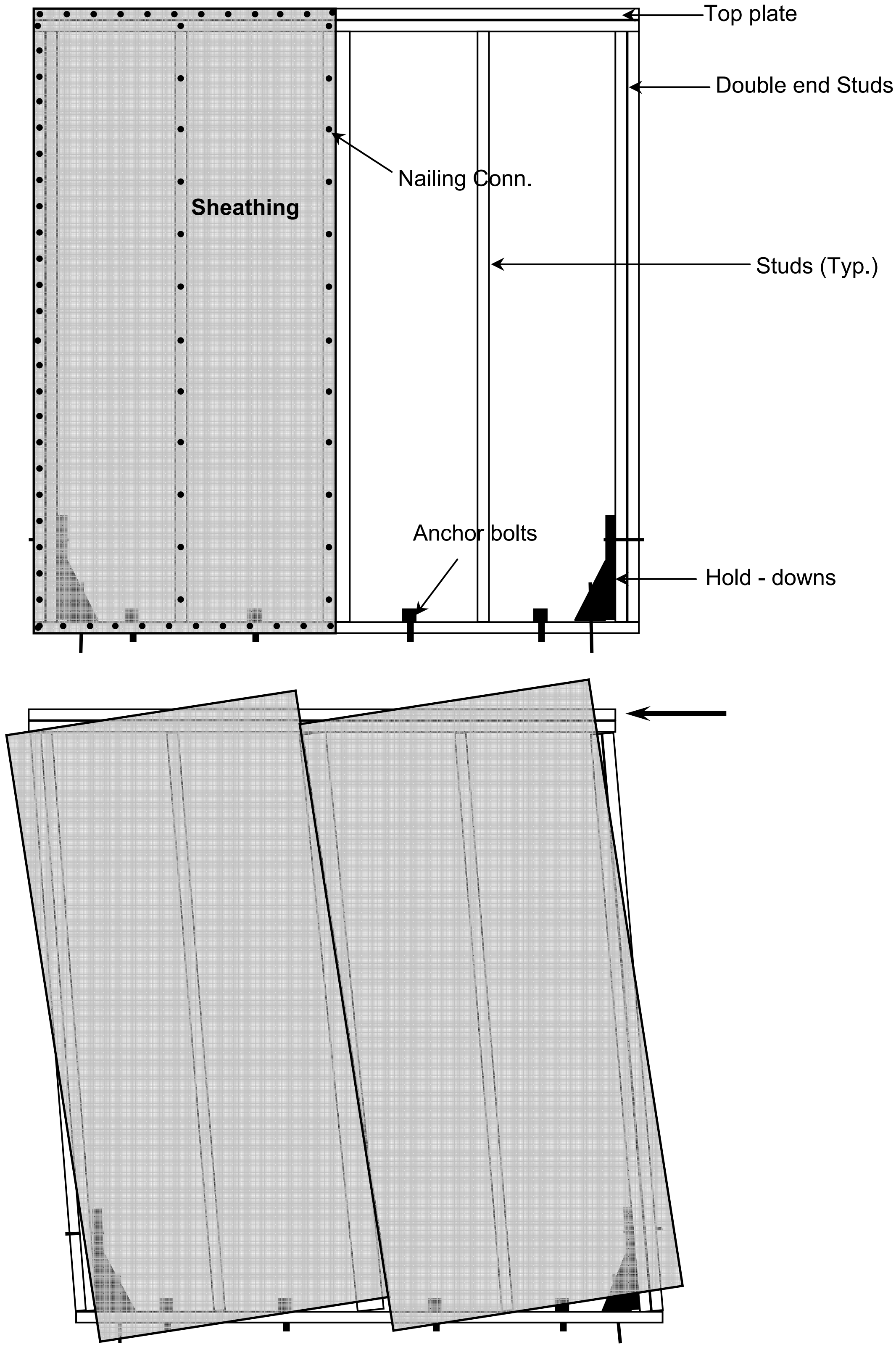

(a)

(b)

Figure 2.15: (a) Typical wood frame sheer wall (b) Racking due to lateral loads

2.8 Inherent Damping Capacity of Wood Frame Structures

The main source of energy dissipation (damping) in wood structures is inelastic behavior of the connectors connecting the framing and sheathing elements, as the material damping for wood is even less than 1% [Basic et al., 1996]. The experimental study conducted by Yasumura (1996) showed that the equivalent viscous damping for arched and moment resisting timber frames is as low as 2-6% when compared to conventional nailed shear wall or braced frame in which the equivalent viscous damping ranges between 10-18% and 15-20% respectively. Such high damping capacity is gained by the high amount of inelastic behavior in the connections making them ineffective for subsequent lateral loading events. Also for the same loading event the damping achieved for a few initial cycles is not same for subsequent cycles, as loosening of the fastener may reduce the inelastic deformation capacity of the connectors. The damping ratio for a shear wall under very low excitation was found to be less than 5% and varied from 1-3% [Dutil, 2004]. Equation 2.5 shows an expression for equivalent damping ratio (ξ_{equi}) in wood frame structures proposed by Filiatrault et al. (2003).

$$\begin{aligned} \xi_{equi} &= 0.5\Delta + 0.02 \qquad && \Delta < 0.36\% \\ &= 0.20 && \Delta \geq 0.36\% \end{aligned} \quad \text{...2.5}$$

where Δ is the drift ratio. Thus, it can be concluded that the damping in wood frame shear walls is very low under elastic behavior. Inelastic behavior of the connectors increases the inherent damping capacity to about 10%. In this study the effectiveness of the friction dampers is checked for a 1%, 5% and 10% critical damping ratio keeping in mind the variable damping which may occur in wood frame shear walls during a single loading history.

2.9 Proposed Device Configuration

A simple sliding wall configuration with a permanent flexible magnet sheet sandwiched between two plywood sheets is proposed as an energy dissipation device based on the principle of dry friction (Coulomb damping). The sliding wall can be configured to fit any part of the wood frame structure.

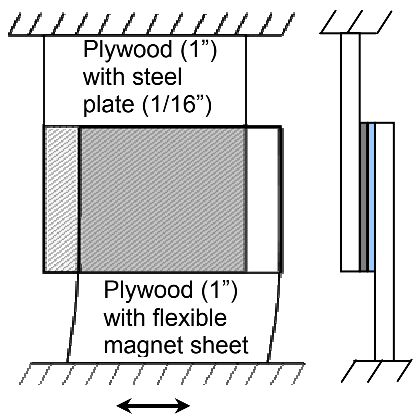

Figure 2.16: Proposed friction damper configuration

As shown in the Figure 2.16 the friction device consists of two overlapping plywood sheets. Each plywood sheet has a 1/16 in. thick steel plate adhered to it. The unmagnetized surface of a flexible permanent magnet sheet is further adhered to one of the steel plates. Connection between the steel plate and plywood as well as that between flexible magnet and steel plate can be achieved using commercially available adhesives (e.g. liquid nail®). Adhesive coated flexible sheets can also be used provided no slip is anticipated between the adhered surfaces at the maximum anticipated lateral load. The two plywood sheets now will be under the influence of normal force of attraction between the flexible magnet and steel plate. It is proposed to adhere the flexible magnet sheets to the steel plate instead of direct attachment to the plywood to achieve flat surface which enables full contact of the magnet and steel plate in the overlapping zone. The overlapping area and strength of magnet can easily be adjusted depending on the anticipated seismic hazard. Plywood sheets should be rigidly attached to the corresponding top and bottom plates. The separation of the magnet from the steel plate can easily be prevented by inducing loose bolts in long slotted holes in the sliding walls. The problem of separation of the magnetic sheet from the steel plate due to the torsional mode of vibration can be addressed by placing the dampers towards the centroid (as interior partition walls).

Chapter 3

Permanent Magnets

A permanent magnet is a perennial source of magnetic field in space. Unlike a current carrying conductor, a magnet provides a constant magnetic field without any supply of electric power or production of heat. Thus, a permanent magnet is an energy storage device, which retains the energy supplied to it when first magnetized [Cullity, 1972].

3.1 Magnetism in Matter

All materials respond to an externally applied magnetic field in some way or the other, since matter always has a large number of randomly oriented magnetic domains (group of magnetic dipoles aligned in one direction) depending on its atomic structure, electron spin and arrangements. However, the intensity of response is spread over a wide spectrum. The response of non-magnetic materials can only be observed using very sensitive equipment. On the basis of the response of the material to an externally applied magnetic field, it is classified as Diamagnetic, Paramagnetic, Antiferromagnetic, Ferromagnetic, or Ferrimagnetic material.

Diamagnetic materials are those which develop an opposing weak magnetic field when exposed to an approaching external magnetic field. Such a weak field is a result of small current (eddy current) developed to oppose the external field. Graphite and Bismuth show the strongest diamagnetic properties apart from silver, wood, water, etc. Magnetic levitation is a property of diamagnetic material. Paramagnetism arises due to unpaired electrons in external orbital resulting in unbalanced magnetic moments. Materials exhibiting paramagnetism when exposed to an external magnetic field produce a weak force of attraction as the unbalanced moments get aligned in the direction of the applied field. Aluminum, Calcium, Platinum, etc. are paramagnetic materials. Antiferromagnetism is very similar to paramagnetism except that the unpaired electrons of the neighboring atoms are aligned opposite to each other resulting in very low or no magnetism. At high temperatures antiferromagnetic materials behave very similar to paramagnetic materials. Thus, diamagnetic, paramagnetic and antiferromaganetic material can be categorized to a common group of non-magnetic materials where as ferromagnetic and ferrimagnetic materials are considered as magnetic materials.

Ferromagnetism is the most common behavior exhibited by magnetic material. The net magnetic moment due to unpaired electrons gets aligned to the externally applied magnetic field generating a strong force of attraction. Iron and Nickel are the most common ferromagnetic materials. Unlike antiferromagnetism, ferrimagnetism is caused by unequal opposing magnetic moments resulting in a net alignment in one direction on application of an external magnetic field. Ferrimagnetic materials can be thought of as a weak form of ferromagnetic materials. Barium Ferrite is a common example of ferrimagnetic material. Magnetic materials can also be classified as hard or soft. Soft magnetic materials align their magnetic dipoles in the direction of applied external magnetic field very easily. Orientation of magnetic dipoles of hard magnetic material remains unchanged under the influence of an external magnetic field. This property of hard magnetic material is utilized in the production of permanent magnets.

3.2 Definitions

The coercive force, residual induction and maximum energy product are the principal magnetic properties of permanent magnet materials. The values of these properties give an idea of the strength and resistance of a magnetic material to demagnetization. Further, the sensitivity of the magnetic properties to the temperature of the magnetic material can be predicted from corresponding reversible temperature coefficients. Following are the definitions of the principal magnetic properties and other general terms.

Magnetic Field Strength, (H): Magnetic field strength is the ability of a magnetic body or current carrying conductor to produce a magnetic flux at a given point in space. Unit of field strength is Oersteds.

Coercive Force, (H_c): It is the external demagnetizing force/magnetic field strength required to reduce the residual induction of a magnetic material to zero. It is measured in Oersteds.

Air-gap: The length of non-magnetic material in the path of magnetic field is termed as air-gap.

Residual Induction, (B_r): Flux density induced in a magnet after saturation is called residual induction or residual flux density. It corresponds to zero magnetizing force and is measured in Gauss (G). Tesla (T) is a larger unit of magnetic flux density and is equivalent to 10000 Gauss. Thus, 10 G = 1 mT. Residual induction can only be observed at zero air-gap.

Intrinsic Induction, (B_i): The inherent capacity of a magnetic material to contribute to the total magnetic induction; It is denoted as 'B'.

Intrinsic Coercive Force, (H_{ci}): The material's inherent ability to resist demagnetization is called intrinsic coercive force and is measured in Oersteds.

Maximum Energy Product, (BH_{max}): A measure of energy which can be supplied by a magnet to an external magnetic circuit at any point of operation on its demagnetization curve. The point on the demagnetization curve where the product of B and H is a maximum is an indication of the power of a magnet. It is measured in Mega Gauss Oersteds, MGOe.

Maximum Service Temperature, (T_{max}): It represents the maximum temperature beyond which the efficiency of the magnet may be reduced due to change in its material structure.

Curie Temperature, (T_c): It is the temperature at which the magnet will become demagnetized. Both reversible as well as irreversible losses may occur if the temperature is raised above T_{max} but below T_c.

Reversible temperature Coefficient: It is a factor expressed as percent change of magnetic property (e.g. Magnetic flux density, maximum energy product etc.) per unit change of temperature.

Holding Force: The normal force of attraction between a ferromagnetic material and a permanent magnet is defined as holding force. Holding force decreases rapidly with increase in air-gap.

Sliding Force: It is the shear/slip resistance achieved between the magnet and ferromagnetic material.

3.2.1 Hysteresis Loop

The hysteresis loop for a magnetic material represents the variation of flux density with respect to an applied external magnetic field. The loop is a unique property for a magnetic material and it describes the cyclic behavior of the magnet as it is brought to saturation, demagnetized, saturated in the opposite direction and again demagnetized under the influence of an external field of intensity H [DESIGN, 2000][1]. As shown in Figure 3.1 (a) curve O-1-H represents magnetization of unmagnetized material when exposed to an external field of intensity H. If H is now reduced to zero there is a residual flux in the material represented by a point B_r. Further if H is increased from zero in the opposite direction the curve B_r-3-H_c-4-H is obtained. B_r and H_c are defined as residual flux density

[1] Design Guide. Magnet Sales and Manufacturing Company, [online], 2000, www.magnetsales.com/Design/DesignG.htm (Accessed: 13 June 2004)

and coercive force respectively. H' represents the saturation point (point at which flux density remains unchanged with increase in the strength of external magnetic field) in the opposite direction. Reduction of force to zero and further increasing the same in the original direction follows the curve H-5-B_r-6-H_c-7-H. The second quadrant of the hysteresis loop is called the *demagnetization curve* and it represents the working condition (without any external magnetic field) of a permanent magnet. $(BH)_{max}$ is defined as the maximum energy product of a magnet and is given by a point on the demagnetization curve for which the product of B and H is maximum. The total flux density (B) is the summation of the material's intrinsic characteristic to produce flux and that produced by an externally applied field [McCaig, 1977]. As shown in Figure 3.1 (b) the variation of the material's intrinsic properties (B_i, H_i) is represented by the intrinsic curve, whereas the normal curve represents the variation of the total flux density (B) with the magnetic field intensity.

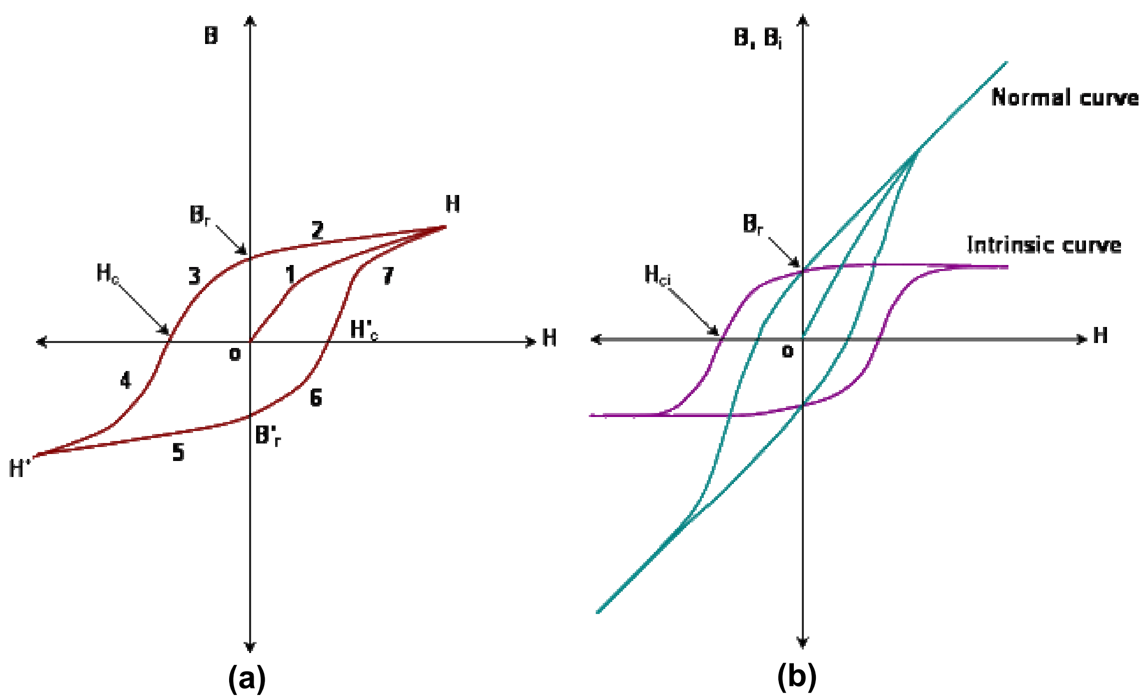

Figure 3.1: Hysteresis loops for magnetic material

3.3 Permanent Magnet Materials

The Magnetic Materials Producers Association (MMPA) defines permanent magnet material as a material which has a coercive force (H_c) greater than 120 Oersted. A large array of permanent magnet materials have been discovered in past years, however, not all are produced on a commercial scale. Table 3.1 lists commercially available permanent magnet materials and references to a corresponding section of standards. Table 3.2 compares different types of permanent magnet materials produced commercially on a large scale. The maximum energy product which is representative of the strength of the permanent magnet material, resistance to demagnetization and the maximum operating temperature are the basis of comparison. Figure 3.2 shows the demagnetization curves (second quadrant of the Hysteresis loop which typically represents the amount of magnetic flux induced by the magnetic material in the space and the resistance of the magnet against demagnetization) for different types of magnetic materials. It is clear that ferrite magnets are the weakest when compared to Alnico and other Rare earth permanent magnets which are discussed in the following sections.

TABLE 3.1
Permanent magnet materials [MMPA 0100-00]*

Magnetic Material	MMPA Standards
Alnico	II
Ferrite	III
Rare Earth Metals	IV

*Reproduced with permission from MMPA- Magnet Materials Producers Association now IMA – International Magnetics Association

TABLE 3.2
Comparison of permanent magnet materials [REFDEX, 1998]

Material	Max. Operating Temp ˚C	Max. Energy product MGOe	Resistance to Demagnetization
NdFeB	150	50	High
SmCo	300	32	High
Alnico	550	9.0	Low
Ferrite (Ceramic)	300	4	Moderate

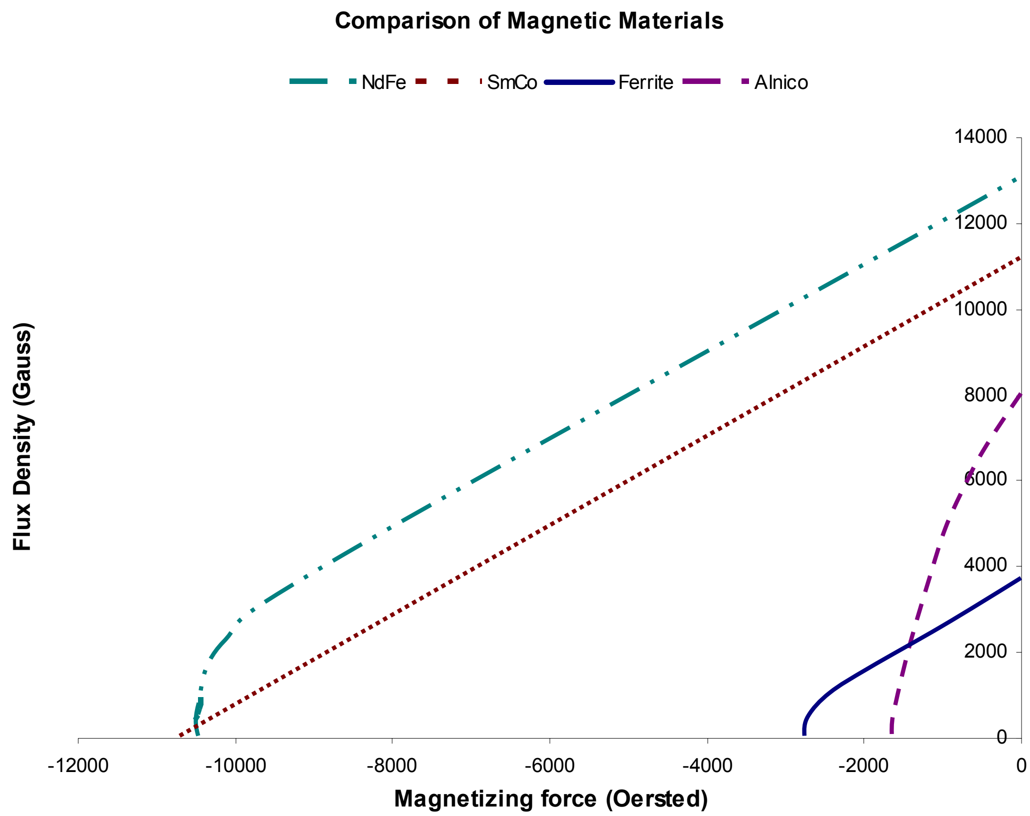

Figure 3.2: Comparison of permanent magnet materials [REFDEX, 1998]

3.3.1 Alnico

Alnico is an alloy of Aluminum, Nickel, Iron, Cobalt and Tin. The maximum energy product for Alnico permanent magnet ranges from 1.5 MGOe to 9.0 MGOe. They are produced by casting molten alloy or by pressing and sintering (the process by which the powdered mixture of metals is converted to solid with melting) fine powder mix. Sintered alloy, being fine grained, is mechanically stronger, however it possess inferior magnetic properties as compared to coarse grained cast alloys.

Alnico is very hard and brittle. It is stable over a wide temperature range higher than 500°C, with very low reversible change of -0.02% per degree Centigrade. Exposure to high temperatures may cause about 5% of irreversible losses which can be easily recovered by remagnetization [Arnold, 2004][2]. Alnico has strong corrosion resistance and hence, does not need any surface coating. Alnico magnets are used in temperature–sensitive applications such as electronic sensors apart from other traditional applications. Table 3.3 summarizes the magnetic properties and chemical composition of different grades of Alnico magnets. MMPA designation in the form of *Maximum energy product* $(BH)_{max}$/*Intrinsic Coercive force* H_{ci} is assigned to all the types of magnetic material. For instance 1.4/0.48 in Table 3.3 represents an Alnico magnetic material with Maximum energy product of 1.4 MGOe and Intrinsic Coervice force of 0.48 kOe. The physical properties of Alnico magnets are listed in Table 3.4.

TABLE 3.3

Magnetic properties and chemical composition of ALNICO [MMPA 0100 - 00]

MMPA Desig.	MMPA class	Chemical Composition (Balance Fe)					Magnetic Properties			
		Al	Ni	Co	Cu	Ti	Max. Energy Product $(BH)_{max}$	Residual Induction B_r	Coercive Force H_c	Intrinsic Coercive Force H_{ci}
							MGOe	gauss	Oe	Oe
Isotropic* Cast ALNICO										
1.4/0.48	Alnico1	12	21	5	3	-	1.4	7200	470	480
1.7/0.58	Alnico2	10	19	13	3	-	1.7	7500	560	580
1.35/0.50	Alnico3	12	25	-	3	-	1.35	7000	480	500
Anisotropic Cast ALNICO**										
5.5/0.64	Alnico5	8	14	24	3	-	5.5	12800	640	640
7.5/0.75	Alnico 5-7	8	14	24	3	-	7.5	13500	740	740
3.9/0.80	Alnico 6	8	16	24	3	1	3.9	10500	780	800
5.3/1.9	Alnico 8	7	15	35	4	5	5.3	8200	1650	1860
9.0/1.5	Alnico9	7	15	35	4	5	9.0	10600	1500	4500
Isotropic Sintered ALNICO										
1.5/0.57	Alnico2	10	19	13	3	-	1.5	7100	550	570
Anisotropic Sintered ALNICO										
3.9/0.63	Alnico5	8	14	24	3	-	3.9	10900	620	630
2.9/0.82	Alnico6	8	15	24	3	1	2.9	9400	790	820
4.0/1.7	Alnico8	7	15	35	4	5	4.0	7400	1500	1690

* Materials exhibiting equal magnetic properties in all directions.
** Materials exhibiting varied magnetic properties in different directions.

[2] Arnold Magnetic Technologies – Permanent Magnets. Arnold Engineering Company, [onlilne], www.arnoldmagnetics.com/products/alnico/index.htm (Accessed: 13 June 2004)

TABLE 3.4

Physical properties of ALNICO [MMPA 0100-00]

MMPA Brief Designation	Original MMPA class	Density lbs/in^3	Tensile strength Ksi	Transverse Modulus of Rupture Ksi	Hardness (Rockwell C)	Coefficient of Thermal Expansion 10^{-4} per ˚C	Electrical Resistivity Ohm-cm x 10^{-4} at 20 ˚C
1.4/0.48	Alnico1	0.249	4	14	45	12.6	75
1.7/0.58	Alnico2	0.256	3	7	45	12.4	65
1.35/0.50	Alnico3	0.249	12	23	45	13.0	60
5.5/0.64	Alnico5	0.264	5.4	10.5	50	11.4	47
7.5/0.75	Alnico 5-7	0.264	5	8	50	11.4	47
3.9/0.80	Alnico 6	0.265	23	45	50	11.4	50
5.3/1.9	Alnico 8	0.262	10	30	55	11.0	53
9.0/1.5	Alnico9	0.262	7	8	55	11.0	53
1.5/0.57	Alnico2	0.246	65	70	45	12.4	68
3.9/0.63	Alnico5	0.25	50	55	45	44.3	50
2.9/0.82	Alnico6	0.25	55	100	45	11.4	54
4.0/1.7	Alnico8	0.252	50	55	45	11.0	54

Table 3.5 lists the thermal properties of Alnico magnets. The reversible temperature coefficient for residual induction, maximum energy product and coercive force are listed along with the Cure temperature (temperature at which the magnetic material is demagnetized) and recommended maximum service temperature. Figure 3.3 shows demagnetization curves for different grades of cast and sintered Alnico magnets, it is clear from the plot that cast Alnico magnets are stronger as compared to the sintered variety.

TABLE 3.5

Thermal properties of ALNICO [MMPA 0100- 00]

MMPA Brief Designation	Original MMPA class	Reversible Temperature Coefficient % Change per ˚C			Curie Temperature ˚C	Max. Service Temperature ˚C
		Near (B_r) Residual Induction	Near Max. Energy Product $(BH)_{max}$	Near Coercive Force (H_c)		
1.5/0.57	Alnico2	-0.03	-0.02	-0.02	810	450
5.5/0.64	Alnico5	-0.02	-0.015	+0.01	860	525
3.9/0.8	Alnico6	-0.02	-0.015	+0.03	860	525
5.3/1.9	Alnico8	-0.025	-0.01	+0.01	860	550
9.0/1.5	Alnico9	-0.025	-0.01	+0.01	860	550

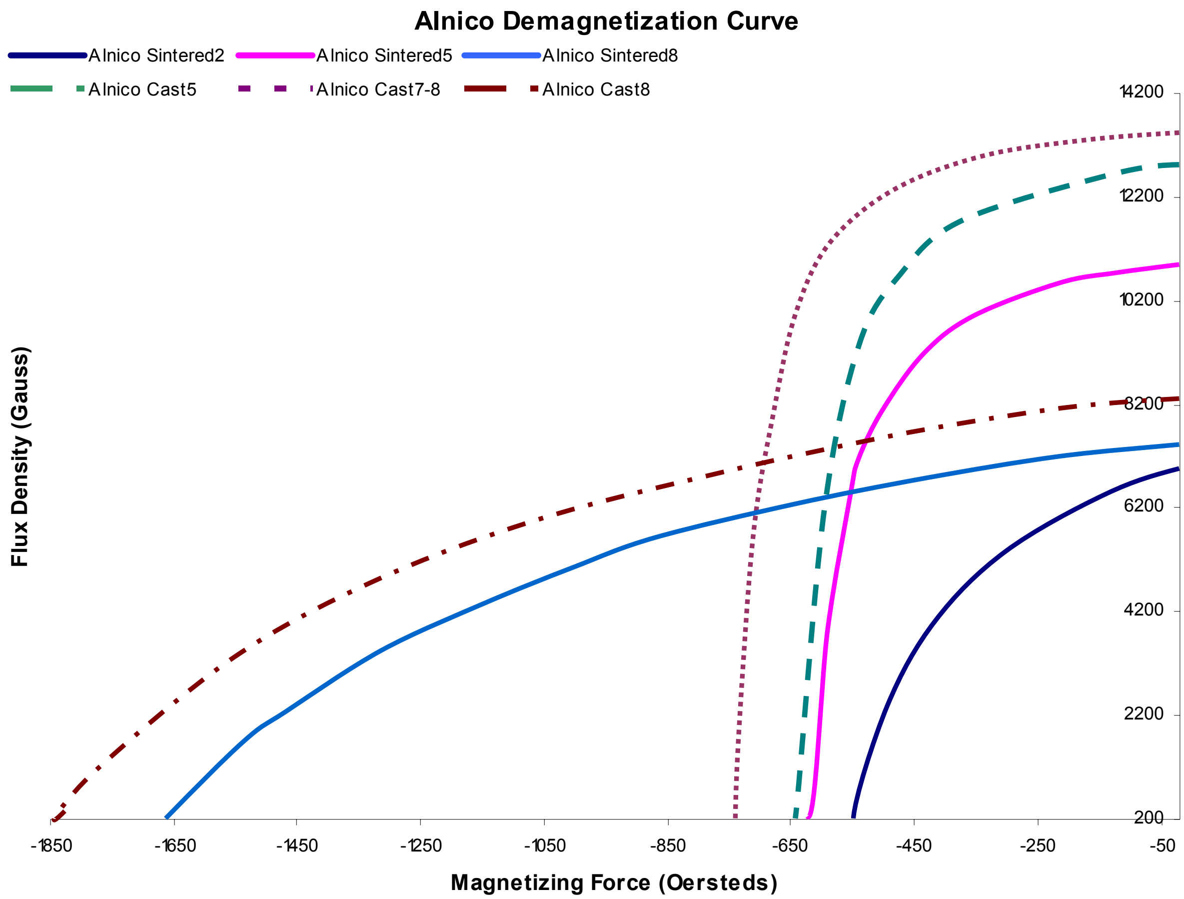

Figure 3.3: Demagnetization curve Alnico material [REFDEX, 1998]

3.3.2 Ferrite / Ceramic

Ceramic magnets are composed of Iron oxide, Barium and Strontium. The chemical composition of ceramic magnet material is $MO \cdot 6Fe_2O_3$, where M represents either Barium or Strontium or combination of both [MMPA 0100-00]. Ceramic magnets, being inexpensive, are the most widely used permanent magnets and represent more than 75 % of the world magnet consumption [Arnold, 2004][3].

[3] Arnold Magnetic Technologies – Permanent Magnets. Arnold Engineering Company, [onlilne], www.arnoldmagnetics.com/products/ferrite/index.htm (Accessed: 13 June 2004)

Ferrite is available in both isotropic and anisotropic form. The maximum energy product for ferrite materials ranges from 1 MGOe to 3.5 MGOe. It has excellent corrosion resistance, good temperature stability, high coercive force and resistance to demagnetization. Both reversible and irreversible changes in magnetic properties occur due to change in temperature, reversible change in magnetic induction occurs at a rate of about -0.2% per degree centigrade whereas coercivity changes at a rate of about 0.27% per degree centigrade. Exposure of ferrite magnets to low temperatures results in irreversible changes which can be restored by remagnetization.

Ferrite magnets are manufactured by compression or extrusion molding followed by sintering. They are also known as ceramic magnets to emphasize the process by which they are manufactured. Flexible and rigid bonded ferrite magnets are formed using ferrite powder and polymer binders. Magnetic and chemical composition of ferrite magnets are listed in Table 3.6 followed by physical and thermal properties in Table 3.7. Figure 3.4 shows demagnetization curves for Ceramic 1 (1.0/3.3), Ceramic 5 (3.4/2.5) and Ceramic 8 (3.5/3.1) ferrite magnets. It should be noted that both normal and intrinsic curves are shown in all the demagnetization curves.

TABLE 3.6

MMPA Magnetic properties and chemical composition of ferrite magnets [MMPA 0100-00]

MMPA Designation	MMPA class	Chemical Composition (M represents Barium, Strontium or combination of the two)	Magnetic Properties			
			Max. Energy Product $(BH)_{max}$	Residual Induction B_r	Coercive Force H_c	Intrinsic Coercive Force H_{ci}
			MGOe	Gauss	Oe	Oe
1.0/3.3	Ceramic1	MO. $6Fe_2O_2$	1.05	2300	1860	3250
3.4/2.5	Ceramic5	MO. $6Fe_2O_2$	3.40	3800	2400	2500
2.7/4.0	Ceramic7	MO. $6Fe_2O_2$	2.75	3400	3250	4000
3.5/3.1	Ceramic8	MO. $6Fe_2O_2$	3.50	3850	2950	3050

TABLE 3.7

Physical and thermal properties of ferrite magnets [MMPA 0100- 00]

Property	Typical Value
Density	0.177 lbs/in^3
Modulus of Elasticity	2.6 x 10^4 ksi
Poisson ratio	0.28
Compressive strength	130 ksi
Tensile Strength	5 ksi
Flexural strength	9 ksi
Reversible temperature coefficient for residual induction	-0.11%/°F
Curie Temperature	450°C
Maximum Service Temperature	800°C

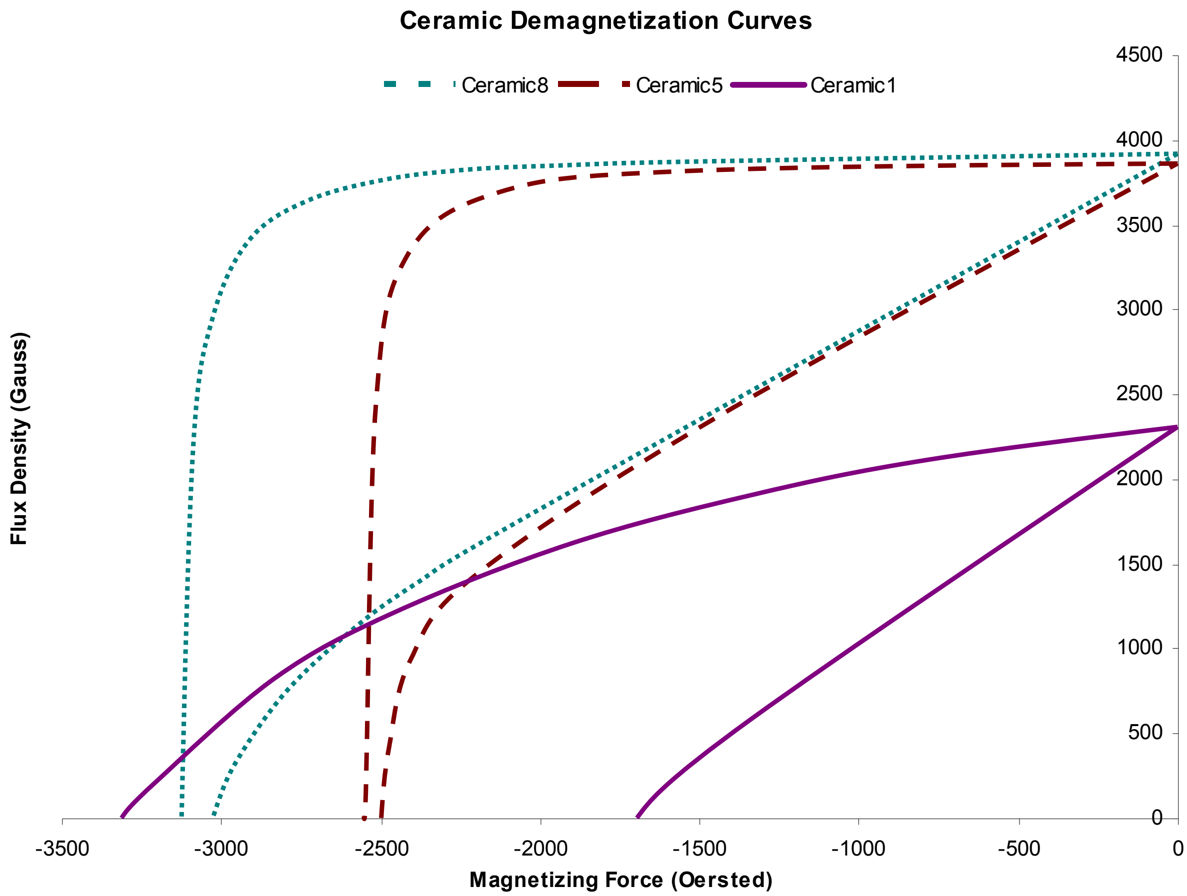

Figure 3.4: Demagnetization curve Ceramic magnet material [REFDEX, 1998]

3.3.3 Bonded Flexible Magnets

Bonded Flexible magnets consist of magnetic material in a matrix of binder such as nitrile rubber, polyethylene, nardel etc. Such magnets can be machined with no loss in magnetic energy. Bonded magnets, being relatively weak and flexible, can be handled easily.

Ferrite is a common magnetic material used for the production of flexible magnets. However, products consisting of rare earth magnet materials are also manufactured for high strength requirements. The maximum energy product for ferrite and rare earth bonded flexible magnets varies from 0.6 MGOe to 1.8 MGOe and 8 MGOe to 10 MGOe respectively [BOND, 2004][4]. Hybrid flexible magnets composed of a mixture of ferrite and rare earth magnet materials with the maximum energy product ranging from 1.6 MGOe to 4 MGOe are also manufactured. Flexible magnets are manufactured by the process of extrusion or by calendaring. Extrusion is the process wherein heated slurry of magnetic material and binder is squeezed through a shaped die, and then magnetized after cooling. The slurry can also be calendared and compressed between rollers to form a sheet, cut to desired width and magnetized. Sheets of flexible magnets are available in the form of rolls of width 24 in. with varying thickness of 0.01 in. to 0.063 in. In general flexible bonded magnets are available up to thickness of 0.375 in. Such magnets are magnetized on one face with multiple poles. The number of magnetic poles per inch which varies from 2 to 60 [FLEXDEX, 1998][5] is directly proportional to the holding force of the magnet where as it is inversely proportional to the reach of magnetic flux. A 30 mil (mili-inch) "SafeMag"[6] flexible ferrite magnetic sheet manufactured by Arnold Magnetic Technologies with

[4] Bonded Magnets – abbreviated product list. Arnold engineering company, [online], 2004, www.arnoldmagnetics.com/products/pdf/bonded_list.pdf (Accessed: 18 June 2004)

[5] Flexible Sheet Magnet Material. Dexter Magnetic Technologies, [online], 1998, www.dextermag.com/Page90.aspx (Accessed: 13 June 2004)

[6] "Safemag" - Backcoated flexible magnetic sheet. Flexmag Industries (Arnold Engineering Company), [online], 2004, www.arnoldmagnetics.com/products/flexible/pdf/flexmag_safemag.pdf (Accessed: 18 June 2004).

maximum energy product of 0.78 MGOe is capable of holding 85 lb/ft^2. High energy bonded flexible ferrite magnets have holding force as high as 150 lb/ft^2 to 190 lb/ft^2. The rare earth flexible magnets are more than 10 times stronger than ferrite flexible magnets.

Bonded flexible ferrite magnets, like ferrite magnets, degrade linearly with increase in temperature. Magnets with binder like polyethylene or nitrile rubber perform well up to temperatures in the range of 120°C. Higher temperatures may result in dimensional change accompanied with loss in flexibility. Rare earth metals being chemically reactive to the binder, above 80°C and much harder, may result in tearing of the binder matrix at such high temperatures when binder is relatively soft.

Table 3.8 shows the magnetic properties of selected flexible bonded magnets manufactured by Arnold Magnetic Technologies. It should also be noted that the maximum service temperature for the flexible magnets ranges from 80-150 °C.

TABLE 3.8

Magnetic properties of bonded flexible magnets [BOND, 2004]

Magnet Material	Binder	Magnetic Properties				
		Max Temp °C	Max. Energy Product $(BH)_{max}$	Residual Induction B_r	Coercive Force H_c	Intrinsic Coercive Force H_{ci}
			MGOe	Gauss	Oe	Oe
BaFerrite	Polyamide	125	1.9	2800	2250	3000
BaFerrite	Hypalon	80	1.2	2250	1990	3250
BaFerrite	Hypalon	80	1.4	2480	2040	3050
SrFerrite	Hypalon	80	1.8	2730	2390	3040
SmCo 8	Nylon 12	150	8.5	6100	5300	16000
NdFeB	Nylon 12	150	5.2	5200	4200	14000
NdFeB	Epoxy	120	10.0	6800	5200	9500
BaFe & Neo	Nylon 12	150	4.0	4550	3450	8200

SmCo- Samarium Cobalt, NdFeB – Neodymium Iron Boron, BaFerrite – Barium Ferrite, SrFerrite – Strontium Ferrite.

3.3.4 Rare Earth Permanent Magnets

3.3.4.1 Neodymium Iron Boron

Neodymium Iron Boron and Samarium Cobalt magnets are known as rare earth magnets as they are composed of rare earth or Lanthanide series of the periodic table. NdFeB is the most commonly produced rare earth magnet material. The maximum energy product for NdFeB permanent magnet material ranges from 24MGOe to 50 MGOe. Thus, they are strong enough to magnetize and demagnetize small sizes of Alnico and flexible material. It is very difficult to demagnetize NdFeB. Corrosive NdFeB magnets need inert coating for efficient performance. Structurally NdFeB is a very brittle and hard material. NdFeB, being susceptible to high temperatures, is not used for applications where temperature may rise beyond 150°C. It has high reverse temperature coefficient of magnetic induction causing degrading performance with increasing temperatures. Figure 3.5 shows demagnetization curves for three different varieties of NdFeB magnets. NdFeB magnets are produced by compacting the powdered alloy followed by sintering. High energy bonded flexible magnets are also manufactured using Neodymium rare earth permanent magnet material. The demagnetization curve for these magnets is a straight line as shown in Figure 3.5.

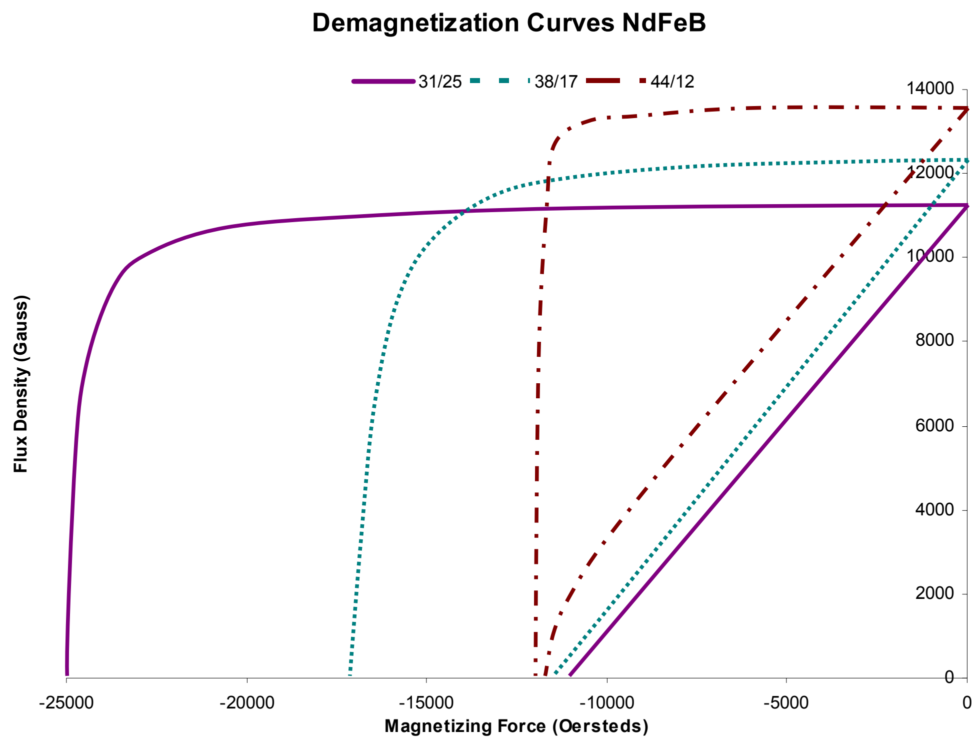

Figure 3.5: Demagnetization curve NdFeB magnet material [REFDEX, 1998]

3.3.4.2 Samarium Cobalt

The maximum energy product for Samarium Cobalt (SmCo) ranges from 16 MGOe to 30 MGOe. It is manufactured in two forms Sm_1Co_5 and Sm_2Co_{17}, where the later has higher stability and is cheaper as compared to former. It has excellent thermal stability and anti-corrosion properties. SmCo can be used in high temperature and humid environments up to 350°C. It has reasonably low reversible temperature coefficient of magnetic induction in the range of -0.035% to -0.04% per degree change in temperature [Arnold, 2004][7] as seen in Table 3.10. Thus, reversible losses are less with increase in temperature. SmCo is expensive as compared to NdFeB magnets. Figure 3.6 shows demagnetization curves for different grades of SmCo magnets. Table 3.9 and Table 3.10

[7] Arnold magnetics – permanent magnets. Arnold Engineering Company, [onlilne], www.arnoldmagnetics.com/products/samarium/index.htm (Accessed: 13 June 2004)

summarize the physical and thermal properties of the rare earth magnets. Table 3.11 shows the physical and chemical composition of both the types of rare earth magnets.

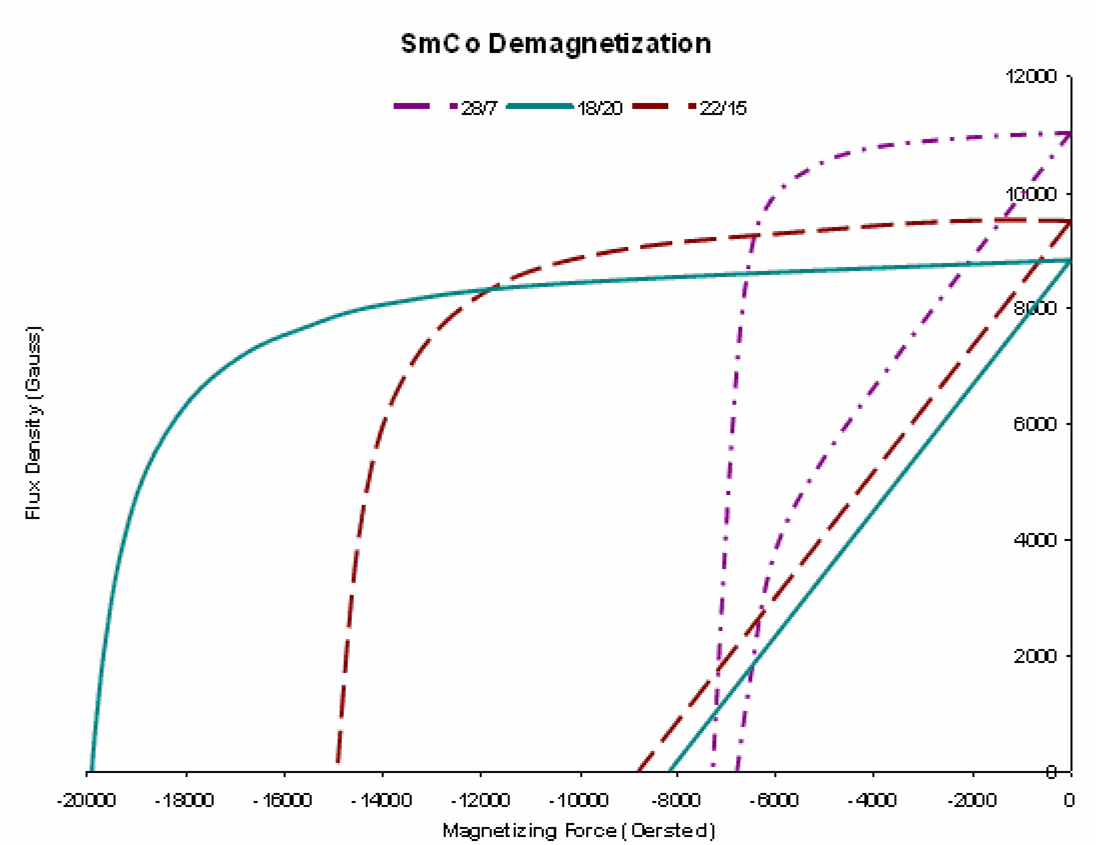

Figure 3.6: Demagnetization curve SmCo magnet material [REFDEX, 1998]

TABLE 3.9

Physical properties of rare earth permanent magnet materials [MMPA 0100-00]

Material	**Density lbs/in^3**	**Tensile strength ksi**	**Transverse Modulus of Rupture Ksi**	**Coefficient of Thermal Expansion 10^{-6} per °C**	**Electrical Resistivity Ohm-cm x 10^{-4} at 20 °C**
1-5 SmCo	0.303	6	23 x 10^6	13	53
2-17 SmCo	0.303	5	17 x 10^6	11	86
NdFeB	0.267	12	22 x 10^6	4.8	160

TABLE 3.10

Thermal properties of rare earth permanent magnet materials [MMPA 0100-00]

Material	Reversible Temperature Coefficient % Change per ˚C Near Residual Induction (B_r)	Curie Temperature ˚C	Max. Service Temperature ˚C
1-5 SmCo	-0.04	750	300
2-17 SmCo	-0.035	825	350
NdFeB	-0.090	310	150

TABLE 3.11

MMPA Magnetic properties and chemical composition of rare earth magnets [MMPA 0100-00]

MMPA Brief Designation	Chemical Composition	Magnetic Properties			
		Max. Energy Product $(BH)_{max}$	Residual Induction B_r	Coercive Force H_c	Intrinsic Coercive Force H_{ci}
		MGOe	Gauss	Oe	Oe
16/19	$RECo_5$	16	8300	7500	19000
18/30	$RECo_5$	18	8700	8500	30000
20/16	$RECo_5$	20	9000	8500	16000
20/30	$RECo_5$	20	9000	8800	30000
22/16	$RECo_5$	22	9500	9000	16000
RE (Rare Earth Elements) = Sm (Samarium) for 16/19 and 18/30, Sm or Pr (Praseodymium) for rest; Co - Cobalt					
24/7	RE_2TM_{17}	24	10000	6000	7000
24/26	RE_2TM_{17}	24	10000	9300	26000
26/10	RE_2TM_{17}	26	10500	9000	10000
26/26	RE_2TM_{17}	26	10700	9750	26000
28/7	RE_2TM_{17}	28	10900	6500	7000
28/26	RE_2TM_{17}	28	11000	10300	26000
30/24	RE_2TM_{17}	30	11600	10600	24000
RE (Rare Earth Elements) = Sm; TM (Transition Metal) = Fe (Iron), Cu (Copper), Co, Zr (Zirconium), Hf (Hafnium)					
24/41	$RE_2TM_{14}B$	24	10000	9600	41000
26/32	$RE_2TM_{14}B$	26	10500	10090	31500
28/32	$RE_2TM_{14}B$	28	10730	10490	31500
30/27	$RE_2TM_{14}B$	30	11300	10800	16000
32/31	$RE_2TM_{14}B$	32	11600	11100	31000
36/26	$RE_2TM_{14}B$	36	12200	11700	26000
38/23	$RE_2TM_{14}B$	38	12400	12000	23000
42/15	$RE_2TM_{14}B$	42	13100	12700	15000
44/15	$RE_2TM_{14}B$	44	13500	13000	15000
50/11	$RE_2TM_{14}B$	50	14100	10300	11000
RE (Rare Earth Elements) =Nd (Neodymium), Pr, Dy (Dysprosium); TM (Transition Metal) = Fe, Co					

3.4 Effect of Size on Magnetic Flux Density and Magnetic Force

Permanent magnets are available in any shape over a wide range of sizes including the standard shapes such as disc, cylinder, cube, plate and ring. A range of available sizes is tabulated in Table 3.12. Also they are available in variety of magnetic orientation depending on their preferred direction (direction in which maximum magnetic strength can be achieved) of magnetization. The proposed magnetic dampers will be installed in the buildings and hence it is very important to learn the effects of strong static magnetic field on its occupants i.e. humans. It is very important to understand the flux densities produced by different magnetic materials and its variation with distance so as to know the exposure level of the occupants. This section discusses the variation of flux density for disc and rectangular shaped ceramic magnets.

TABLE 3.12

Maximum and minimum sizes of rare earth magnets

Ring Magnet	Outer Dia (mm)	Inner Dia (mm)	Thickness (mm)
Maximum	200	180	50
Minimum	2.6	1.8	0.5
Block Magnet	Length (mm)	Width (mm)	Thickness (mm)
Maximum	200	80	50
Minimum	2.0	1.5	0.5
Disc Magnet	Diameter (mm)	Thickness (mm)	-
Maximum	200	50	-
Minimum	1.2	0.5	-

The following relationships derived from Biot-Savart law, are used to calculate magnetic flux density along the axis of a given cylinder/disc shaped shape permanent magnet.

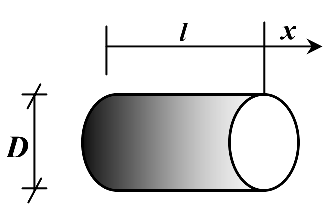

l – Length /thickness of cylinder/disc shaped magnets

x **-** Distance along the centroidal axis from the free surface of magnet

D **–** Diameter

$$B_x = \frac{B_r}{2}\left(\frac{(l+x)}{\sqrt{(D/2)^2+(l+x)^2}} - \frac{x}{\sqrt{(D/2)^2+x^2}}\right) \qquad 3.1$$

where, B_x - Magnetic flux density at distance x in. (Gauss)

B_r – Residual flux density at distance (Gauss)

The above equation is true for magnetic materials having straight line demagnetization curve (e.g. ceramic and rare earth magnets) [DESIGN, 2000].

For a ceramic magnet with residual flux density of 3300 Gauss the effect of varying diameter of disc magnet keeping thickness on the magnetic flux density at various distances along the centerline of the disc are shown in Figure 3.7. Figure 3.8 shows the effect of varying thickness of disc magnet, keeping the diameter constant, on the magnetic flux density at various distances along the centerline of the disc.

As shown in Figure 3.7, it is observed that adding material in the direction normal to the direction of magnetization (i.e. increasing the diameter) increases the flux density up to certain limit and then further adding results in a decrease of magnetic flux density. However, increasing thickness causes a huge increase in flux density but as the shape of disc magnet starts approaching a cylinder like configuration this increase more or less ceases. Also the magnetic flux density decreases sharply with distance which is clear from Figure 3.7. Equation 3.1 can also be applied to steel plate backed magnets by substituting 2 ℓ instead of ℓ [DESIGN, 2000]. For such a configuration, the same pattern is observed except that the magnitude has increased as compared to that of the magnet alone. The value of flux density at 3 in. was found to be as low as 50-10% of the residual flux density. For the strongest available rare earth magnet with residual flux density of about

1400 mT the value of flux density decreases to 0.1 mT at a distance of 2 ft from the surface of the disc magnet of size 3 in. diameter and 1 in. thickness.

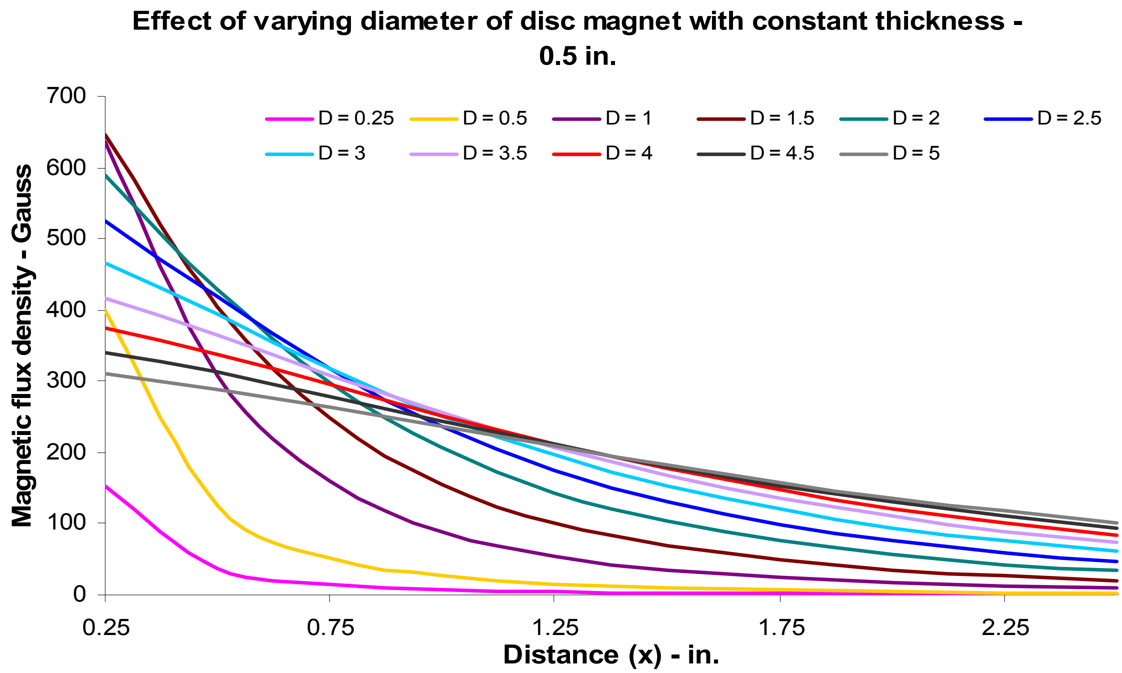

(a)

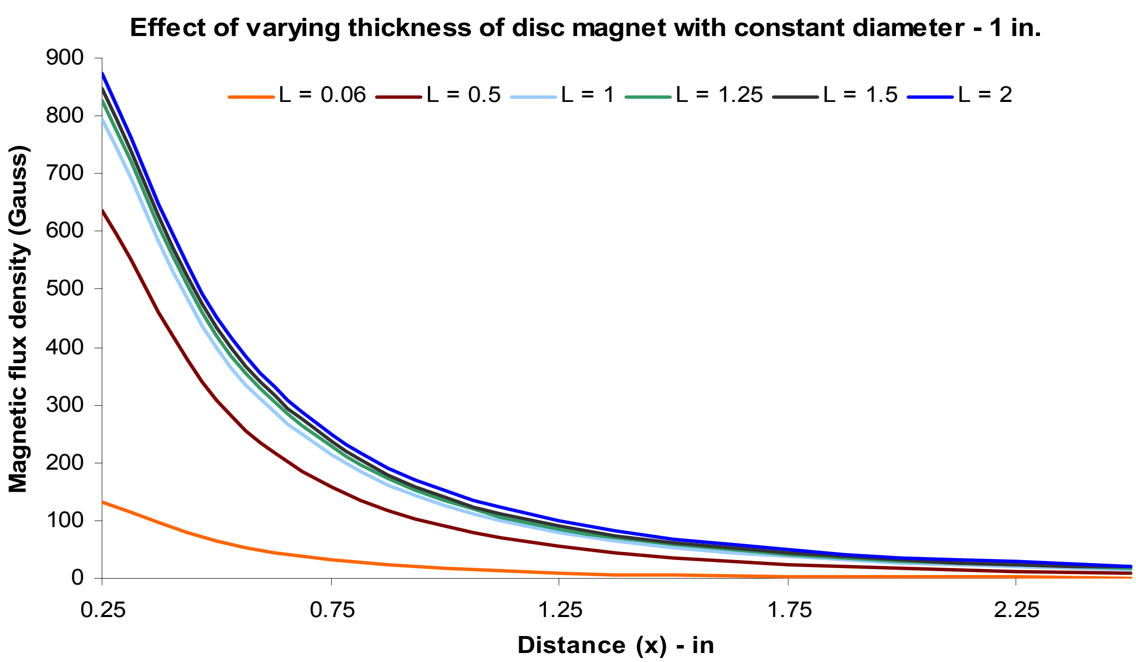

(b)

Figure 3.7: (a) Effect of varying diameter of a ceramic (3300 Gauss) of disc magnet 0.5 in. thick

(b) Effect of varying length/thk. of a ceramic (3300 Gauss) disc magnet 1 in. diameter

The force of attraction between a magnet with straight line demagnetization curve and any ferromagnetic material can be approximated using equation 3.2.

$$F_a \approx 0.58 B_r L \sqrt{A} \quad \text{...3.2}$$

F_a – Force of attraction (lb)

B_r – Residual flux density (Gauss)

L – Length of the magnet

A – Cross-section area of magnet (pole of magnet)

Equation 3.1 can be extended to rectangular cross section with a few changes. Effects of varying the length of the rectangular magnet keeping the width and thickness constant is shown in Figure 3.8

$$\mathrm{B_x} = \frac{\mathrm{B_r}}{\pi}\left(\tan^{-1}\frac{(lw)}{\sqrt{4x^2+l^2+w^2}} - \tan^{-1}\frac{(lw)}{2(t+x)\sqrt{4(t+x)^2+l^2+w^2}}\right) \quad \text{................3.3}$$

B_x - Magnetic flux density at distance x in. (Gauss)

B_r – Residual flux density (Gauss)

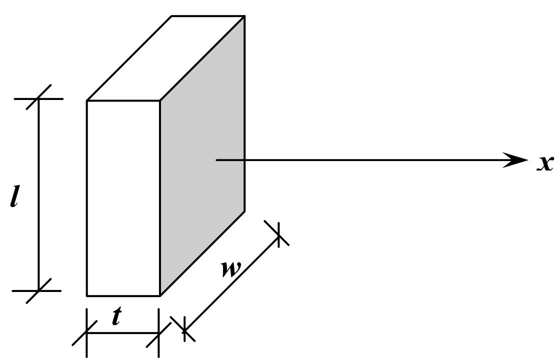

l – Length of rectangular magnet

w - Width of rectangular magnet

x - Distance along the centroidal axis for the free surface of magnet

t – Thickness in the direction of magnetization of rectangular magnet.

As shown in Figure 3.8 (a) almost the same type of behavior was found for rectangular magnets magnetized in the direction of the thickness (t). In spite of increasing area/volume, the flux density decreases when the width of the magnet is increased where as a tremendous increase in magnetic flux density is found as the thickness is increased for the same dimensions as shown in Figure 3.8 (b). Increasing width, keeping the other two parameters constant causes a decrease in magnetic flux density, the same is the case when length is increased as shown in Figure 3.8 (a).

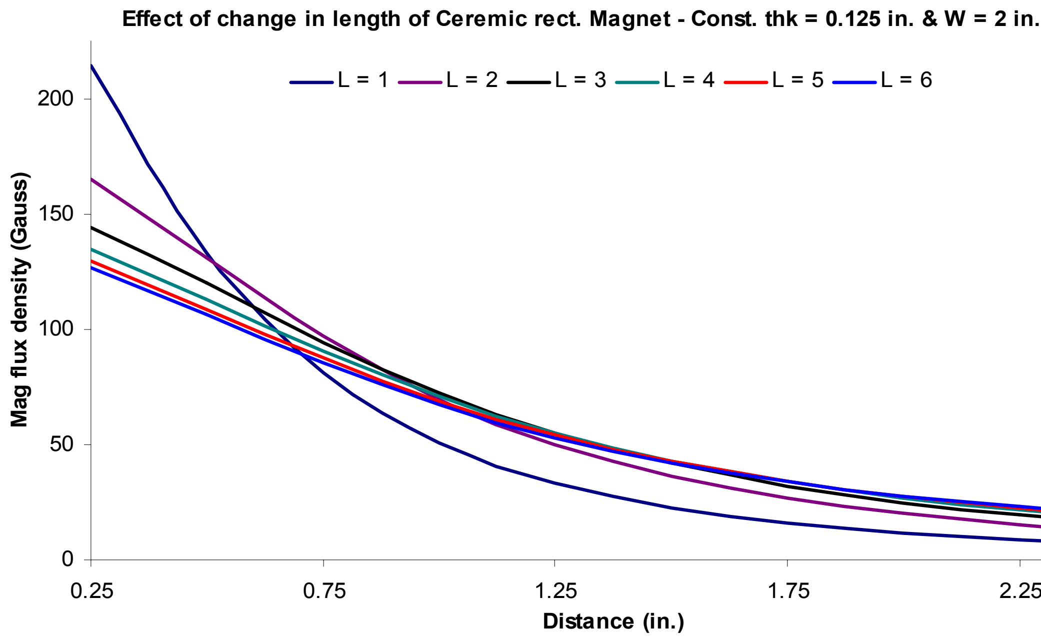

(a)

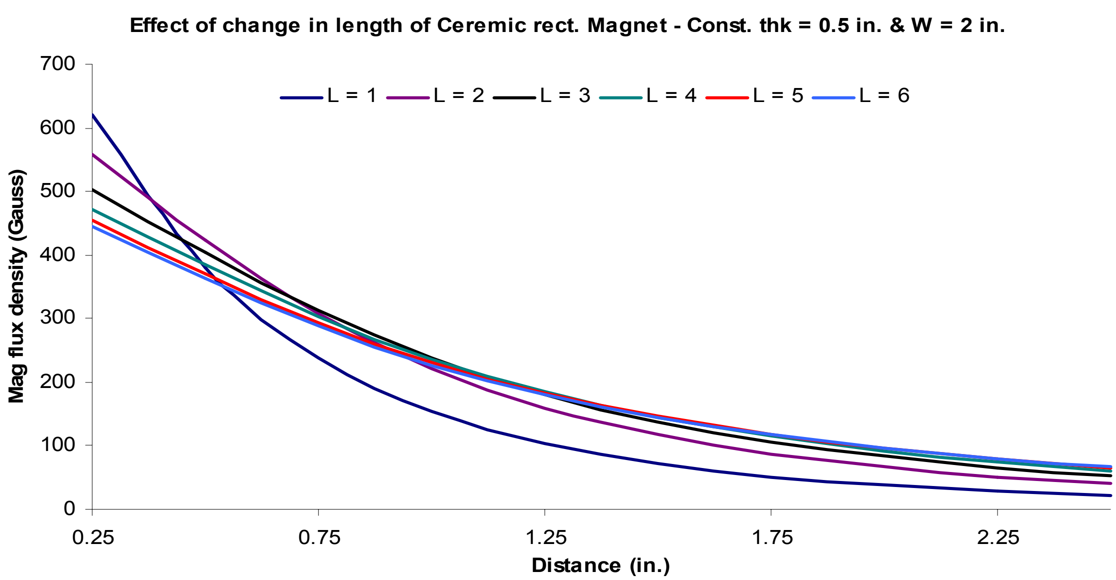

(b)

Figure 3.8: Effect of varying dimensional parameters on rectangular ceramic magnets

Chapter 4

Effects of Static Magnetic Field on Humans

4.1 General

The objective of this study is to find the effects of strong permanent magnets on human beings. Biological systems such as human cells exhibit diamagnetic properties and hence experiences magnetic force when exposed to static magnetic field. Studies indicate that ‘unlike’ the electric field, the magnetic field cannot be shielded using insulators and hence, is capable of penetrating almost all common materials [John, 2004]. Unlike the effect of certain bacteria, viruses or carcinogens on the human body, magnetic fields do not directly affect biological systems, but they may create a condition that may hinder its functioning. Unit used for flux density is Tesla (T) or Gauss (G), where 1 T = 10000 G. Magnetic field strength is measured in the units of Oersted (Oe).

4.2 Effects of Static Magnetic Field on Humans

All humans are exposed to the Earth's magnetic field ranging from 0.03-0.07 miliTesla (mT). Also exposure to static magnetic field of about 0.02 mT produced by direct current carrying power lines is common [John, 2004]. Static magnetic fields induced by Magnetic Resonance Imaging (MRI) ranges from 400-2500 mT. This may be the highest exposure level experienced by common man. The residual magnetic flux density B_r, achieved only at zero air-gap, of the flexible magnets to be used may vary from 170-700 mT and magnetic intensity varies from 2400-6000 Oe which is *equivalent*[1] to 240-600 mT. For all other permanent magnets, the residual flux density varies from 230-1400 mT. It was found that magnetic flux density of permanent magnets decreases by 1-5% of B_r near the source and 50-90% of B_r at about 3 in. away from the source. The above variation depends on the size of the magnet. The presence of multiple poles in flexible magnetic sheet limits the reach of magnetic flux within a very short distance. The physical and biological effects of static magnetic fields of varying strength are as follows:

Physical Effects

- People with metallic tooth fillings may experience strange taste sensation when exposed to fields of 1500 mT [Myers, 2004].
- Bundinger (1985) and Saunder (1984) studied the effect of static magnetic field on the workers in nuclear physics laboratories. No detrimental effects were observed on the health of the workers when exposed to 2000 mT for a few hours and 500 mT for long period.
- Arms exposed to 10000 mT field experiences cold, pain in bones, and a sensation of ants crawling on skin [Myers, 2004].
- Metallic devices such as pins or rods embedded in human bodies may prove to be detrimental when exposed to strong magnetic fields.
- Working of sensitive equipment like cardiac pacemakers may be influenced by magnetic fields. It was concluded by Pavlicek et al. (1983) that cardiac pacemakers shifted to asynchronous mode when exposed to magnetic field greater than 1.7 mT and hence individuals bearing cardiac pacemakers should not be exposed to the field beyond this strength. American Conference of Governmental Industrial Hygienists

[1] Magnetic field intensity and flux density can be considered equal when exposure of non-ferromagnetic material to static magnetic field is studied [John, 2004].

(ACGIH) recommends exposure restriction of 0.5 mT to be imposed for persons with pacemakers [John, 2004].

Biological Effects

- Red blood cells and retinal tissues react to external magnetic field without any detrimental effects [Env-health, 1987].
- Budinger (1981) showed that enzymatic reactions are affected by strong magnetic fields such as 20000 mT.
- Studies conducted by Chandra and Stefani (1979), Bellossi and Toujas (1982) and, Tenforde and Shifrine (1984) showed that static magnetic fields up to 1150 mT do not have any consistent effects on tumor and cell growth.
- Reduction in growth rate of tumor cells exposed to 7000 mT for 64 hours was observed by Raylman et al. (1996). Schiffer et al. (2003) observed no effect on human cell growth when exposed to static magnetic field of 1500 mT and 7050 mT for durations varying from 2 hr to 24 hr. Wiskirchen et al. (2000) also showed that repetitive magnetic field exposure do not affect cell growth.
- Magnetic field interacts with blood flow and periodic movement of the chest and heart. Blood flow in the presence of high magnetic field may induce potential across the blood vessels. It is evident that a magnetic field of 2500 mT is capable of producing the potential of 40mV which may depolarize cardiac muscles [GUIDELINES, 2002][2].
- Unlike carcinogens and radioactive radiations static magnetic fields do not cause any alteration in DNA structure [Env-health, 1987].

[2] "Guidelines on exposure to electro magnetic fields from magnetic resonance clinical system – safety code 26 (continued)". (Consumer and Clinical Radiation Protection), [online] May 9 2002, http://www.hc-sc.gc.ca/hecs- sesc/ccrpb/publication/87ehd127/chapter4.htm (Accessed: May 19 2004)

- Except for the cells stimulated to divide, human immune system cells when exposed to 10 T field did not show any loss/death [John, 2004].
- Haugsdal et al. (2001) showed that production of human melatonin hormone (which prevents cancer) was unaffected when the specimens were exposed to 2-7 mT static fields.
- Mur et al. (1998) concluded that the fertility of male workers of aluminium industry was not affected by static magnetic field ranging from 4–30 mT.
- No consistent evidences, for decrease in fertility, cause of birth defects or increase in miscarriage rates for MRI operators exposed to static magnetic field, were found [John, 2004].

4.3 Recommended Exposure Guidelines

- Guidelines published by US Lawrence Livemore National Laboratory suggest that the peak exposure should be limited to 2000mT of static magnetic field. Daily exposure limits are set to 0.06 T [Env-health, 1987].
- It was concluded that no health hazard was posed on the human body for exposure to static magnetic field density of 2000 mT for a short period of time [Env-health, 1987].
- US Department of energy recommends that full time (8 hour) exposure of whole body and hands should be limited to 0.01 mT and 0.1 mT respectively. Furthermore, body and hand exposure should be limited to 0.1 mT and 1 mT only for short duration of 1 hour [Env-health, 1987].
- National Radiation Protection Board (NRPB-UK) recommends the occupational exposure limit of 200 mT with peak exposure limited to 2000 mT. A higher limit of

5000 mT has been recommended for limbs. General exposure limit of 40 mT is also recommended [Review-NRPB, 2004][3].

- American Conference of Governmental Industrial Hygienists (ACGIH) recommends a limit of 60 mT and 600 mT for whole body and limbs respectively [John, 2004].
- International Commission on Non-Ionizing Radiation Protection (ICNIRP) also recommends similar exposure guidelines as NRPB.

4.4 Conclusions

- Scientific data on biological effects of static magnetic fields show no detrimental effect on human cell growth and division, enzymatic reactions, blood vessels and blood flow, DNA structure, fertility, birth defects and hormonal activity for the range of magnetic flux density of permanent magnets proposed to be used.
- Magnetic friction dampers do not pose any health hazard to the occupants. Dampers with strong ceramic or rare earth magnets if installed a few feet away from general occupancy area and electronic devices may not cause any harm as the flux density rapidly decreases with the distance. The use of ferromagnetic material contends the magnetic field thus, decreasing the exposure level to the occupants. Magnetic shield alloys having very high affinity for magnetic field can be used for this purpose.
- Use of ferromagnetic material in the damper prevents flux leakage in atmosphere thus, limiting the exposure levels.
- Flexible permanent magnets cause no health hazard since the multiple pole magnetization limits the reach of the magnetic field.

---

[3] Review of scientific evidence for limiting exposure to electromagnetic field (0-300 Hz). 2004, *Documents of the NRPB,* Vol. **15** (3).

- Electronic devices can be easily affected by very weak magnetic field. For instance a color monitor may show color distortions when exposed to static magnetic field of 0.1 mT. Also loss of data may be experienced when the data storage device is exposed to a moving magnetic field.
- Thus, exposure to varying magnetic field is more detrimental to humans as well as electronic devices like computers when compared to static magnetic field.

Chapter 5

Finite Element Analysis

5.1 General

Finite element analysis of the permanent magnet friction device incorporated in a light-frame wood structure was carried out to understand its behavior when subjected to seismic excitation. Further the effect of varying device modeling and loading parameters on the behavior of the wood frame was studied. Finally, the response of the light-frame with sliding walls was compared to those without such devices to assess the effectiveness of such devices in light-frame wood structures.

Three distinct finite element models of a typical two story wood shear wall structure were analyzed using SAP2000. Only the lateral load resisting structural components were modeled for simplicity. Nonlinear time history analysis was performed with Nonlinear Link elements being used to imitate the sliding behavior. Detailed descriptions of the models and the analysis results are discussed in the following sections of this chapter. The meshing algorithm “WoodFrameMesh” was used to aid the generation of the models.

5.2 Finite Element Model

Finite element models of a wood shear wall structure 60 ft long and 20 ft wide, with story height of 10 ft were generated for the proposed analytical study. As shown in Figure 5.1 the two-wall model (2W) is the configuration with two shear walls per story to resist lateral load with no additional source of damping. The sliding wall/two-wall friction damper (2WFD), on the other hand, is the finite element model representing the addition of sliding walls in the two-wall model. In order to assess advantages and disadvantages of adding a

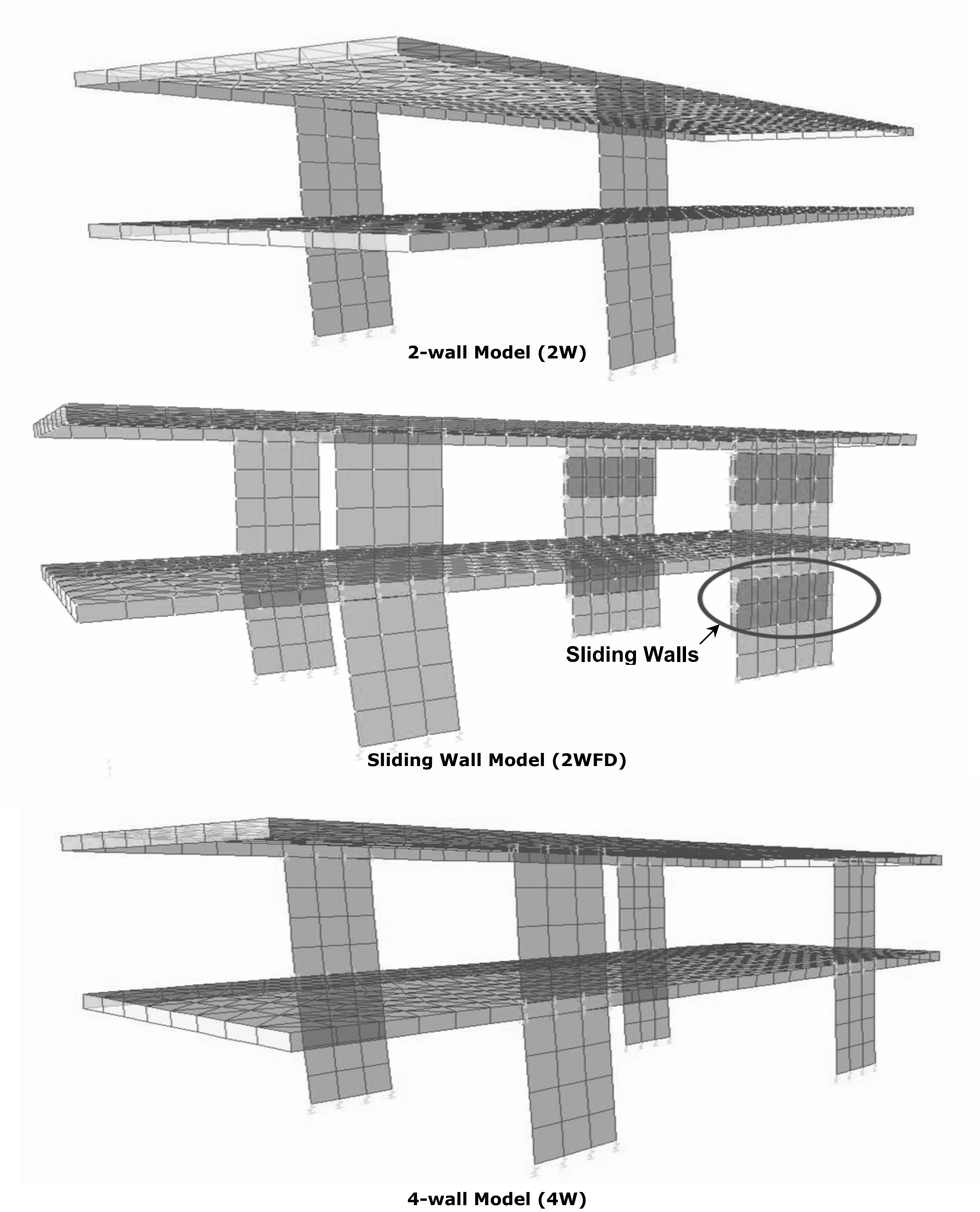

Figure 5.1: Two story wood shear wall structures (2wall, sliding wall and 4-wall models)

normal shear wall in lieu of a sliding wall, a four-wall per story model was also analyzed. Since the main aim of the study is to understand and compare the behavior of the structure with and without friction devices efforts were not made to model the shear walls with framing and sheathing elements connected by nailing connectors. If needed the nailing connections could be modeled using nonlinear link elements with typical force displacement relationship in all the three X, Y and Z directions resulting an extremely complex model. Such modeling technique accounts for the energy dissipated by hysteretic behavior of the connectors thereby representing the damping characteristics of the structure. In this study, the shear walls are modeled as vertical diaphragms and high inherent damping capacity of wood frame structures is incorporated by using a higher value of modal damping in the analysis.

The floor and roof diaphragms were modeled using thin shell elements of 1 in. membrane thickness and large bending thickness to prevent out of plane bending. A diaphragm constraint was applied to each node of the diaphragm so as to eliminate in-plane membrane deformation; it also results in reduction of the size of the eigenvalue problem. An area mass of 1.4 (lb-sec^2/ft/ft^2) and 2.95 (lb-sec^2/ft/ft^2), corresponding to system density of 7 lb/ft^3, was lumped on the top and bottom diaphragm respectively in the final configuration. The filler beam (lip) and shear walls were also modeled using thin shell elements with both bending and membrane thickness of 1 in. The thin thickness formulation was selected for shell elements as the restrained degrees of freedom and applied loading are not expected to induce any transverse shear in walls or diaphragm. It was observed that changes in bending thickness of the shell elements did not affect the analysis results whereas membrane thickness which is used to calculate lateral stiffness and the mass of the shell elements affects the response of the structure. Modulus of elasticity and shear modulus for the shell elements were taken as 1600 ksi and 666.67 ksi respectively to model the properties of wood. The diaphragm and walls were connected through lip elements using linear springs with high linear and rotational stiffness in all the three directions. The shear wall was supported on a very stiff beam element which in turn was supported by linear springs with very high stiffness in the vertical direction (global Z) and horizontal direction (global X) to emulate foundation anchors and transfer the shear force induced to ground/foundation. Figure 5.2 presents the conceptual development of finite element model.

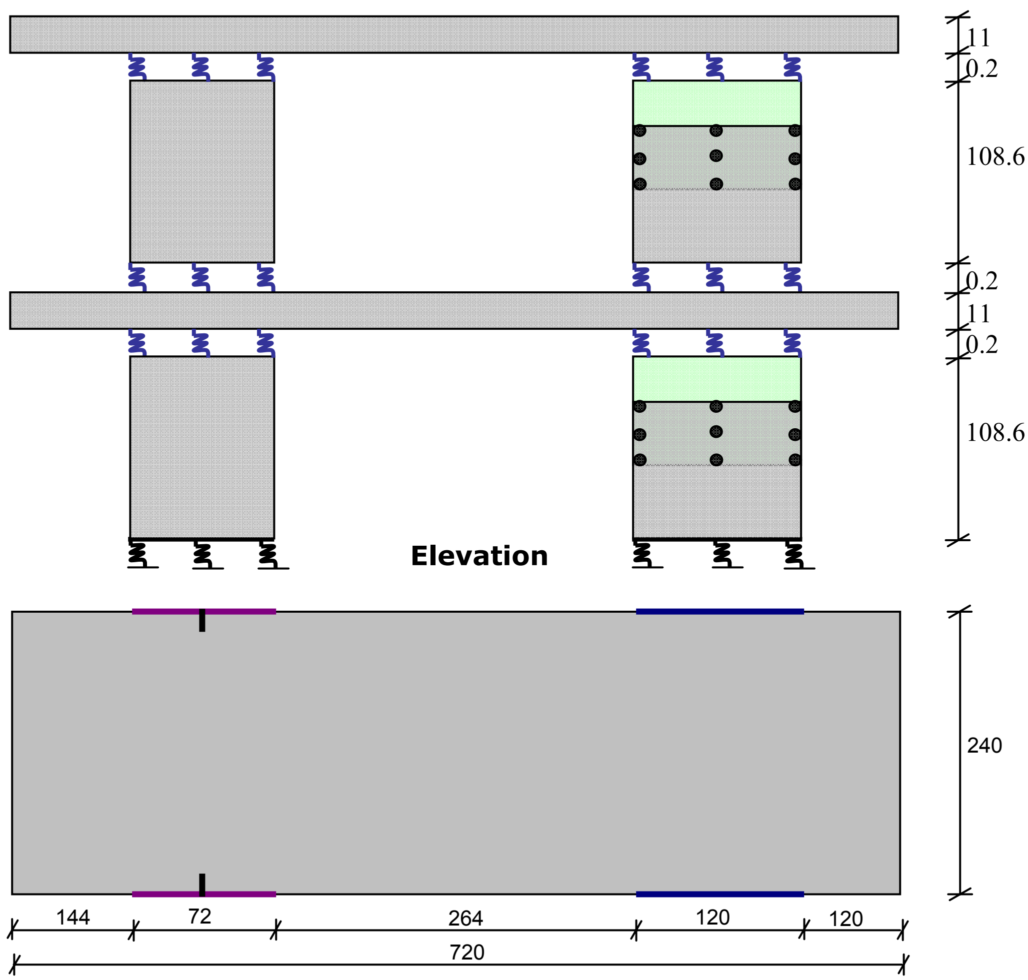

- Spring element with high linear and rotational stiffness (100000 kips/in, 100000 kip-in/rad)

- Nonlinear Link element (Uniaxial Plasticity - Wen model)

- Linear spring with high stiffness in vertical (Z) and horizontal (X) direction (100000 kips/in)

- Wood shear wall

- Sliding wall (Permanent Magnet Friction Damper)

Figure 5.2: Finite element model of wood shear wall structure with sliding walls

5.2.1 Modeling Friction Problem

5.2.1.1 Link Elements

Discrete nonlinearities in a structure can be modeled with ease using the link elements. A link element can be thought of a conglomeration of six linear and/or nonlinear springs where each spring corresponds to one of the six translational or rotational degrees of freedom. Both linear and nonlinear properties can be defined for each degree of freedom. The linear set of properties consists of linear effective stiffness and effective damping. The linear effective stiffness and effective damping are used only for linear analysis or for linear degrees of freedom in nonlinear analysis.

Nonlinear properties are generally incorporated through coupled or uncoupled force displacement relationships for each degree of freedom. This nonlinearity acts only during nonlinear analysis (such as nonlinear modal response history analysis) whereas it is ignored while performing linear analysis. Nonlinear behavior such as multilinear uniaxial elasticity, viscoelastic damping, uniaxial plasticity, multilinear uniaxial plasticity, friction pendulum behavior, biaxial plasticity, gap, hook etc. can be modeled using link elements. It is very important to be aware of the behavior of link elements and the effect of various parameters representing the behavior so as to model the problem correctly. Also, extreme care should be taken in orienting the link elements so as to interpret the results of analysis correctly.

5.2.1.2 Plastic Wen Link Elements

Friction between the steel plate and permanent magnet can be modeled using uniaxial plasticity NLlink elements with high initial elastic stiffness and a flat plastic (post yield) plateau representing slip. The slip load can be represented by fictitious yield strength of the uniaxial element. An array of nonlinear link elements based on the uniaxial plasticity model proposed by Wen (1976) was used to represent the friction surface. Figure 5.3 shows the force deformation relationship for plastic (Wen) NLlink elements.

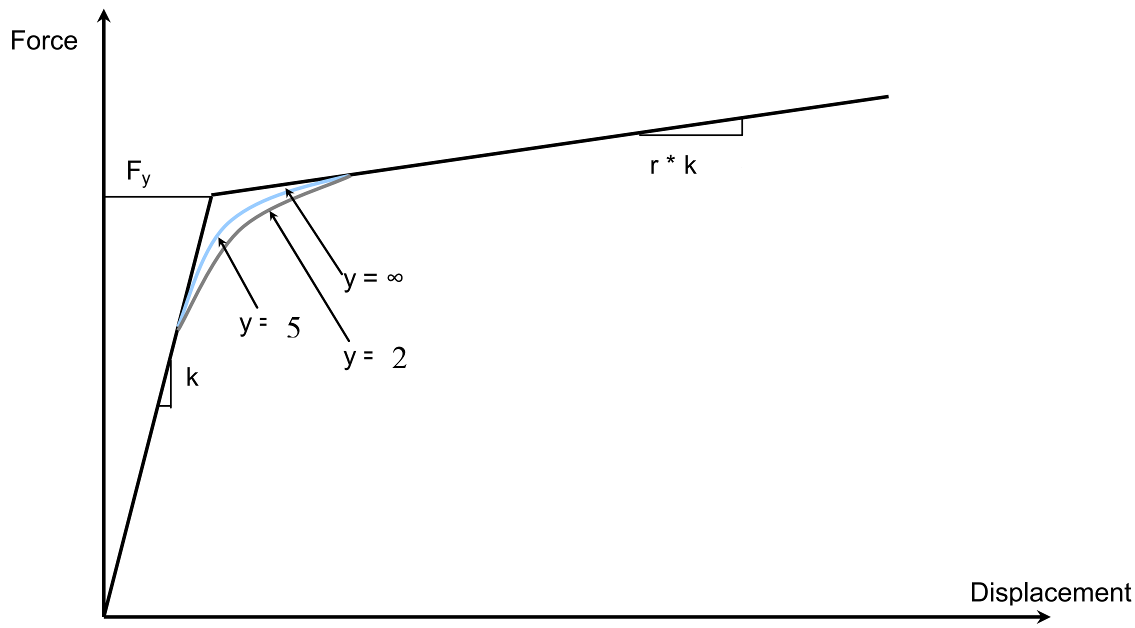

Figure 5.3: Force deformation relationship - uniaxial plasticity (Wen)

The force deformation relationship can be expressed as:

$$F = \left(\frac{k_y}{k}\right) kd + \left(1 - \frac{k_y}{k}\right) F_y Z \quad \text{.......} 5.1$$

Equation 5.1 can be simplified to,

$$F = k_y d + (1 - r)\, F_y Z \quad \text{.......} 5.2$$

Where, k = elastic stiffness, k_y = post yield stiffness, d = deformation, F_y = yield force, r = ratio of post yield stiffness (k_y) to elastic stiffness (k), Z = internal hysteretic constant.

If $|Z| \leq 1$, $|Z| = 1$ which represents yield plateau. For other values of $|Z|$:

$$\dot{Z} = \frac{k}{F_y} \begin{cases} \dot{d}\,(1 - |Z|^{y}) \text{ if } \dot{Z} > 0 \text{ else} \\ \dot{d} \end{cases} \quad \text{.......} 5.3$$

The variable 'y' represents sharpness of yielding, it varies from 1 to ∞.

All the damper link elements were grouped as corner, edge or interior elements according to their location as the mass and yield strength were varied depending on the tributary area. Only translational degrees of freedom were considered of which U2 (vertical shear) and U3 (horizontal shear) were assigned nonlinear properties whereas U1 (axial degree of freedom) was assigned high linear effective stiffness to represent force of attraction between the steel plate and flexible magnet sheet. The nonlinear properties of a typical corner link are as follows:

Mass – 2.94 x 10^{-5} kips-sec^2/in

Linear properties:

Linear effective stiffness (k_e) – 10 k/in

Effective damping – 0 lb-s/in

Location of shear surface (shear spring) from end i of the link = 0.1 in

Nonlinear Properties:

Elastic stiffness (k) – 15000 k/in

Yield strength (F_y) – 0.15 kips

Post yield stiffness ratio (r) – 1 x 10^{-7}

Yield exponent (y) - 5

The slip resistance per sliding wall was taken as 6 kips (150 lb/ft^2 slip resistance for 40 ft^2 of overlap area) thus summing up to 24 kips of slip resistance for four such walls. This slip resistance was later varied to check its effect on the behavior of the structure. It should be noted that the link element should be assigned some mass so that it participates in nonlinear dynamic analyses. Mass of the link element was calculated on the basis of mass density of plywood (5.62 x 10^{-8} kip-sec^2/in^4) 1 in. thick and steel plate 1/16 in. thick (7.345 x 10^{-7} kip-sec^2/in^4) used for both the sliding surfaces. As previously mentioned the value of elastic stiffness was taken as 15000 k/in. to represent high stiffness of the device before slip was initiated. The yield strength depends on the tributary area and strength of magnet sheet used. A very small value of post yield stiffness ratio (r) was chosen to represent perfect plastic behavior (slip) as the slip resistance was overcome. The effect of linear effective stiffness, mass of link element and yield exponent was evaluated to arrive at final values.

5.3 Nonlinear Analysis

Nonlinear dynamic analyses of the models subjected to different ground motions and loading time histories were performed using the Fast Nonlinear Analysis (FNA) method developed by Wilson. The responses were verified using direct time integration of the full equations of motion.

5.3.1 Fast Nonlinear Analysis (FNA)

Linear elastic structural systems with discrete nonlinearities (limited to link elements) can be analyzed efficiently using the FNA method. The analysis time for FNA is significantly less as compared to direct integration method with little or no compromise in the accuracy of the results, provided NLlink properties are rationally selected.

All the nonlinearity in FNA is carried over to the right hand side of the equation of motion and is treated as an unknown variable. The equilibrium equations for a system with discrete nonlinearity in the form of NLlink elements subjected to any loading can be written as [CSIREF, 2002]:

$$M\ddot{u}(t) + C\dot{u}(t) + Ku(t) + F_s(t) = F(t) \qquad 5.4$$

Where K is linear elastic stiffness matrix of structural components and linear degrees of freedom of link elements, C is proportional damping matrix, M is mass matrix and F_s is nonlinear force vector for NLlink elements. $\ddot{u}(t)$ is relative acceleration, $\dot{u}(t)$ is relative velocity and $u(t)$ relative displacement of the mass.

In some cases linear effective stiffness can be defined either to represent initial stiffness of a passive energy device or to stabilize the rigid body modes due to presence of discrete nonlinearity (such as a initially open gap). The effective stiffness is induced in the equilibrium equation by adding it on both sides of the equation which results the following equation:

$$M\ddot{u}(t) + C\dot{u}(t) + (K + k_e)u(t) = F(t) - F_s(t) + k_e u(t) \qquad 5.5$$

where k_e is linear effective stiffness of the link elements. The above equation can be solved using any of the available numerical step by step solution methods. The value of effective stiffness may vary from zero to the device stiffness in case of passive energy system. Linear effective stiffness of the NLlink element is used for modal analysis and hence affects the generated modes and fundamental time period of the structure. The fast nonlinear analysis method utilizes the generated modes after modification which theoretically negates the effect of linear effective stiffness on the analysis results. Ritz vector analysis, which uses the applied loads to generate mode shapes, was used for modal analysis. Linear effective stiffness also affects the convergence rate of nonlinear iteration hence, for all artificial large values of stiffness of nonlinear link elements (as in friction dampers) a very small value of linear effective stiffness should be chosen to avoid large numerical errors [CSIREF, 2002].

5.3.2 Nonlinear Direct – Integration Time - History Analysis

Nonlinear direct integration analysis in SAP2000 is capable of solving fully coupled equations of motion including all types of nonlinearities such as material, geometric nonlinearities etc. Solutions generated by the FNA method vary with the value selected for the linear effective stiffness (K_e) of the NLlink element. The Nonlinear Direct Integration method, being independent of K_e, was used to investigate the sensitivity of the solution to the value of K_e and thus, arrive at the correct value of K_e to be used for the FNA method. The sliding wall model with 1% modal damping was analyzed for the unmodified El Centro ground record using the Hilber-Hughes-Taylor alpha time stepping integration method. It was observed that the analysis results were very sensitive to time step size (t_s) and the value of the numerical damping parameter (α). The numerical damping parameter, used in the time stepping routine introduces artificial damping in the system which improves the rate of convergence of the solution. The value of α (alpha) can vary from 0 to -1/3. In these analyses the parameter α was varied as 0, -1/4 and -1/3 with decreasing size of time steps. Top diaphragm displacement response of friction damped two-wall structure (2WFD) with 1% modal damping subjected to El Centro ground motion is shown in Figure 5.4. The response of the structure before 2.2 sec in response history was same for all the cases representing no effect of these parameters on the elastic behavior and hence, is not presented in Figure 5.4. It was observed that alpha = 0 gives the most accurate results, whereas negative value of alpha particularly for large t_s, resulted in artificially damped response (of higher modes, as suggested by SAP reference manual) which can be observed in Figure 5.4. However, this problem was solved by using smaller size of time steps which eventually gave the same accuracy as alpha = 0. As shown the response of the friction damped structure with alpha = 0 and t_s = 0.002 sec and, alpha = 0 and t_s = 0.0002 sec is same as that of alpha = -1/4 and t_s = 0.0002 sec. Thus, t_s = 0.0002 should be used if alpha is negative and t_s = 0.002 sec should be used when alpha = 0 for the analysis of this problem. Since the solution converged rapidly for negative values of alpha as compared to alpha equals zero, the negative value for alpha resulted in faster analysis.

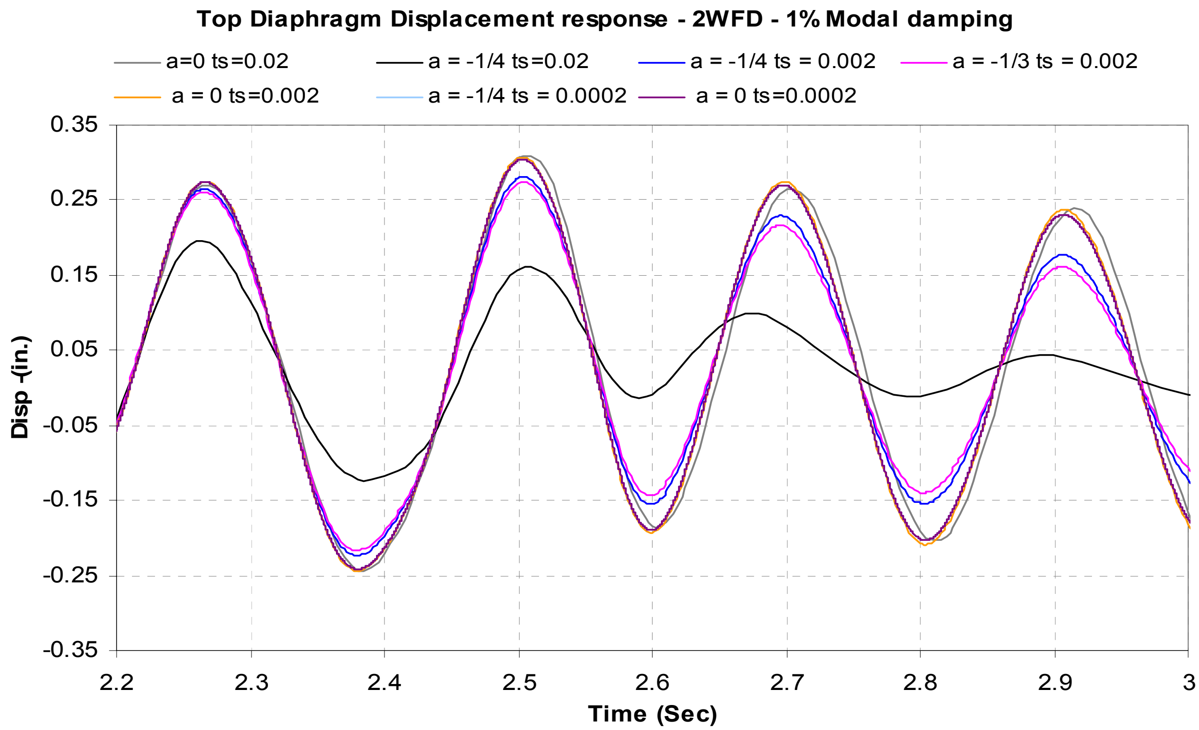

Figure 5.4: Effect of alpha (a = α) and time step size (t_s) in the nonlinear direct integration analysis (El Centro)

5.4 Acceleration Time Histories and Loading Functions Used for Analysis

The El Centro ground acceleration record from the Imperial Valley earthquake (1940) and the Northridge earthquake ground acceleration record (1994) were used for nonlinear time history analyses. These motions were linearly scaled to represent strong ground motion that can be experienced in the western United States. The displacement and pseudo acceleration response spectra for both ground motions are shown in Figure 5.5. It should be noted that the response spectra are plotted only up to 0.2 sec as the fundamental time period for the structures analyzed fall within this range.

Figure 5.6 shows a sinusoidal cyclic lateral load equally applied on the diaphragms of the structure. Note that only one cycle of 100 kip load is applied at a period of 0.1323 seconds and then the induced motion is allowed to decay to study the free vibration response of the structure. The magnitude of the load was chosen such that enough slip is achieved in the devices and the loading frequency is taken same as the fundamental time period of 2WFD structure.

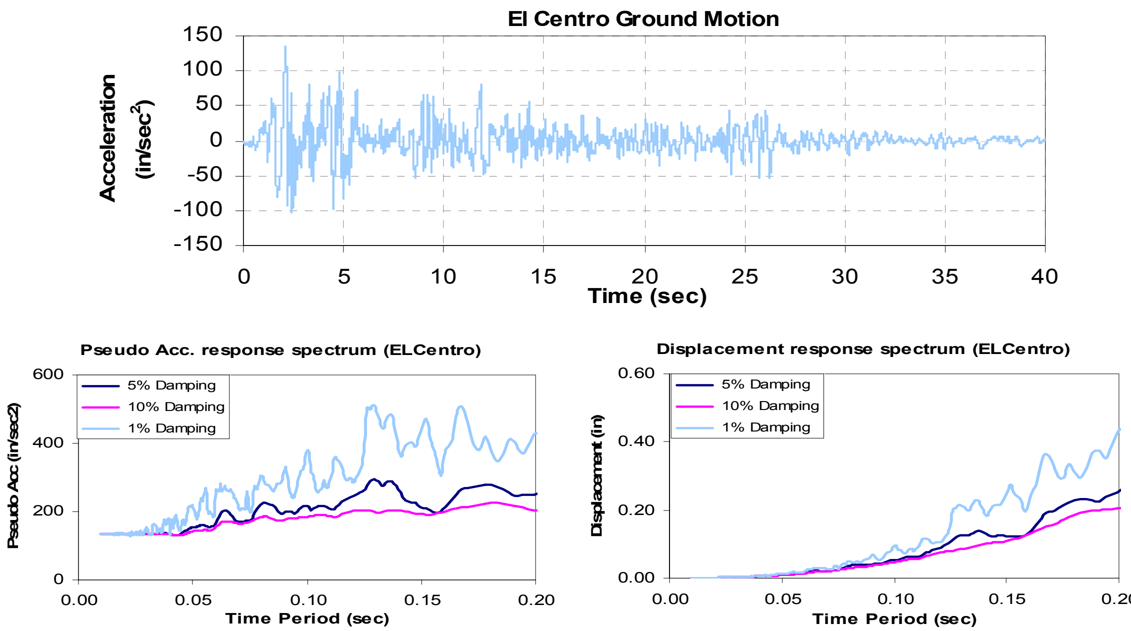

(a)

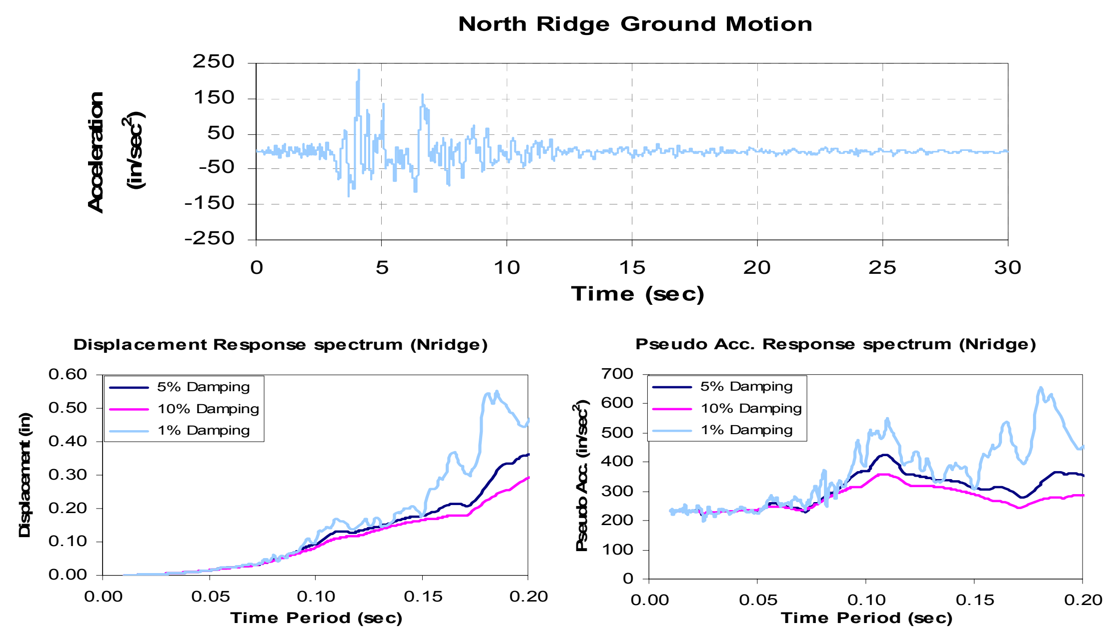

(b)

Figure 5.5: Ground acceleration record and response spectrum (a) El Centro ground motion (b) Northridge ground motion

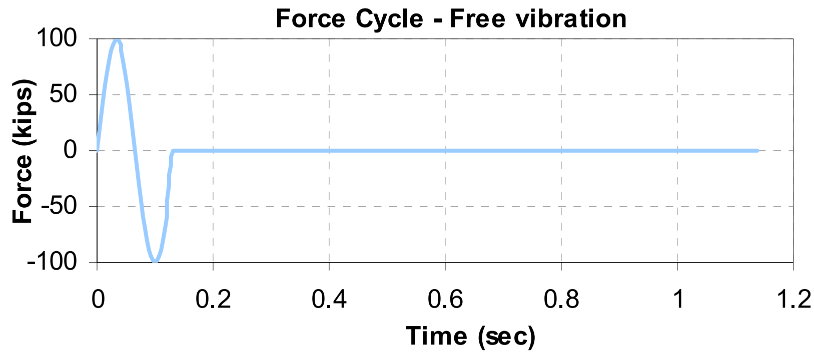

Figure 5.6: Cyclic lateral load time history

5.5 Effect of Linear Effective Stiffness of Nonlinear Link Element

The linear effective stiffness of the NLlink elements was varied over a range of 0-10000 k/in. and the results obtained by the FNA method for the 2WFD structure subjected to El Centro ground motion were compared with that given by nonlinear direct integration analysis which is independent of the value of linear effective stiffness used. A solution time step of 0.02 sec was used for the FNA method. Figure 5.7 and Figure 5.8 (a) show the displacement and base shear response of the structure. Note that the results are presented only for the time interval from 2.2 sec to 3.1 sec to show the effects on the peak response of the structure. Also the response of the structure for all the cases was almost same before 2.2 sec. A reduction in displacement and base shear response is observed as the value of effective stiffness is increased from 0 k/in. to 10000 k/in. The energy induced in the structure for all the cases was more or less same. However, a decrease in hysteretic energy was observed with an increase in linear effective stiffness indicating elastic behavior. Figure 5.8 (b) compares the energy plots for k_e = 10 k/in. with those for other values of k_e. The responses of the structure with effective stiffness of 0 k/in. and 10 k/in. are very close and match with the direct integration solution for alpha = 0 and t_s = 0.0002. Further the results were verified using smaller time step length for k_e = 0 k/in. and k_e = 10 k/in. the only effect found was a decrease in analysis time for smaller time steps. The FNA utilizes the mode shapes and time periods generated by modal analysis which uses the value of k_e to calculate the time period of the structure. Thus, the correct time period of the structures with passive devices can be known only if the value of k_e represents the stiffness of the passive energy device. In order to model the friction dampers, a large artificial value is used to represent the device stiffness before slip. For such cases, matching the value of k_e with the high device stiffness may result in the correct time period but introduces large numerical errors in the solution. Hence as discussed earlier when a large artificial value of elastic stiffness (such as for friction dampers) is used the linear effective stiffness should be taken as small as possible to avoid large numerical errors. This fact is clear from the results of the analyses presented. Thus, for all further analysis the value of linear effective stiffness (k_e) is taken as 10 k/in., keeping in mind the accuracy and time required to analyze the problem. As the name suggests, the FNA is much faster than the Non-linear direct integration method and, hence, is preferred for all the nonlinear analysis performed after here.

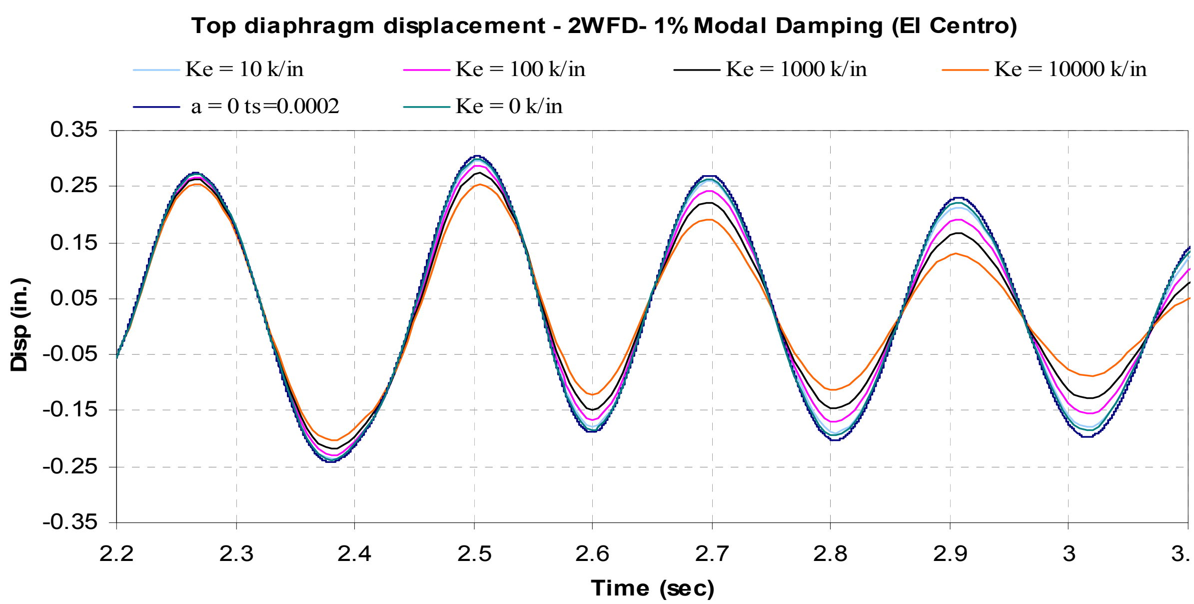

Figure 5.7: Effect of Ke – Top diaphragm displacement response 2WFD- 1% modal damping (El Centro ground motion)

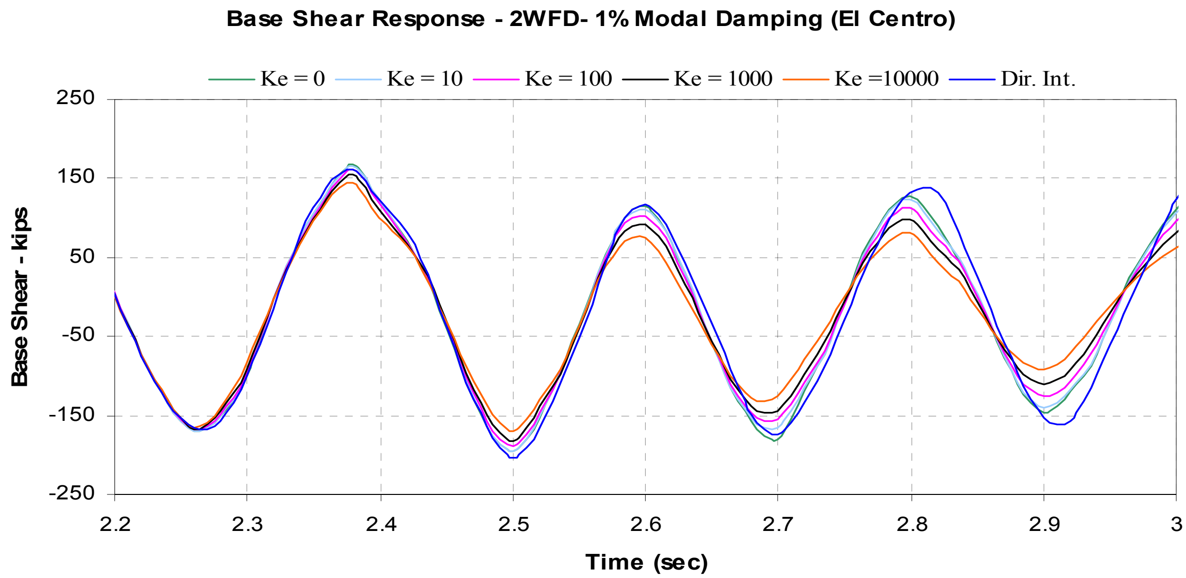

(a)

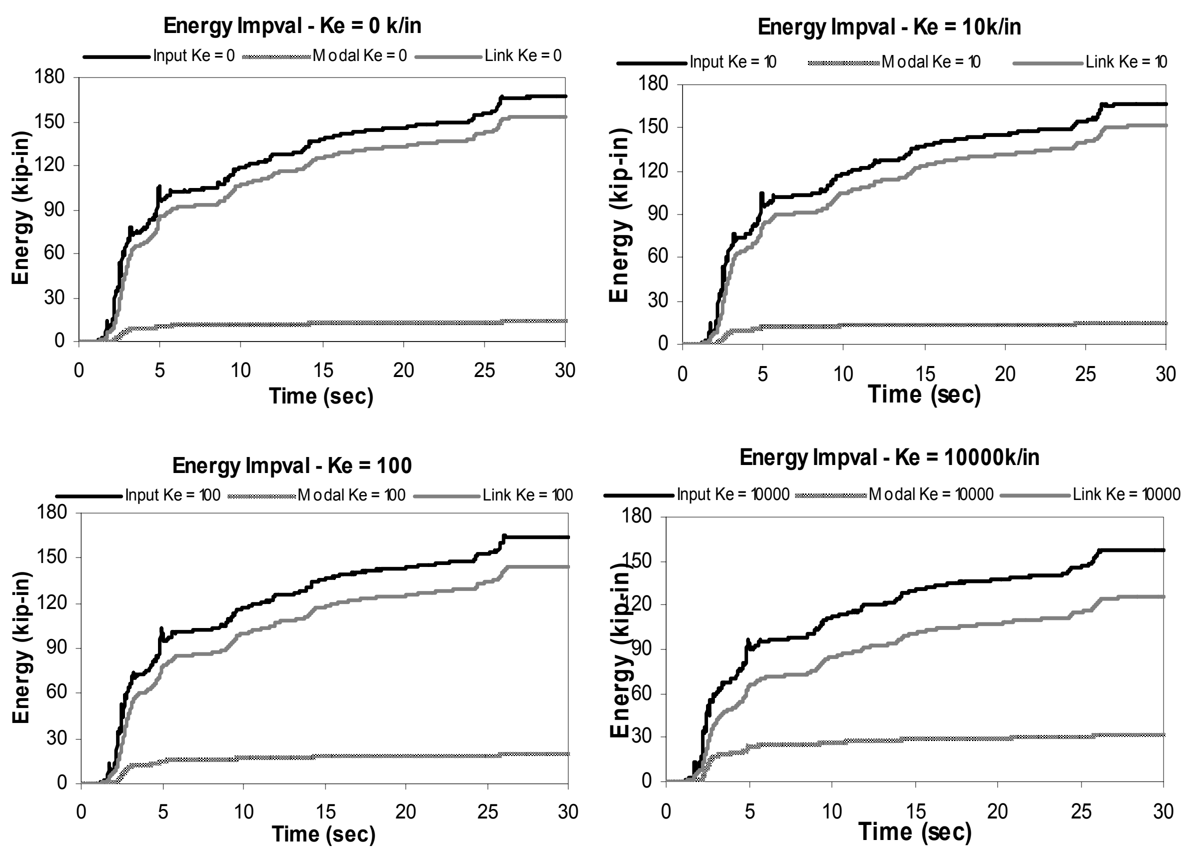

(b)

Figure 5.8: Effect of K_e – (a) Base shear response (b) Energy plots (El Centro ground motion)

5.6 Effect of Yield Exponent – Plastic Wen Elements

The yield exponent ‘y’ of Plastic Wen NLlink element is a measure of sharpness of yielding. It can vary from one to infinity; however practical limit of 20 is considered to be large enough to represent sharp yielding as in case of elastic perfect plastic behavior or the force deformation relationship for a passive energy friction device. Yield exponent was varied as 5, 10, 20, 30, and 50 for 2WFD structure. The lumped mass on the top and bottom diaphragm was taken in accordance to the structure mass density of 12 lb/cu ft. Also, linear behavior of the normal walls was assumed. It was found that the response of the structure did not significantly rely on the value of yield exponent, however the analysis time for smaller values was much less as compared to that for large value such as 50 which represents very sharp yielding. Figure 5.9 shows top diaphragm displacement response and base shear response for El Centro ground motion and 1% modal damping.

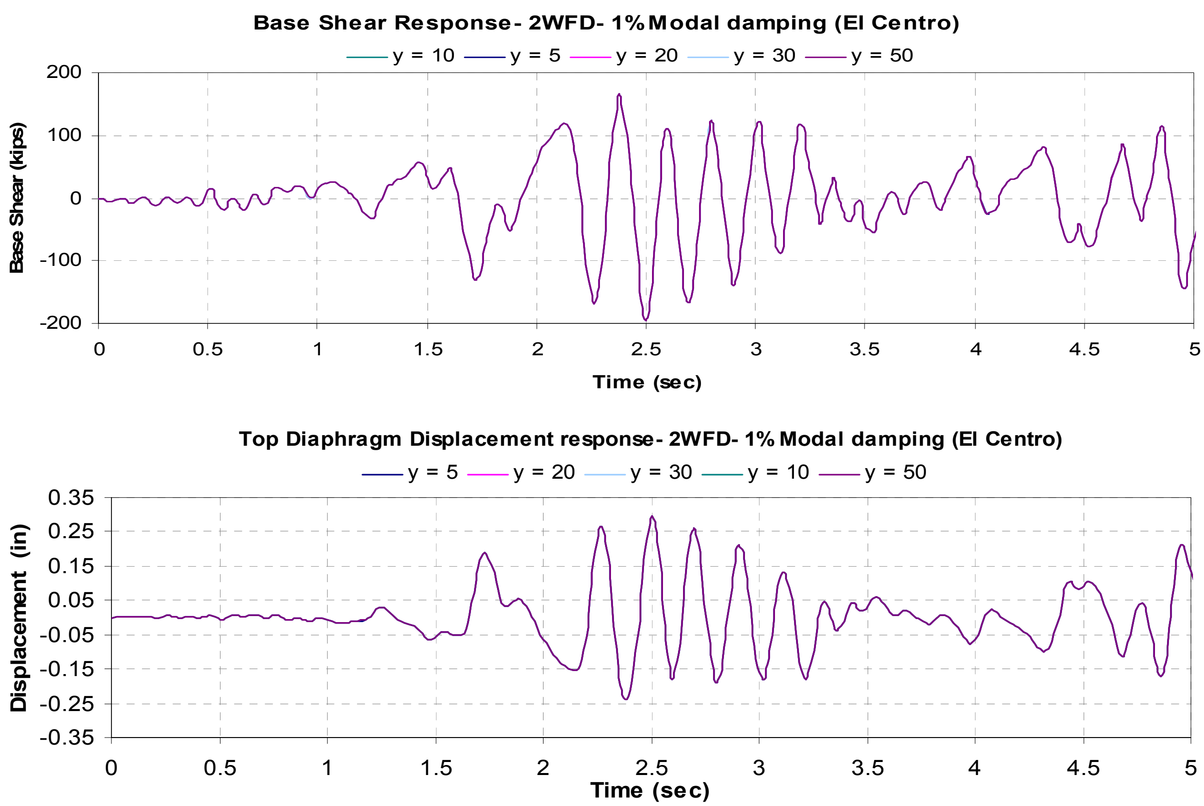

Figure 5.9: Effect of ‘*y*’ – Top diaphragm displacement and base shear response (El Centro)

5.7 Effect of Mass of the NLlink Element on the Response

The mass of the NLlink elements was varied as 0.0001 kips-sec^2/in., 0.001 kips-sec^2/in. and 0.01 kips-sec^2/in. and FNA was performed to evaluate the behavior of the structure with sliding walls (2WFD) for El Centro ground motion with 1% modal damping. As shown in Figure 5.10 higher mass aggravates the response as compared to that of a lower mass. Such behavior can be attributed to increase in time period of the structure due to addition of mass. The displacement response spectrum for El Centro ground motion clearly justifies such a response. Figure 5.11 compares the energy plots for M = 0.001 kips-sec^2/in. with those for other values of M.

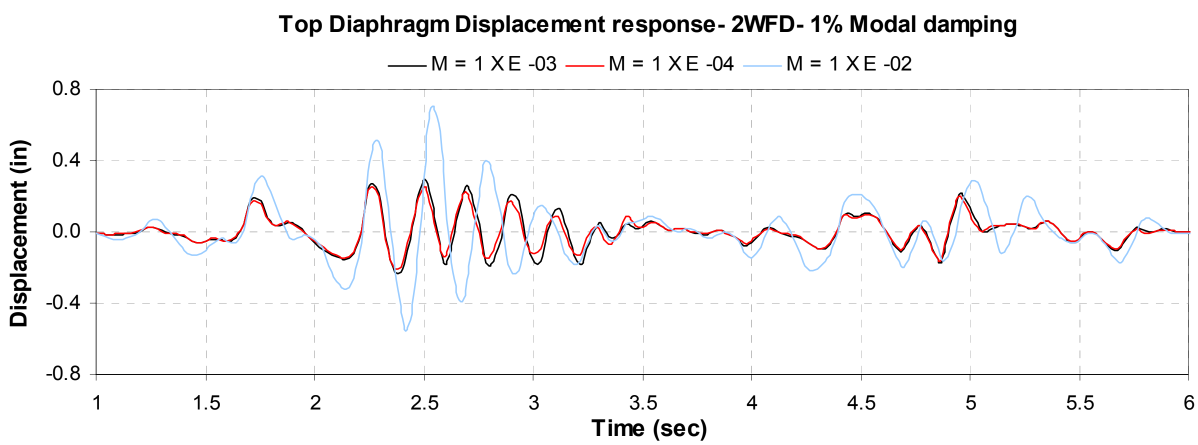

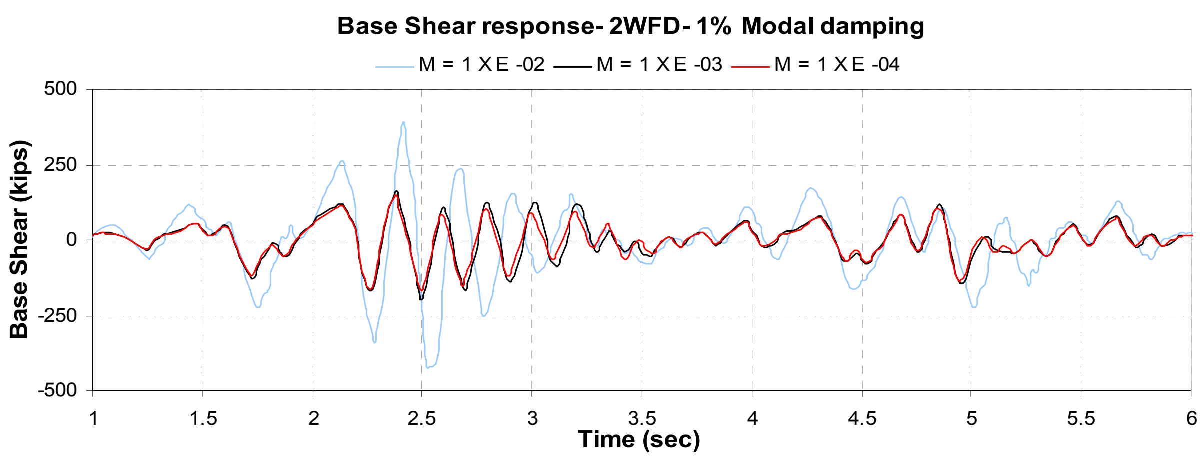

Figure 5.10: Effect of mass of NLlink element – Top Diaphragm Displacement and Base shear response (El Centro Ground motion)

It was observed that input energy for the heavier structure (M = 0.01 kips-sec^2/in.) was much greater as compared to that for the structures with mass of link element equal to 0.001 kips-sec^2/in. and 0.0001 kips-sec^2/in. Such behavior was anticipated as the base shear response for heavier structure was greater as compared to the other two structures. Thus, it can be concluded that the link element should be assigned mass corresponding to its tributary area which will be followed in the analyses after here.

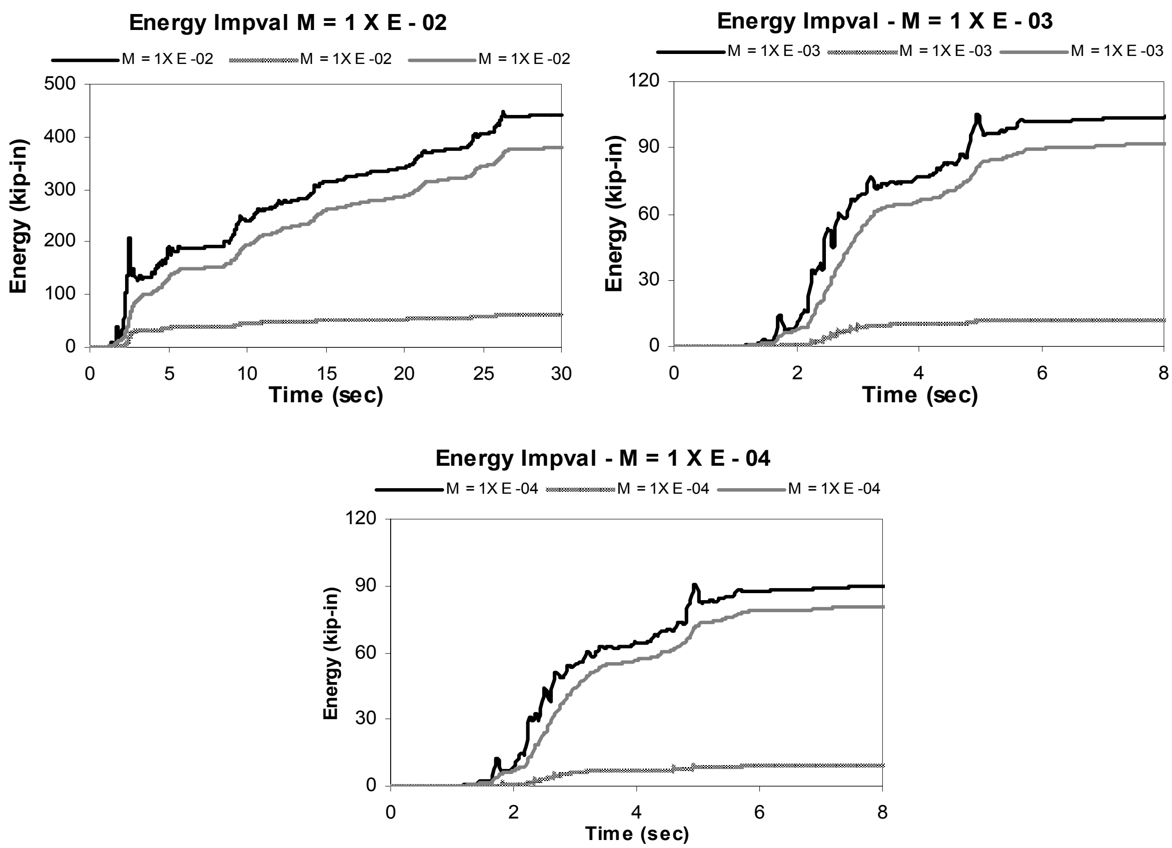

Figure 5.11: Effect of mass of NLlink element – Energy plots

The recommended NLlink properties for nonlinear analysis can be summarized as follows:

Mass – In accordance to tributary area (e.g. 2.94 x 10^{-5} kips-sec^2/in a corner link element)

Linear effective stiffness (k_e) – 10 k/in

Effective damping – 0 lb-s/in

Elastic stiffness (k) – 15000 k/in (artificial high value to represent conditions before slip)

Yield strength (F_y) – 0.15 kips (depends on the strength of the magnetic sheet)

Post yield stiffness ratio (r) – 1 x 10^{-7} (very low to represent flat post yield plateau/slip)

Yield exponent (y) – 5

Lumped mass top diaphragm - 1.4 (lb-sec^2/ft/ft^2)

Lumped mass bottom diaphragm - 2.95 (lb-sec^2/ft/ft^2)

5.8 Forced and Free Vibration Response of the Friction Damped Structure

The two-wall (2W), four-wall (4W) and sliding wall (2WFD) model were analyzed for the forced-free vibration time history. Slip resistance for these analyses was 9 kips and 3 kips per sliding wall, respectively for the bottom and top story sliding walls, which summed up to a total slip resistance of 18 kips in the bottom story and 6 kips in the top story. Note that the slip resistance for the bottom story shear walls is increased by 50 percent from the original 6 kips whereas the top shear wall slip resistance is reduced by 50 percent as compared to 6 kips. Lateral load was applied only on the top diaphragm, only on the bottom diaphragm and equally distributed on top and bottom diaphragm in three different loading cases. All the different configurations were analyzed for 1% modal damping using the FNA method. Note that linear behavior was assumed for the normal walls. Figure 5.12 (a) compares the response of 2WFD for three different loading cases depending on the position of the applied load. It was observed that the decay of vibration was linear and all the motion was damped out within four cycles of damped free vibration which is apparent from the Figure 5.12 (a). Note that the start and the end of damped free vibration of 2WFD are highlighted in all the plots of Figure 5.12. Also the response of the structure varied with the position of applied force. A decreasing trend in displacement and shear response of the structure was observed for load applied only on the top diaphragm, equal distribution of the applied load on top and bottom diaphragm and load applied only on bottom diaphragm respectively. The energy induced in the structure also followed the same trend. This can be attributed to different slip resistance experienced for each position of applied load.

The response of the structure with friction dampers (2WFD; T_1 = 0.1323 s), subjected to equal lateral load on top and bottom diaphragm, was compared to the responses of the two-wall structure (2W; T_1 = 0.158 s) and four-wall structure (4W; T_1 = 0.1105 s) with same loading position. As shown in Figure 5.12 (b) reduction in displacement response of the friction damped structure is observed as compared to the 2W structure. However, the base shear for the 2WFD was greater than that for the 4W in a few initial cycles.

It is found that base shear induced in the 2WFD structure is least throughout the response history when compared to base shear response of 2W and 4W structure, Figure 5.12 (c). It should also be noted that 4W is totally a different system and has fundamental period of vibration different than that of the friction damped and undamped two-wall structures which has the same fundamental period of vibration, prominently observed in Figure 5.13 (a). Note that the time period mentioned earlier for the 2WFD structure and 2W structure are misleading. These values are given by modal analysis which includes the value of linear effective stiffness (k_e) and hence, they do not match. However, the response of the friction damped structure is not in phase with its undamped counterpart (2W structure).

About 85% of the energy induced was dissipated by hysteretic damping due to friction in all the cases. The displacement response of the friction damped structure when compared to the undamped structure, as in Figure 5.13 (a), shows that initially the structure is damped at about 8% equivalent viscous damping which increases to 10% and

12% further in the response history. It should be noted that the friction damped structure was analyzed with 1% equivalent viscous damping. Figure 5.13 (b) denotes occurrence of slip till the motion dies out.

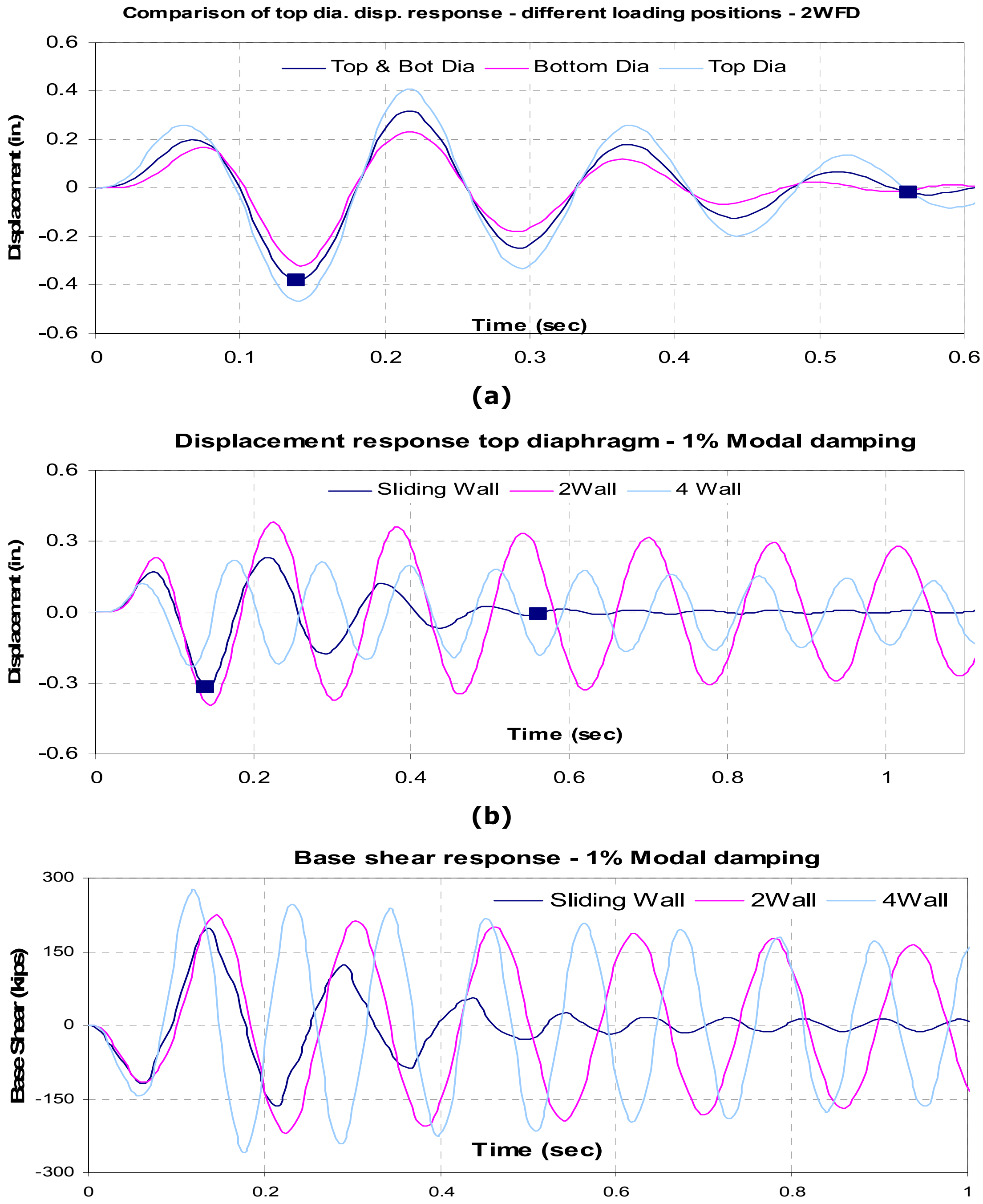

(c)

Figure 5.12: (a) Effect of loading positions: Displacement response – 2WFD 1% modal damping (b) & (c) Disp. and base Shear response – load applied equally to top and bottom diaphragm

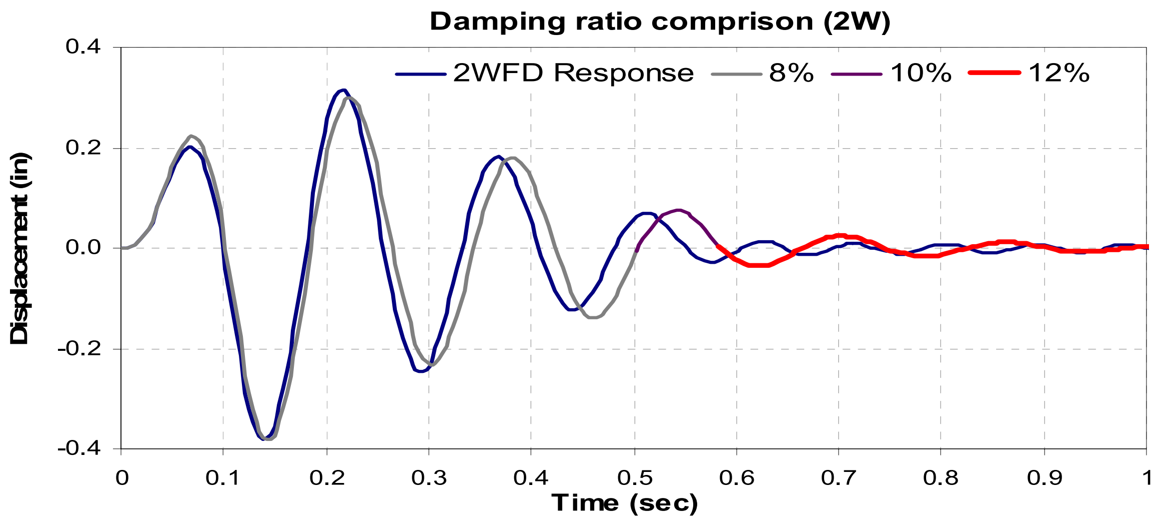

(a)

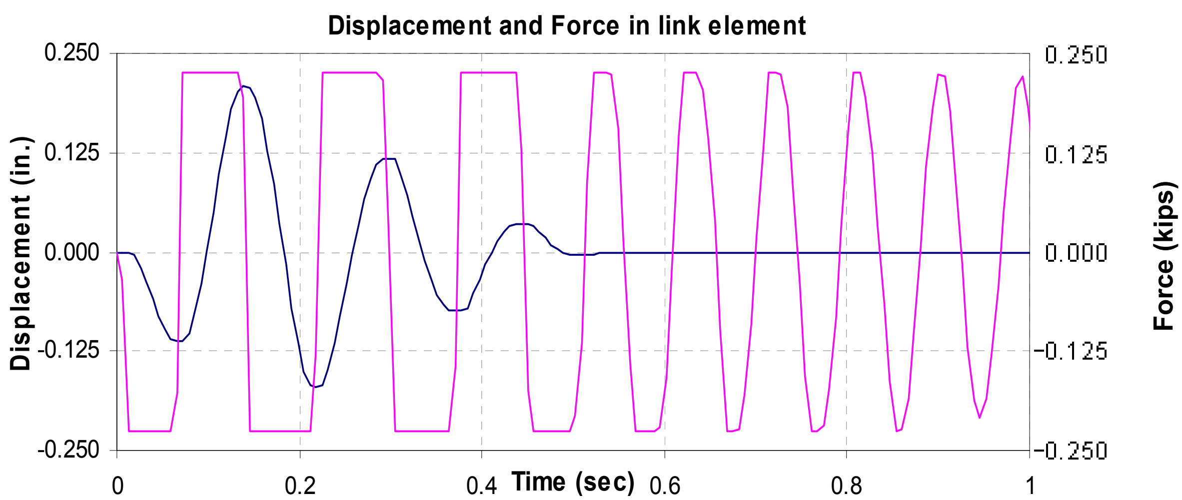

(b)

Figure 5.13: Equal lateral load to top and bottom diaphragm (a) Comparison of friction damping with equivalent viscous damping (b) Force slip response for typical corner link element

A single story model with two normal and two sliding walls with slip resistance of 18 kips was also analyzed for forced and free vibrations. Forcing functions of 36 sin (4πt) and a single load cycle of 100 sin (4πt) were used to observe the free vibration characteristics of the SDOF model. Figure 5.14 shows the friction damped free vibration response of the single degree of freedom model. As seen for each cycle, displacement peaks decrease approximately 50 % per cycle. Figure 5.15 shows the force deformation characteristics of SDOF under forced vibration.

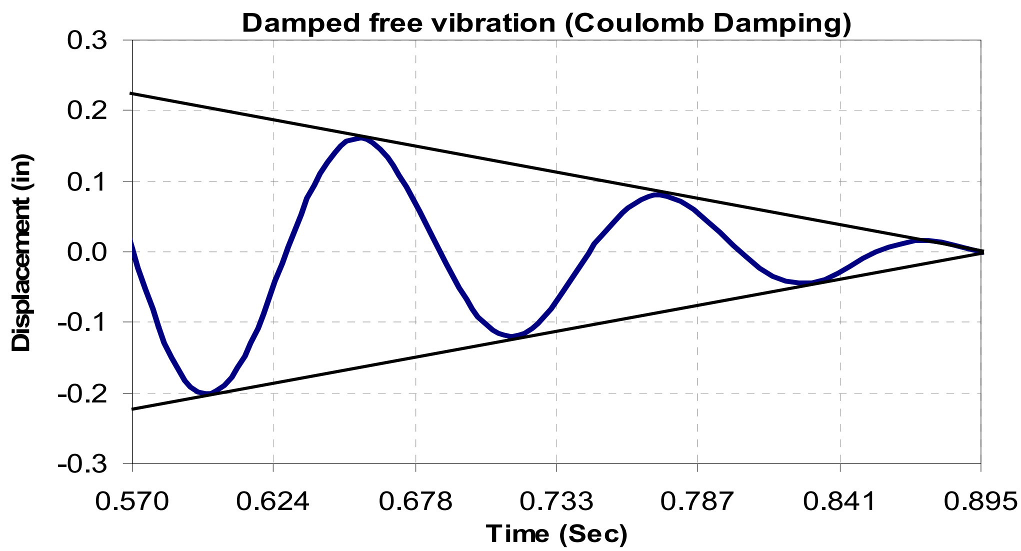

Figure 5.14: Damped free vibration response of SDOF model (T_1 = 0.158 s)

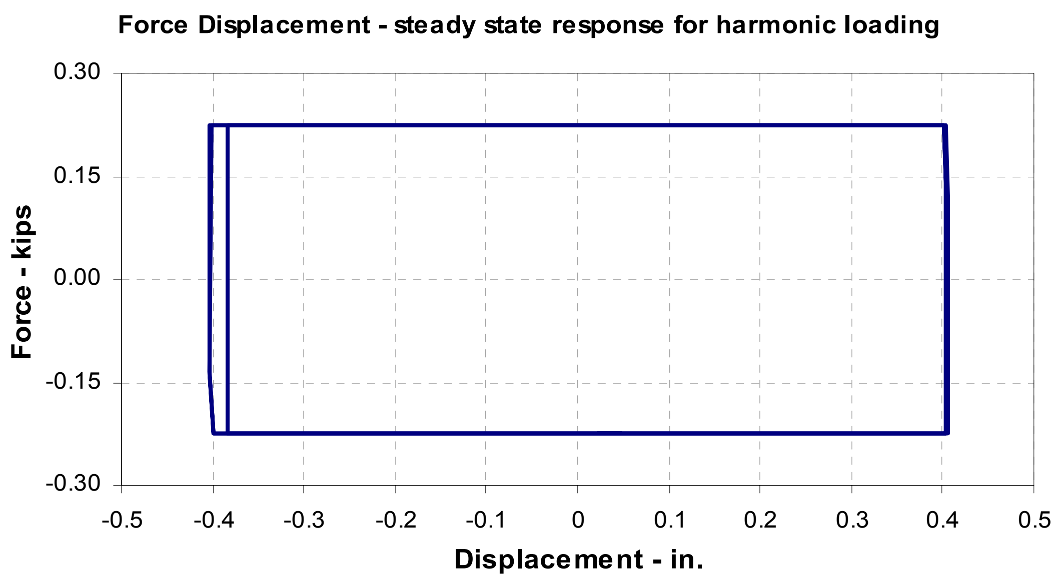

Figure 5.15: Force displacement relationship for harmonic loading

5.9 Effect of Modal Damping on Response of the Friction Damped Structure

The two-wall, two-wall friction damped structure and four-wall structures were analyzed for 1%, 5% and 10% modal damping. The modal damping of 1% and 5% are the representative cases for structures with connectors stressed in their linear elastic range, Plywood shear wall structures or glued timber structures have low inherent damping as compared to highly stressed nailed timber structures which, are represented by 10% modal damping in this study. Nonlinear response history analysis was carried out for 150% El Centro and 150% Northridge ground motions.

5.9.1 Response of the Structures Subjected to 150% El Centro Ground Acceleration

5.9.1.1 1% Modal Damping

The inherent damping capacity of the light-frame nailed wood shear wall structure with elastic behavior is represented by 1% modal damping ratio in this analysis. The analysis results of 2W, 4W and 2WFD subjected to 150% El Centro ground acceleration will be discussed in this section. A reduction of 49.87% was observed in the absolute maximum value of the top diaphragm relative displacement response due to the proposed friction dampers when compared to the 2W structure without any added source of damping, Figure 5.16 (a). The top diaphragm displacement response of the friction damped structure was increased by 17.05% as compared to the 4W structure. As shown in Figure 5.16 (b) such behavior is observed in a few initial cycles when the slip in the dampers is not initiated. Over all a huge reduction in displacement response of the top diaphragm is observed, which indicates a reduction in structural as well as non-structural damage. As shown in Figure 5.17 (a) and (b) the relative acceleration response of the top diaphragm was reduced by 44.34% and 51.46% in the 2WFD structure when compared to the 4W and 2W structures respectively. A reduction of 34.73% and 29.68% in the base shear response of the 2WFD structure was observed as compared to the base shear response of the 2W and 4W structures, Figure 5.18 (a) and (b). About 93% of the input energy (73.11 kip-in.) was dissipated by friction damping in 2WFD structure. A decrease in input energy was also observed when compared to the 2W structure which has no energy dissipating devices induced, Figure 5.18 (c). The maximum values are highlighted in all the figures. The results for 1% modal damping are summarized in Table 5.1.

Table 5.1

1% modal damping response for 2W, 4W and 2WFD structures,

150 % El Centro ground motion

Response	Structure	Time	Max.	% Reduction abs. value
Top Diaphragm Displacement (in)	2W	5.612	0.40	49.87
	4W	4.778	0.17	- 17.05
	2WFD	2.244	0.20	-
Top Diaphragm relative Acceleration (in/s/s)	2W	2.590	581.59	51.46
	4W	4.720	506.65	44.34
	2WFD	2.244	282.30	-
Base Shear (kips)	2W	4.534	211.89	34.73
	4W	4.778	196.67	29.68
	2WFD	2.244	138.29	-
Energy (kip - in)	2WFD	% of Input energy dissipated by Friction damping		93.77

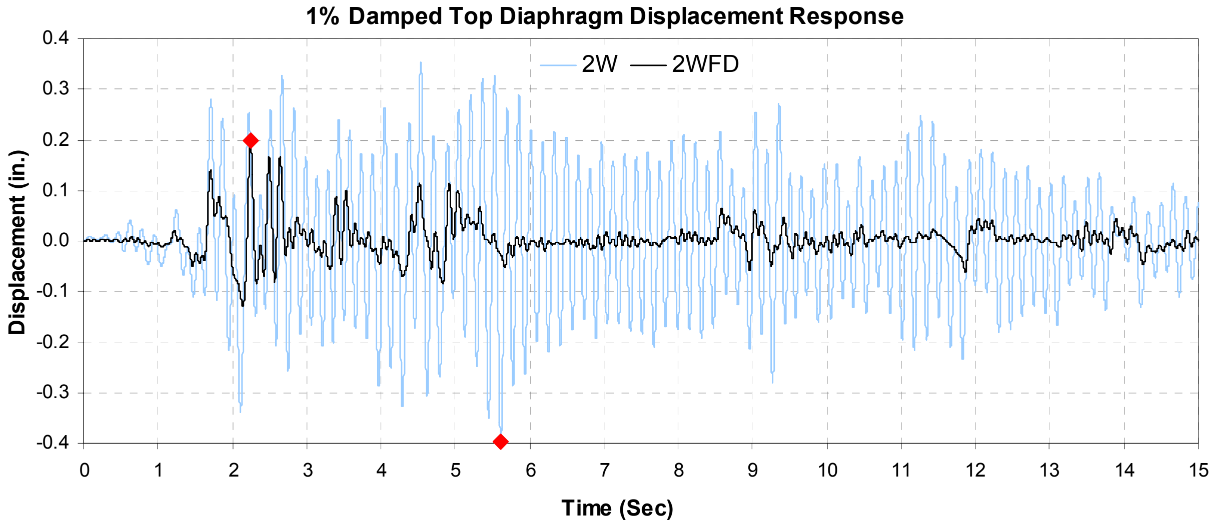

(a)

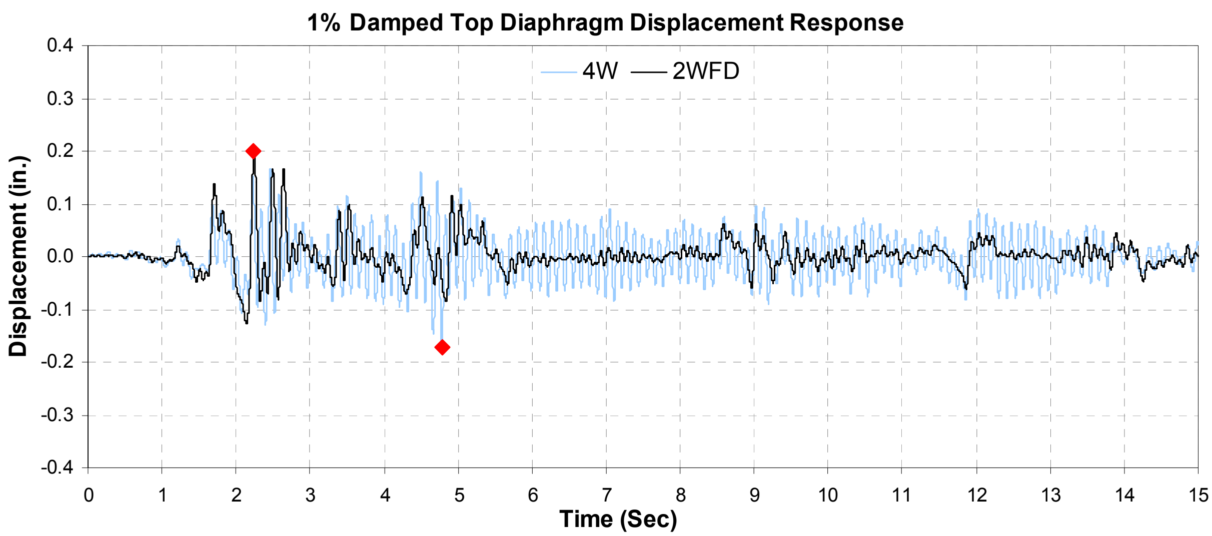

(b)

Figure 5.16: (a) Comparison of the top diaphragm displacement response 2W and 2WFD - 1% MD

(b) Comparison of the top diaphragm displacement response 4W and 2WFD - 1% MD

150% El Centro ground motion

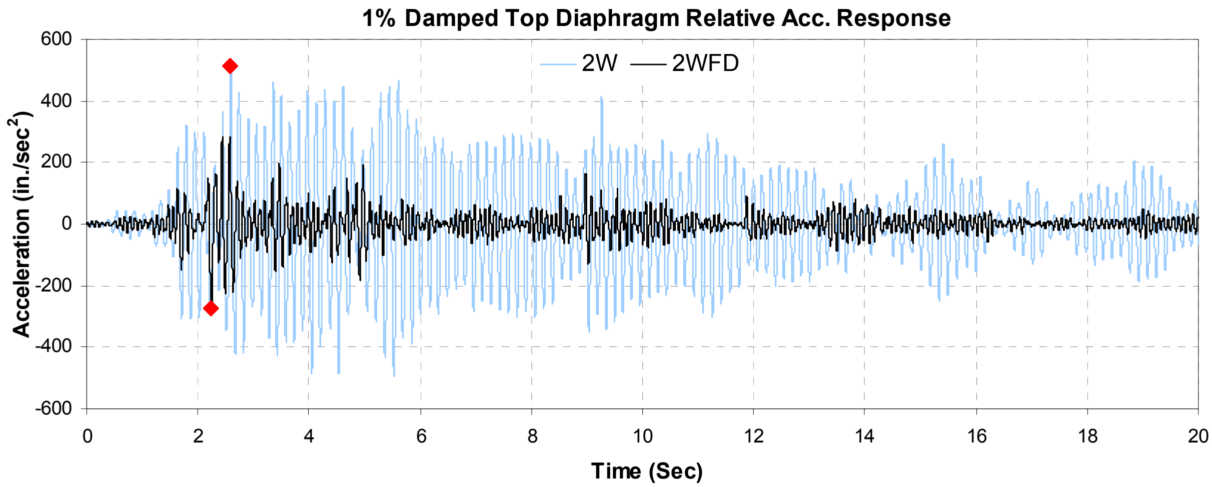

(a)

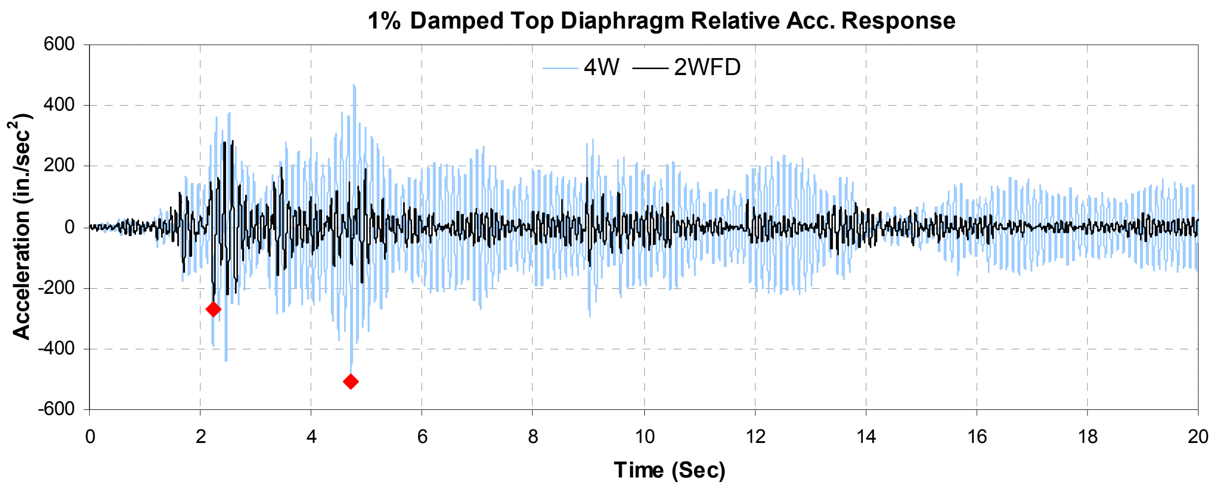

(b)

Figure 5.17: (a) Comparison of the top diaphragm relative acc. response 2W and 2WFD - 1% MD

(b) Comparison of the top diaphragm relative acc. response 4W and 2WFD - 1% MD,

150 % El Centro ground motion

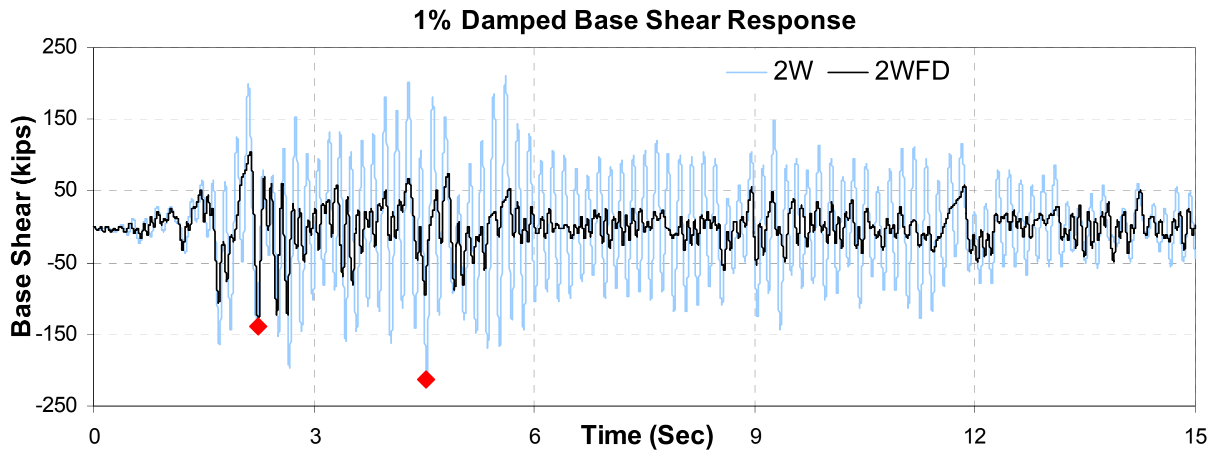

(a)

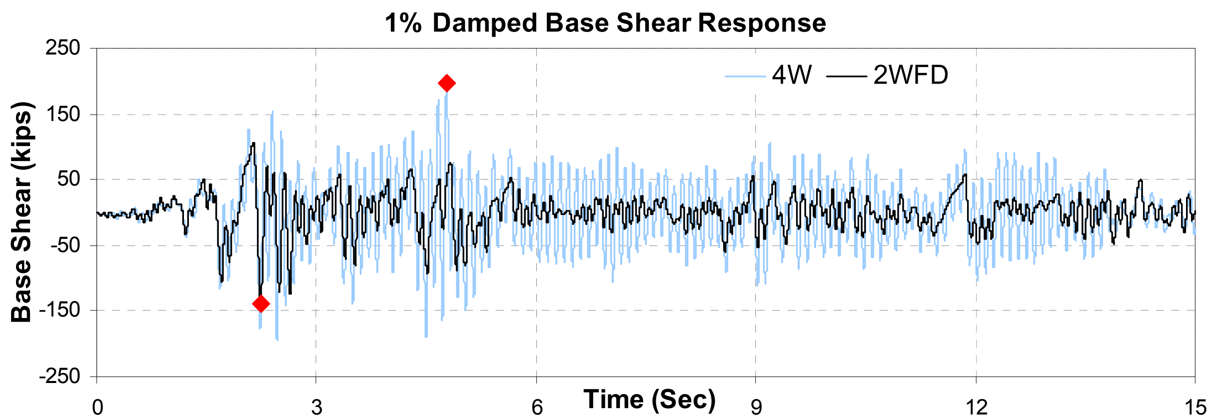

(b)

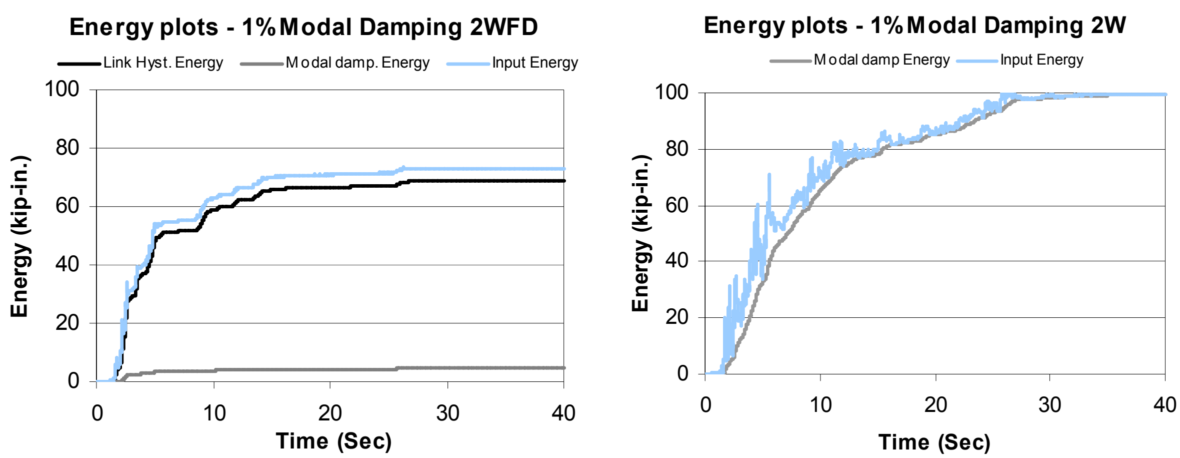

(c)

Figure 5.18: (a) Base shear response - 2WFD and 2W structures; (b) Base Shear response - 2WFD and 4W structures; (c) Energy plots - 1% modal damping, 150% El Centro ground motion

5.9.1.2 5% Modal Damping

Inherent damping capacity of light-frame nailed wood shear wall structure with moderate amount of inelastic behavior can be represented by a 5% modal damping ratio. In this section, response of the 2W, 4W and 2WFD structures subjected to 150% El Centro ground acceleration will be discussed. In general a reduction in displacement as well as acceleration response was observed for the 2WFD structure when compared to the 2W structure. As seen in Figure 5.19 and Figure 5.20 large reductions in the responses of the 2WFD structure are not observed as compared to the 4W structure. However, friction dampers play an important role in curbing the responses later in the time history, thus, reducing cumulative damage in the structure.

A reduction of 26.33% was observed in the absolute maximum value of the top diaphragm relative displacement response due to the proposed friction dampers when compared to the 2W structure without any added source of damping. The top diaphragm displacement response of 2WFD was greater by 45% as compared to the 4W structure. However, a reduction in relative acceleration by 17% and 30.55% was observed in the 2WFD structure as compared to the 4W and 2W structures respectively. The base shear was reduced by about 10% due to friction damping in both 2W and 4W structures.

About 77% of the input energy (70 kip-in.) was dissipated by friction damping in 2WFD structure. The results for 5% modal damping are summarized in Table 5.2. Figure 5.19 (a) and (b) compares the top diaphragm response of the 2WFD structure with the 2W and 4W structure respectively.

The top diaphragm relative accelerations of the friction damped structure are compared with the 2W and 4W structures in Figure 5.20 (a) and (b) respectively. Similarly Figure 5.21 (a) and (b) compares the base shear response of the 2WFD structure with that of the 2W and 4W structure respectively. The energy plots for undamped (2W) and friction damped (4WFD) structures are also presented in Figure 5.21 (c). The maximum values are highlighted in all the figures.

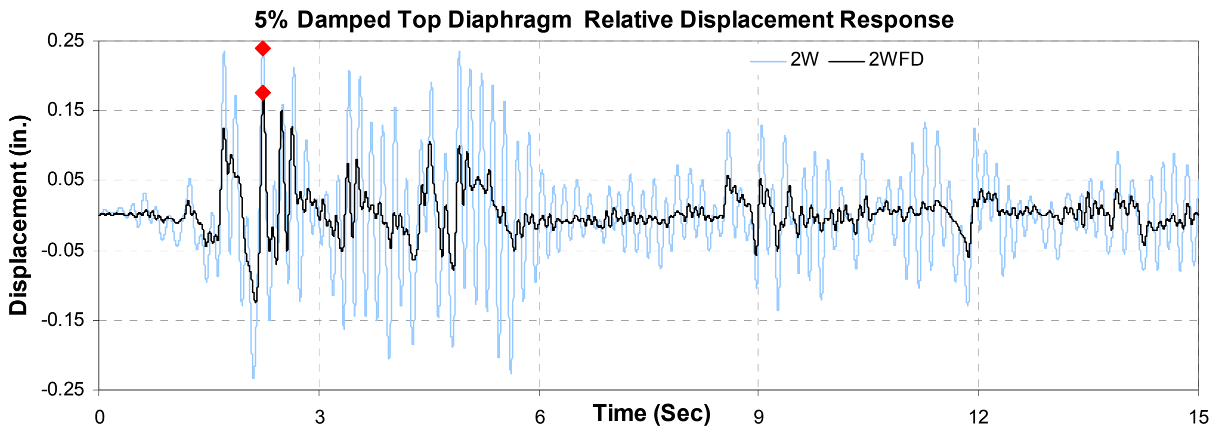

(a)

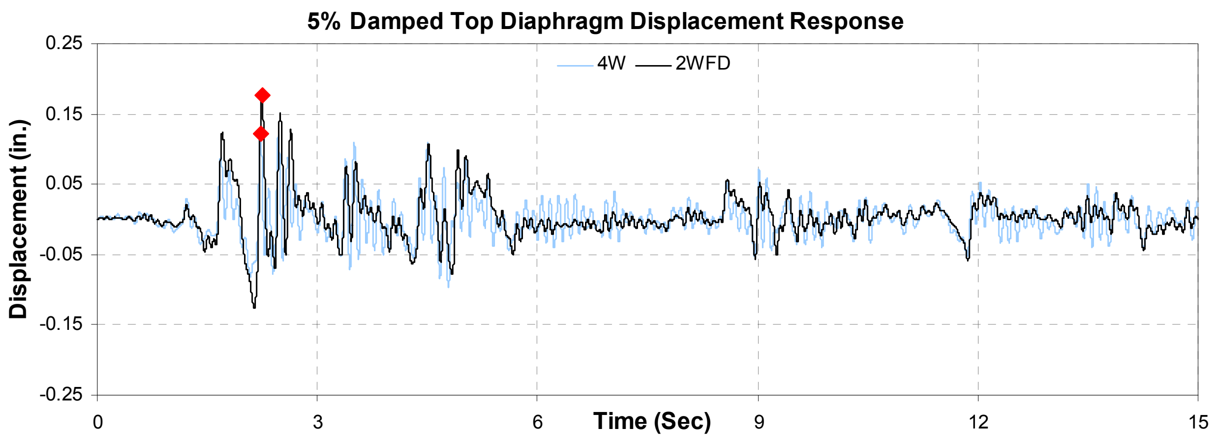

(b)

Figure 5.19: (a) Comparison of the top diaphragm displacement response 2W and 2WFD - 5% MD

(b) Comparison of the top diaphragm displacement response 4W and 2WFD - 5% MD

150% El Centro ground motion

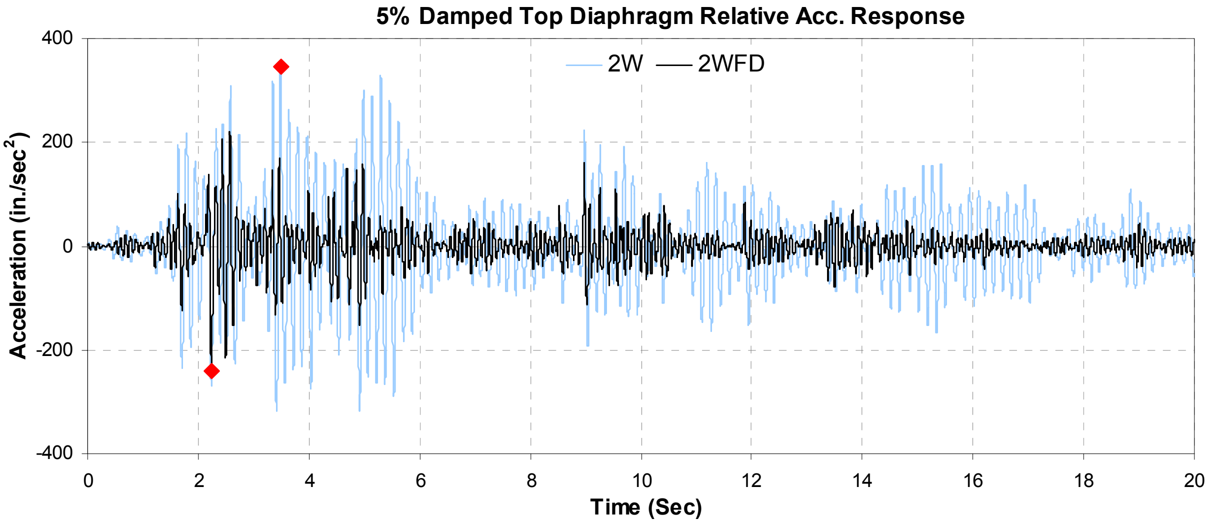

(a)

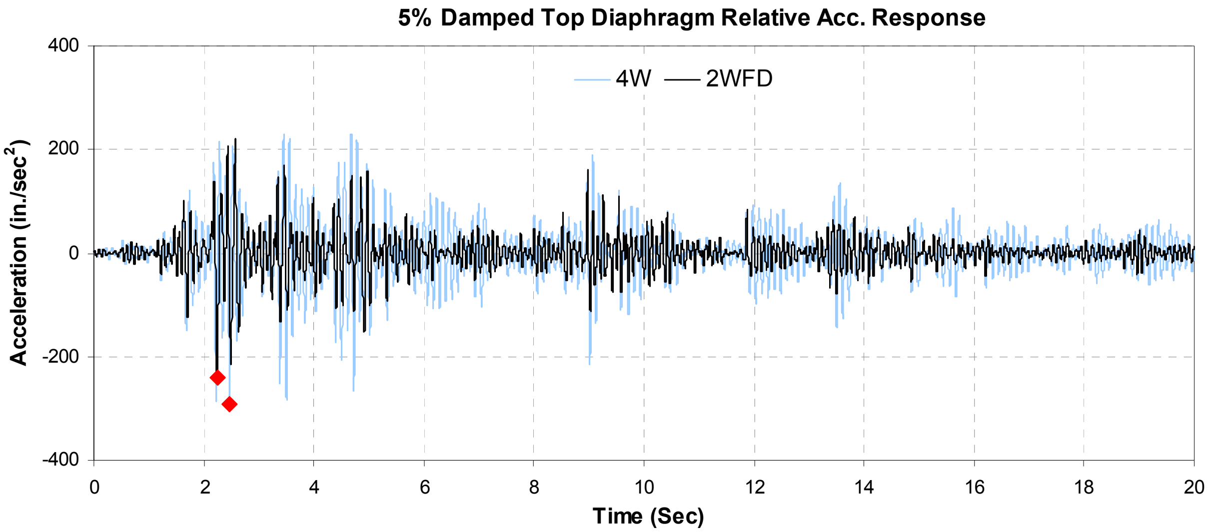

(b)

Figure 5.20: (a) Comparison of the top diaphragm relative acc. response 2W and 2WFD - 5% MD

(b) Comparison of the top diaphragm relative acc. response 4W and 2WFD - 5% MD,

150% El Centro ground motion

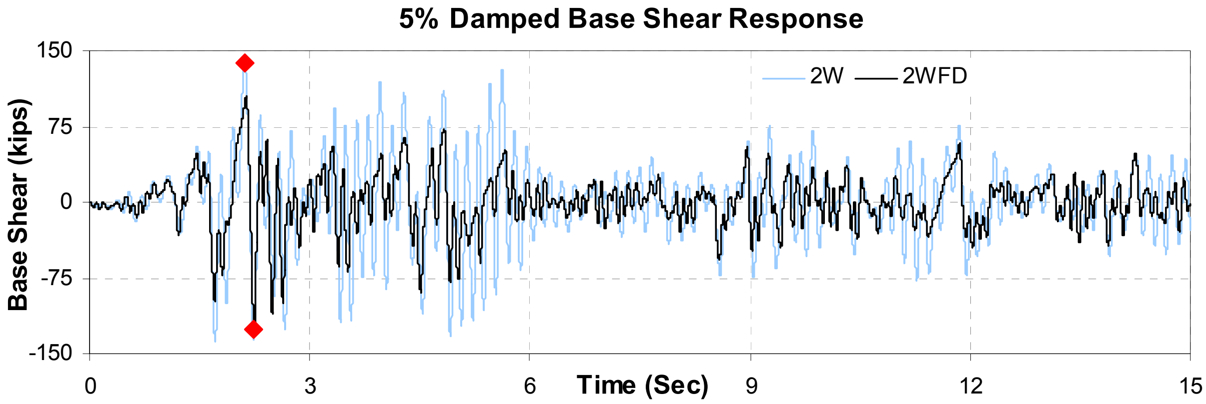

(a)

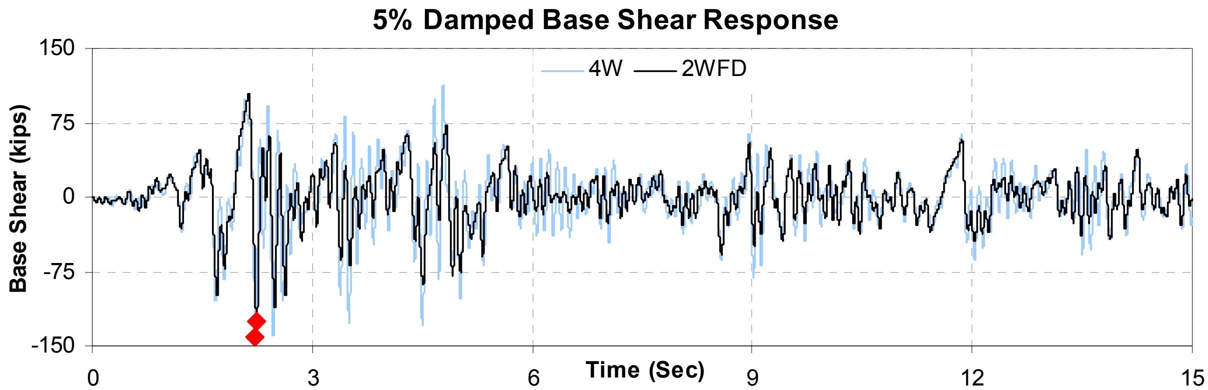

(b)

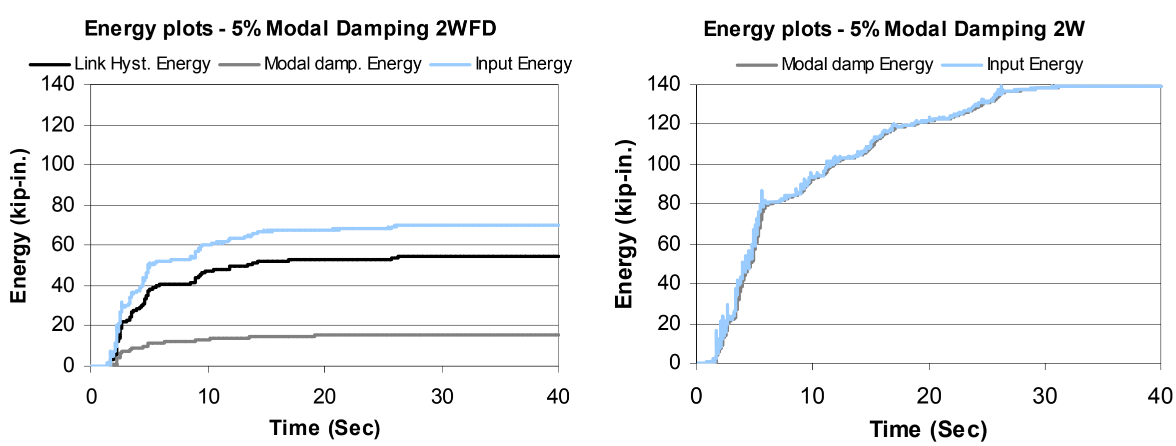

(c)

Figure 5.21: (a) Base shear response - 2WFD and 2W structures; (b) Base shear response - 2WFD and 4W structures; (c) Energy plots - 5% modal damping, 150 % El Centro ground motion

Table 5.2

5% modal damping response for 2W, 4W and 2WFD structures

150 % El Centro ground motion

Response	Structure	Time	Max.	% Reduction abs. value
Top Diaphragm Displacement (in)	2W	2.238	0.24	26.33
	4W	2.226	0.12	- 45
	2WFD	2.244	0.18	-
Top Diaphragm relative Acceleration (in/s/s)	2W	3.486	347	30.55
	4W	2.468	290.50	17.05
	2WFD	2.242	240.97	-
Base Shear (kips)	2W	2.110	138.05	9.07
	4W	2.226	140.85	10.87
	2WFD	2.244	125.53	-
Energy (kip - in)	2WFD	% of Input energy dissipated by Friction damping		77.48

5.9.1.3 10% Modal Damping

A high amount of inelastic behavior in connectors for a typical wood frame shear wall structure in this study is represented by 10% modal damping ratio. The response of the 2W, 4W and 2WFD structure is summarized in Table 5.3. A significant reduction in top diaphragm displacement and relative acceleration response of the 2WFD structure as compared to the 2W structure is observed in Figure 5.22 and Figure 5.23 respectively. No significant reduction in response of the 2WFD structure was observed as compared to the 4W structure. As shown in Figure 5.23 (a) and (b) no significant improvement occurs in the base shear response of the 2W as well as 4W structure. However, about 66% of the input energy (65.43 kip-in) is dissipated by hysteretic damping, Figure 5.23 (c).

An overall decrease in displacement, acceleration and base shear response was observed for 2W structures by using friction dampers. The magnitude of reduction is 30-35% for both 5% and 10% modal damping. The displacement response of the 2WFD structure seems to be more intense as compared to the 4W structure. This can be attributed to ineffectiveness of friction dampers at high inherent damping as the displacement response may not be enough to cause slip. The displacement response history for 10% damping also suggests that the structure may vibrate about its displaced position due to lack of force to reverse the displacement cycle and thereby resulting in high absolute displacement. However, the displacement may be less than the corresponding 4W or 2W structure in absence of such phenomena.

Such behavior also suggests fewer stress reversals in the connectors which may be beneficial in resisting future seismic events. In spite of a decrease in energy dissipation demand of the two-wall structure, 65-70% of input energy was dissipated by friction damping in all the cases. The top diaphragm acceleration response is curbed with both 5% and 10% modal damping, which is clear from Table 5.2 and Table 5.3. The amount of reduction in peak base shear response is nearly the same for both 5% and 10% modal damping cases. The degrading inherent damping capacity of wood frame structures after few loading cycles in a seismic event is not taken into account which may increase the effectiveness of the friction dampers after few initial cycles in loading history.

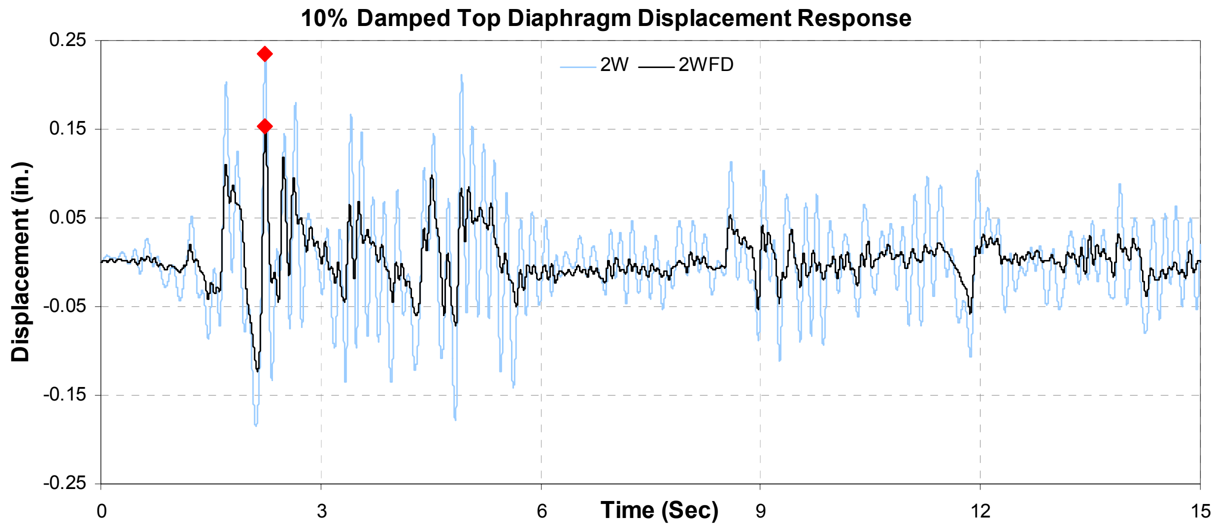

(a)

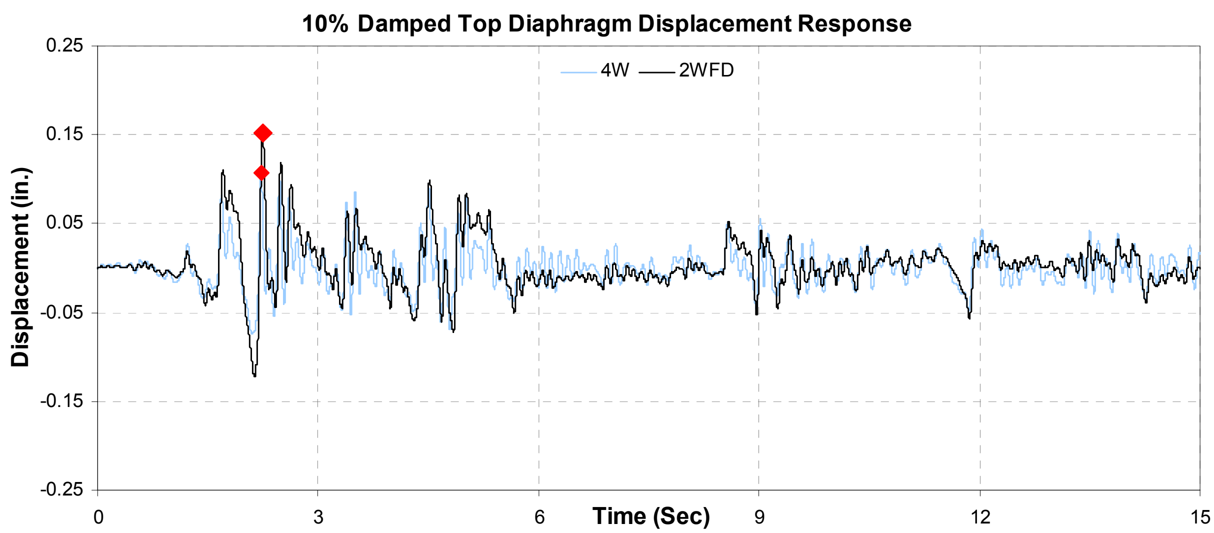

(b)

Figure 5.22: (a) Comparison of the top diaphragm displacement response 2W and 2WFD - 10% MD

(b) Comparison of the top diaphragm displacement response 4W and 2WFD - 10% MD

150% El Centro ground motion

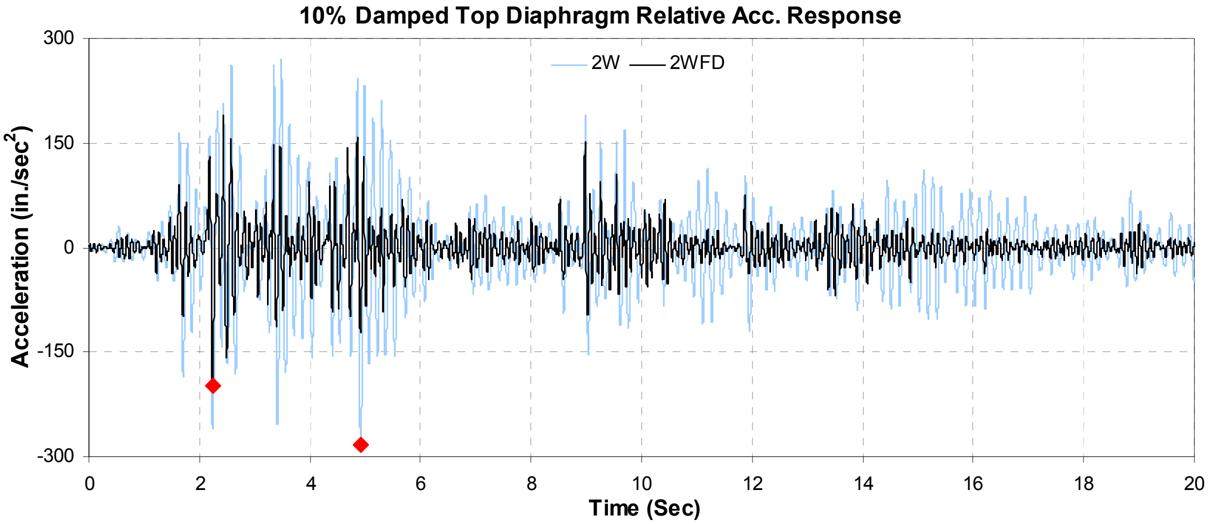

(a)

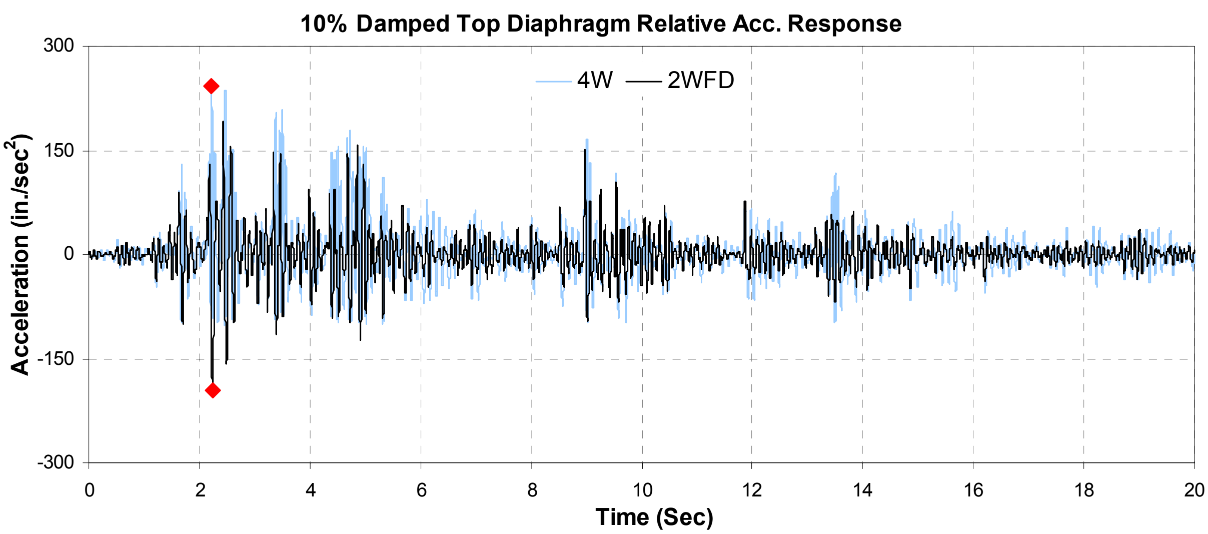

(b)

Figure 5.23: (a) Comparison of the top diaphragm relative acc. response 2W and 2WFD - 10% MD

(b) Comparison of the top diaphragm relative acc. response 4W and 2WFD - 10% MD

150% El Centro ground motion

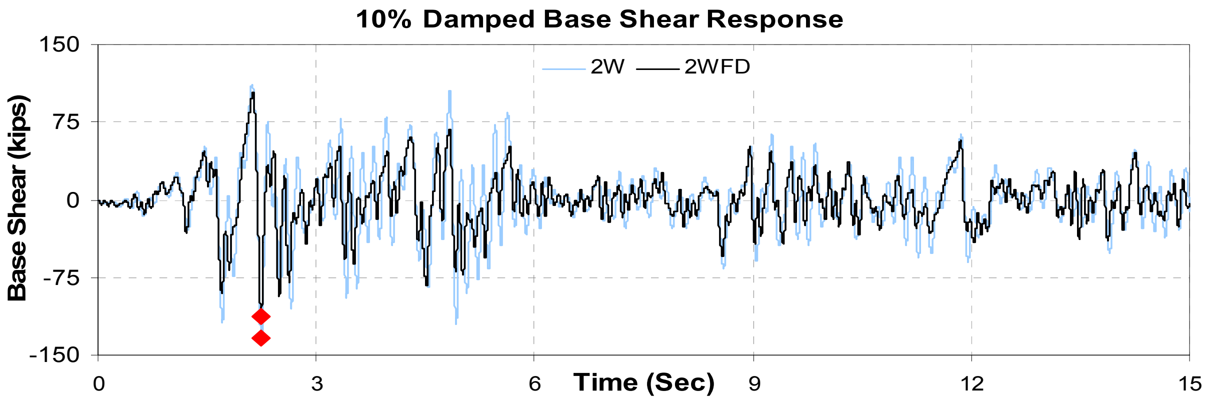

(a)

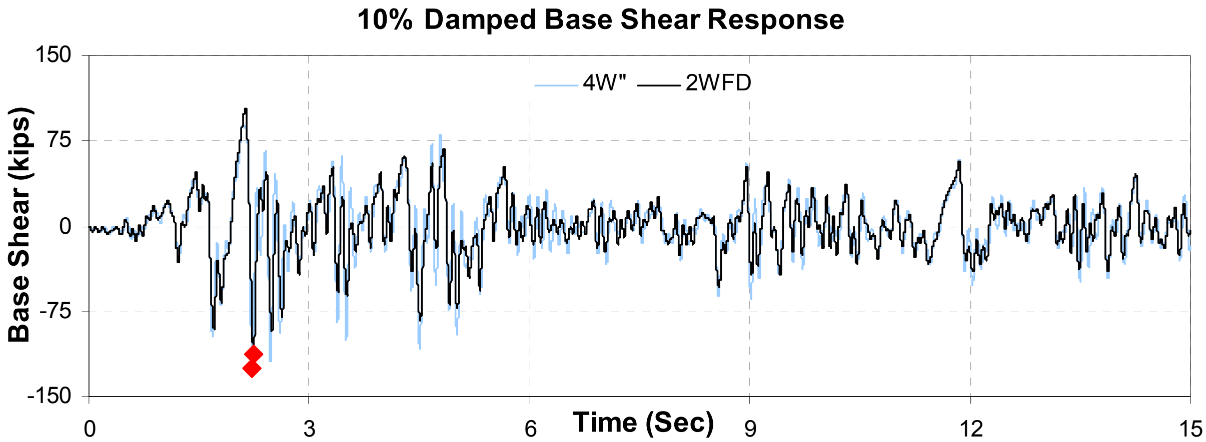

(b)

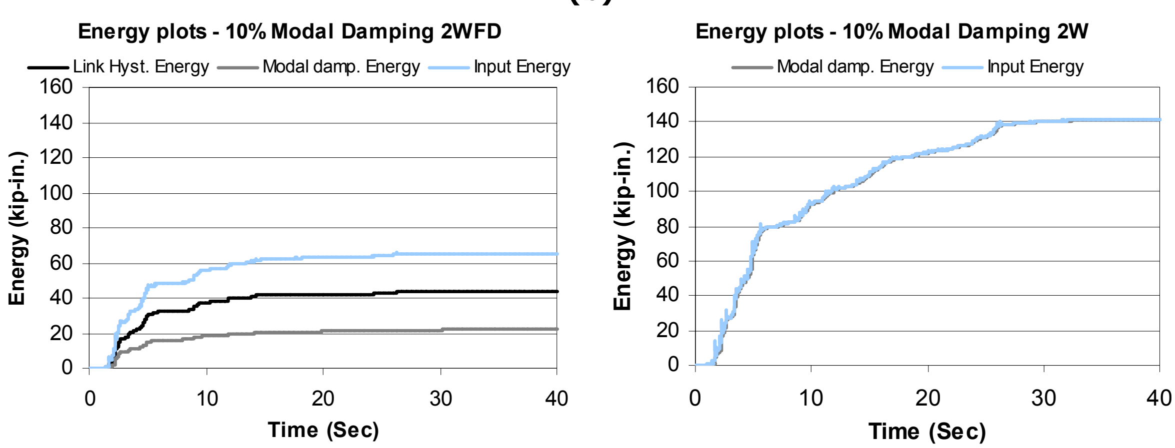

(C)

Figure 5.24: (a) Base Shear response - 2WFD and 2W structures; (b) Base Shear response - 2WFD and 4W structures; (c) Energy plots - 10% modal damping, 150% El Centro ground motion

Table 5.3

10% modal damping response 2W, 4W and 2WFD structures

150% El Centro ground motion

Response	Structure	Time	Max.	% Reduction abs. value
Top Diaphragm Displacement (in)	2W	2.244	0.24	34.78
	4W	2.224	0.11	-43
	2WFD	2.246	0.15	-
Top Diaphragm relative Acceleration (in/s/s)	2W	4.916	281.98	29.54
	4W	2.220	243.52	18.40
	2WFD	2.244	198.72	-
Base Shear (kips)	2W	2.244	134.30	16.42
	4W	2.224	124.95	10.36
	2WFD	2.244	112.60	-
Energy (kip - in)	2WFD	% of Input energy dissipated by Friction damping		66.43

5.9.2 Response of the Structures Subjected to 150% Northridge Ground Acceleration

5.9.2.1 1% Modal Damping

The 2W, 4W and 2WFD, with 1% modal damping representing inherent damping capacity of the structures, were also analyzed for the 150% Northridge ground acceleration record. As shown in Figure 5.25 (a) the absolute maximum value of the top diaphragm relative displacement was reduced by 57.07% for the friction damped structure (2WFD) when compared to the 2W structure without any added source of damping. Unlike the response to El Centro ground acceleration the top diaphragm displacement response of the 2WFD was reduced by 9.14% as compared to the 4W structure, Figure 5.25(b). As shown in Figure 5.26 (a) and (b) the top diaphragm relative acceleration response was reduced by 54% and 63% in the 2WFD structure when compared to the 4W and 2W structures respectively. Also the base shear response of the 2WFD structure is compared to the base shear response of the 2W and 4W structures, Figure 5.27 (a) and (b). The amount of input energy (71.26 kip-in) dissipated due to friction damping was same as for 1% 2WFD subjected to 150% El Centro ground motion. A decrease in input energy was also observed when compared to the 2W structure which has no energy dissipating devices induced, Figure 5.27 (c). All the results for 1% modal damping subjected to 150% Northridge ground acceleration are summarized in Table 5.4. It was observed that the friction dampers were more effective in curbing the response for the Northridge ground motion as compared to the El Centro ground acceleration.

Table 5.4

1% modal damping response comparison for 2W, 4W and 2WFD structures

150 % Northridge ground motion

Response	Structure	Time	Max.	% Reduction abs. value
Top Diaphragm Displacement (in)	2W	8.224	0.56	57.07
	4W	4.102	0.30	9.14
	2WFD	4.120	0.28	-
Top Dia. Relative Acceleration (in/s/s)	2W	8.224	735.03	63.61
	4W	4.160	653.13	59.07
	2WFD	4.012	267.48	-
Base Shear (kips)	2W	8.226	320.31	38.43
	4W	4.102	357.21	50.35
	2WFD	4.12	197.19	-
Energy (kip - in)	2WFD	% of Input energy dissipated by Friction damping		94.06

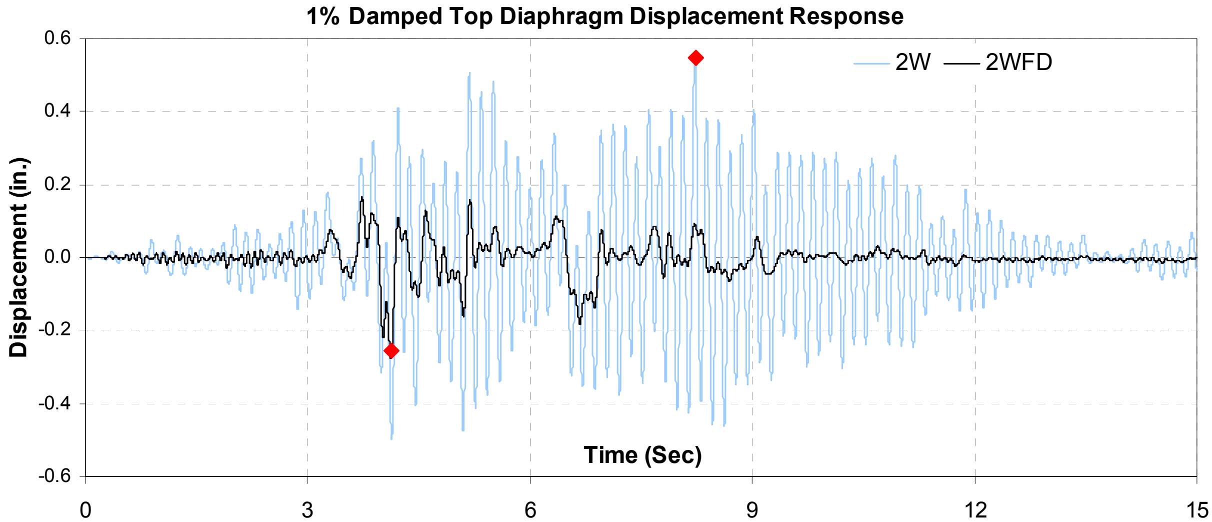

(a)

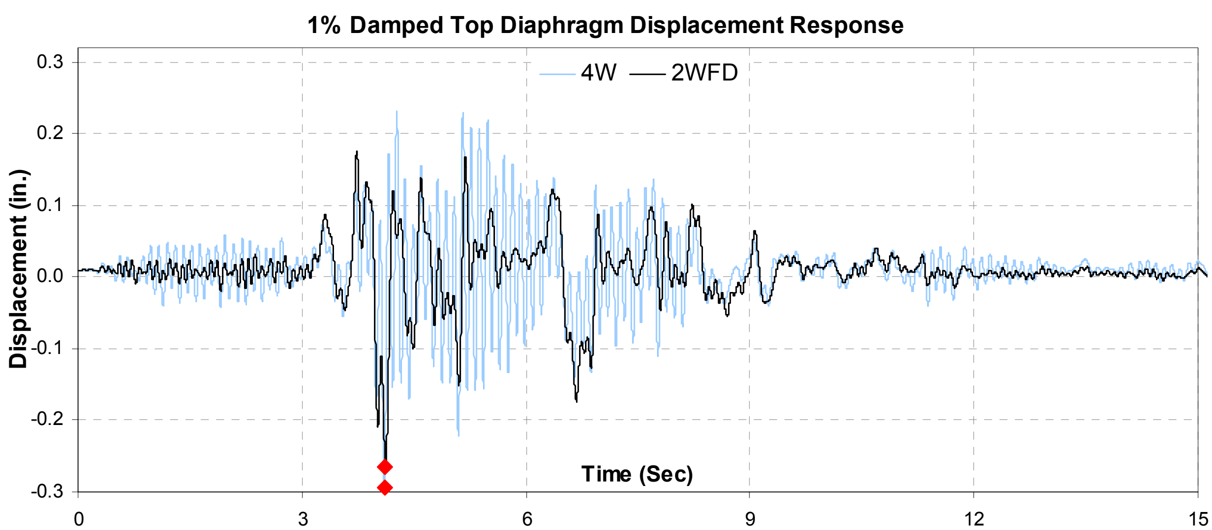

(b)

Figure 5.25: (a) Comparison of the top diaphragm displacement response 2W and 2WFD - 1% MD

(b) Comparison of the top diaphragm displacement response 4W and 2WFD - 1% MD

150% Northridge ground motion

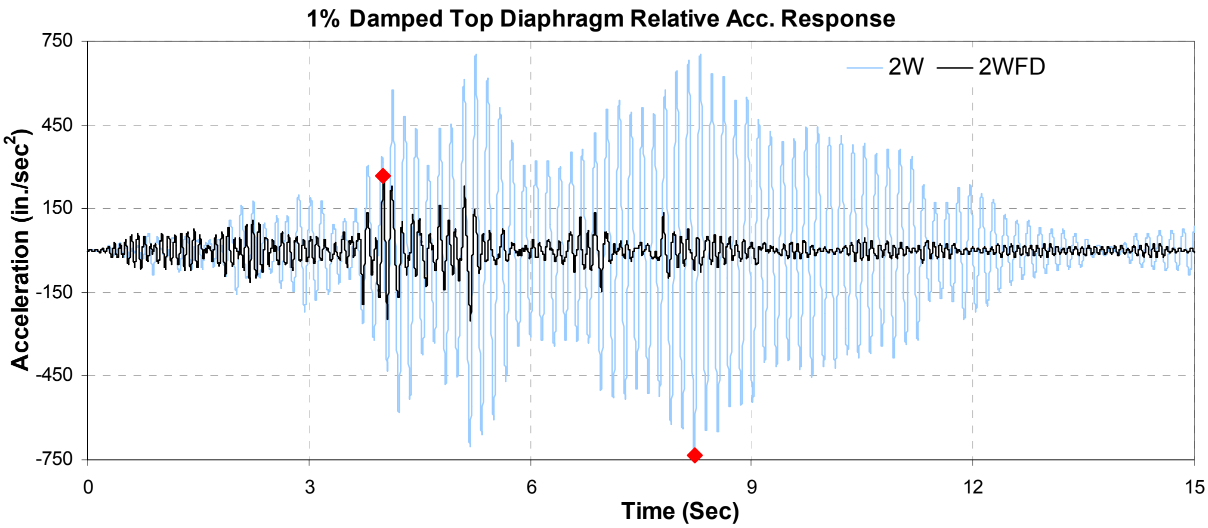

(a)

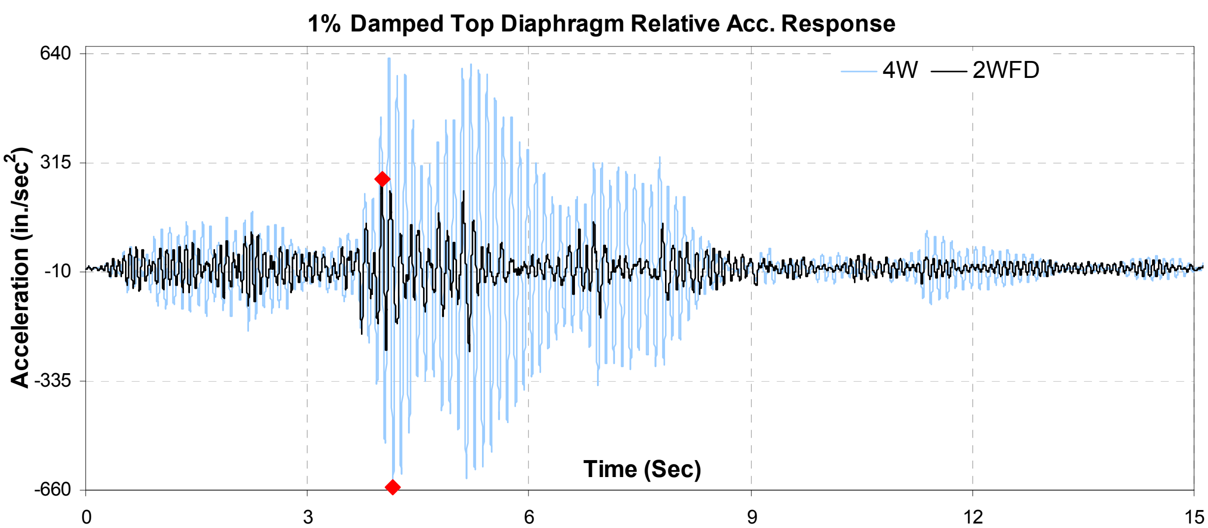

(b)

Figure 5.26: (a) Comparison of the top diaphragm relative acc. response 2W and 2WFD - 1% MD

(b) Comparison of the top diaphragm relative acc. response 4W and 2WFD - 1% MD,

150 % Northridge ground motion

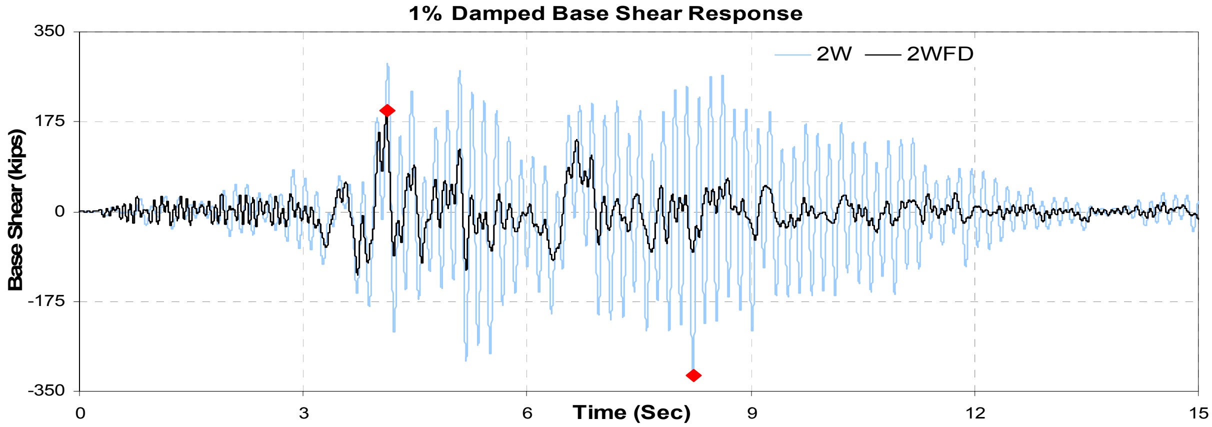

(a)

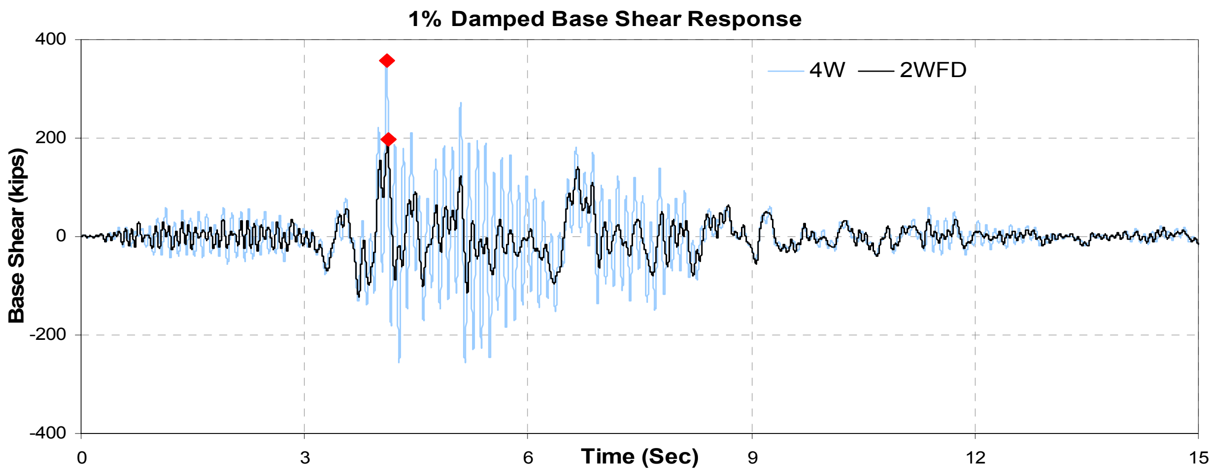

(b)

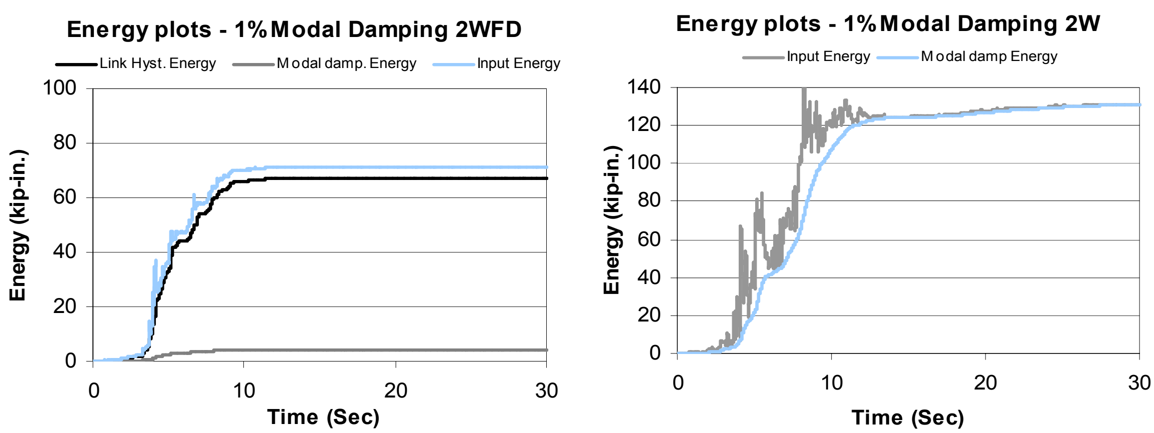

(C)

Figure 5.27: (a) Base shear response - 2WFD and 2W structures; (b) Base Shear response - 2WFD and 4W structures; (c) Energy plots - 1% modal damping, 150% Northridge ground motion

5.9.2.2 5% Modal Damping

In general a reduction in displacement as well as acceleration response was observed for the 2WFD structure subjected to 150% Northridge ground motion, when compared to the 2W structure. As seen in Figure 5.28 and Figure 5.29, though large reductions in the top diaphragm displacement response and relative acceleration response of the 2WFD structure were not observed as compared to the 4W structure, friction dampers play an important role in curbing the peak responses. The base shear response of the friction damped structure is compared with that of the 2W and 4W structures in Figure 5.30 (a) and (b). As seen in Figure 5.30 (c) about 78% of the input energy (70.23 kip-in.) was dissipated by friction damping in 2WFD structure. The input energy the undamped structure is almost double that of the friction damped structure. The results for the structures with 5% modal damping subjected to the 150% Northridge ground motion are summarized in Table 5.5. The maximum values are highlighted in all the figures. Again the friction dampers are found to be more effective in curbing the response when subjected to the Northridge ground acceleration as compared to the El Centro ground motion.

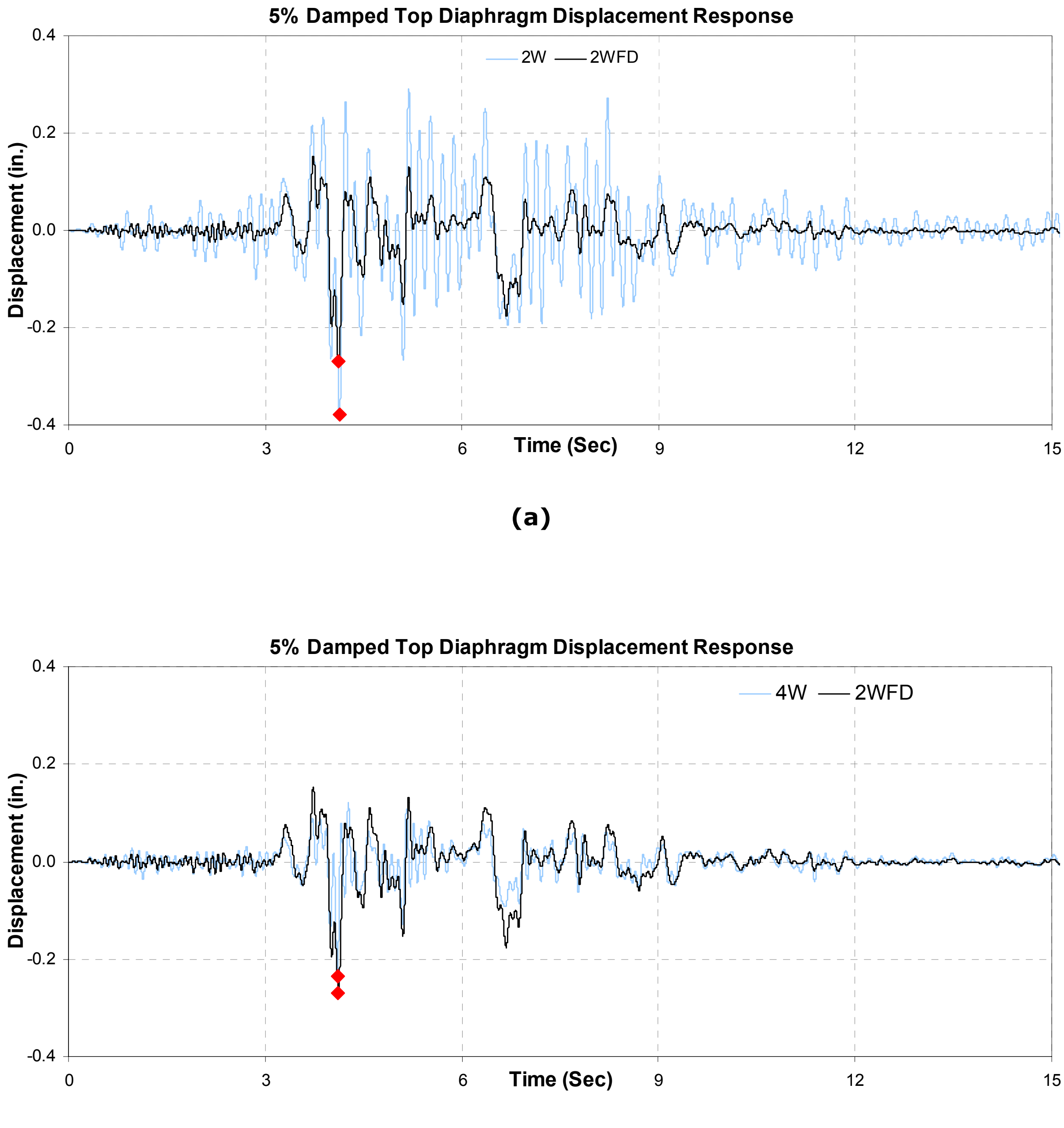

Figure 5.28: (a) Comparison of the top diaphragm displacement response 2W and 2WFD - 5% MD

(b) Comparison of the top diaphragm displacement response 4W and 2WFD - 5% MD

150% Northridge ground motion

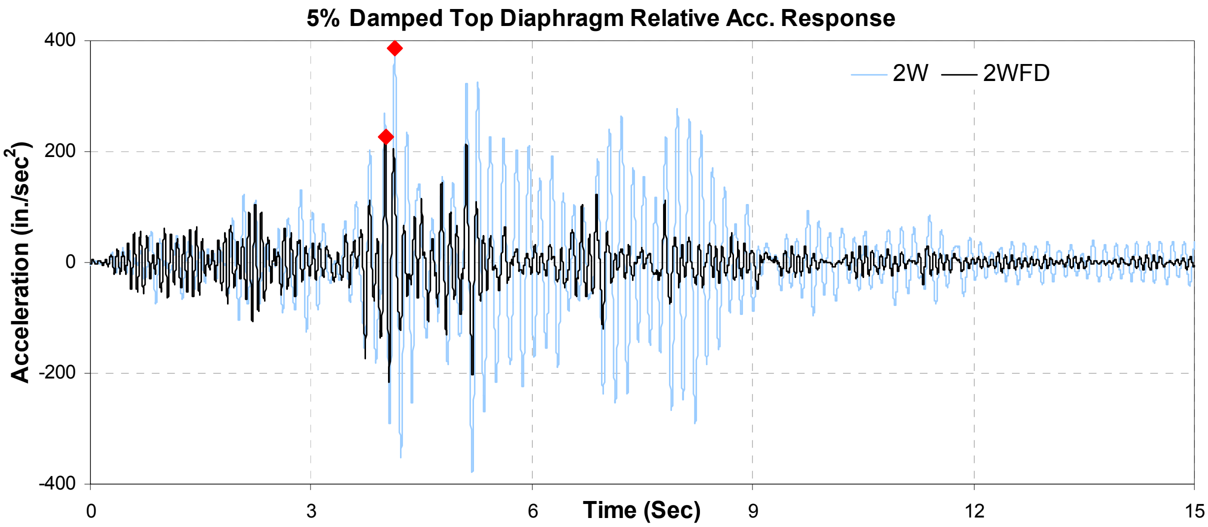

(a)

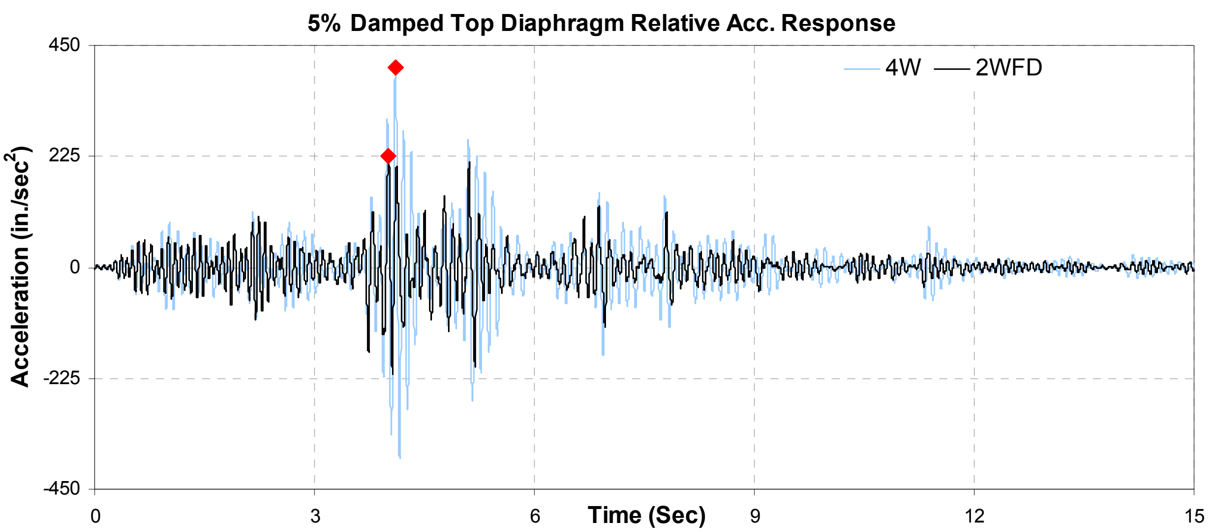

(b)

Figure 5.29: (a) Comparison of the top diaphragm relative acc. response 2W and 2WFD - 5% MD

(b) Comparison of the top diaphragm relative acc. response 4W and 2WFD - 5% MD,

150% Northridge ground motion

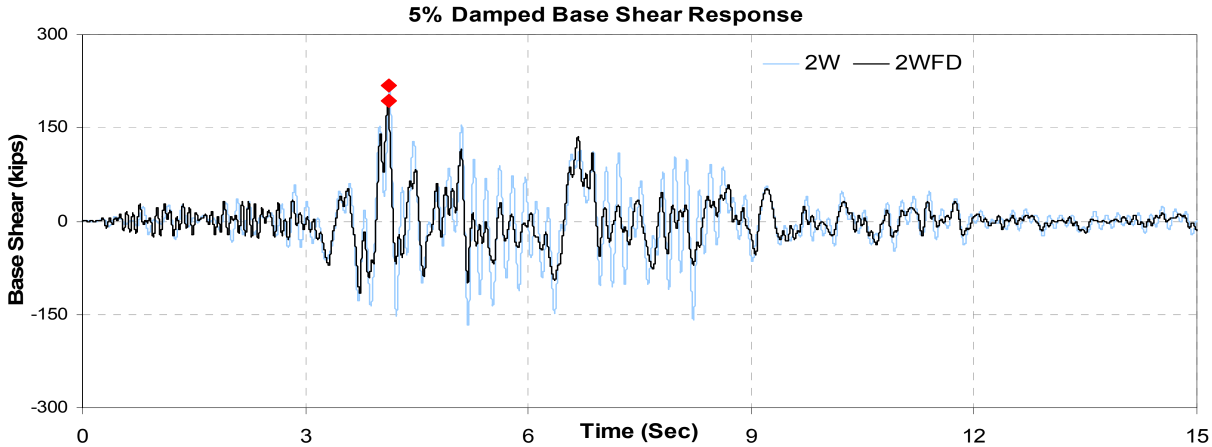

(a)

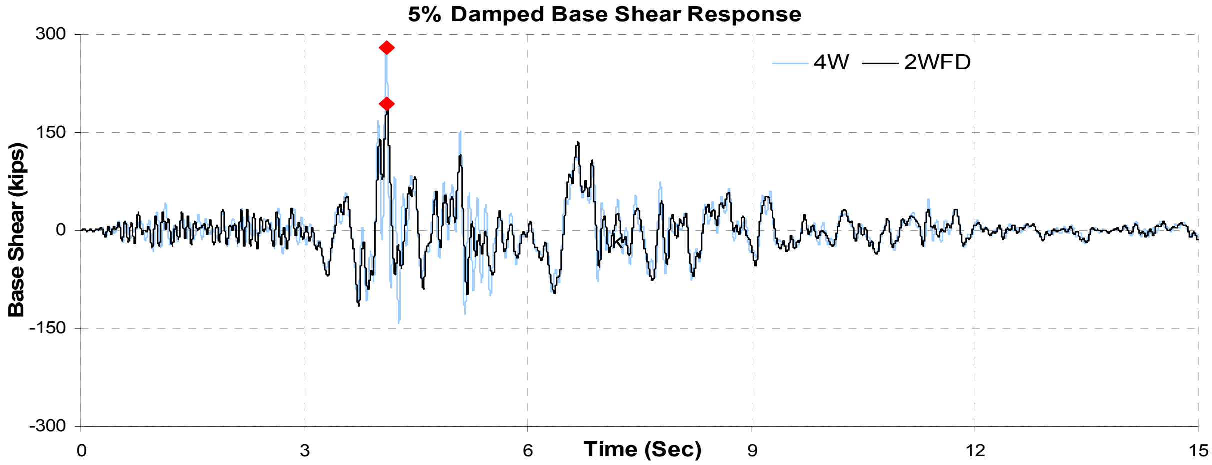

(b)

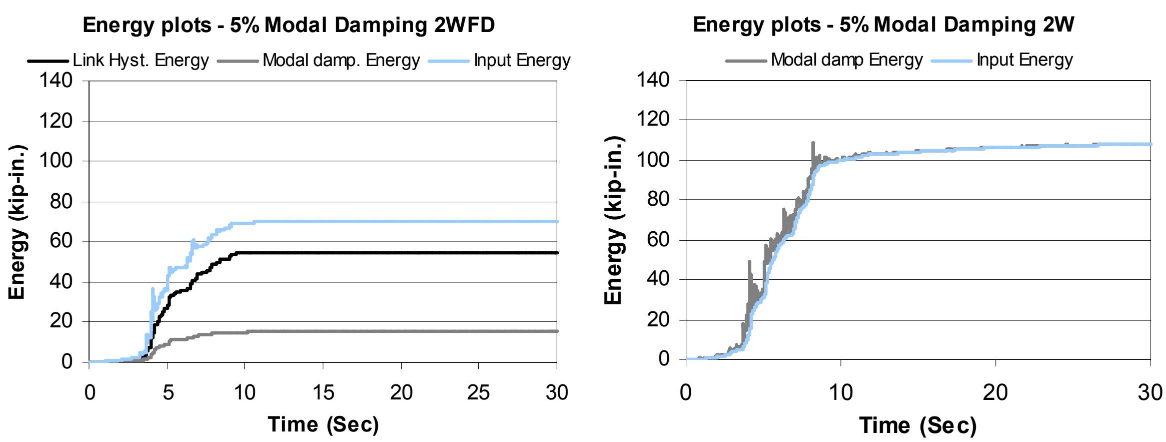

(c)

Figure 5.30: (a) Base Shear response - 2WFD and 2W structures; (b) Base Shear response - 2WFD and 4W structures; (c) Energy plots - 5% modal damping, 150 % Northridge ground motion

Table 5.5

5% modal damping response for 2W, 4W and 2WFD structures

150 % Northridge ground motion

Response	Structure	Time	Max.	% Reduction abs. value
Top Diaphragm Displacement (in)	2W	4.132	0.38	28.82
	4W	4.102	0.24	-13.86
	2WFD	4.118	0.27	-
Top Dia. Relative Acceleration (in/s/s)	2W	4.138	387.00	41.29
	4W	4.104	404.15	43.78
	2WFD	4.010	227.19	-
Base Shear (kips)	2W	4.132	218.97	11.2
	4W	4.102	279.86	30.52
	2WFD	4.116	194.46	-
Energy (kip - in)	2WFD	% of Input energy dissipated by Friction damping		78.03

5.9.2.3 10% Modal Damping

The responses of the 2W, 4W and 2WFD are summarized in Table 5.6. A significant reduction in top diaphragm displacement and relative acceleration response of the 2WFD structure as compared to the 2W structure is observed in Figure 5.31 and Figure 5.32 respectively. Significant reduction in response of the 2WFD structure was not observed when compared to the 4W structure, except some reduction in peak values. As shown in Figure 5.33 (a) and (b) no improvement occur in the base shear response of the 2W as well as 4W structure. About 66% of the input energy (69.35 kip-in) is dissipated by hysteretic damping in the 2WFD structure, Figure 5.23 (c).

Table 5.6

10% modal damping response for 2W, 4W and 2WFD structures 150% Northridge ground motion

Response	Structure	Time	Max.	% Reduction abs. value
Top Diaphragm Displacement (in)	2W	4.132	0.32	24.51
	4W	4.102	0.20	-30.34
	2WFD	4.116	0.26	-
Top Dia. Relative Acceleration (in/s/s)	2W	4.136	294.00	35.31
	4W	4.104	283.36	32.88
	2WFD	5.110	190.19	-
Base Shear (kips)	2W	4.130	189.36	-0.54
	4W	4.102	237.36	19.86
	2WFD	4.114	190.22	-
Energy (kip - in)	2WFD	% of Input energy dissipated by Friction damping		66.33

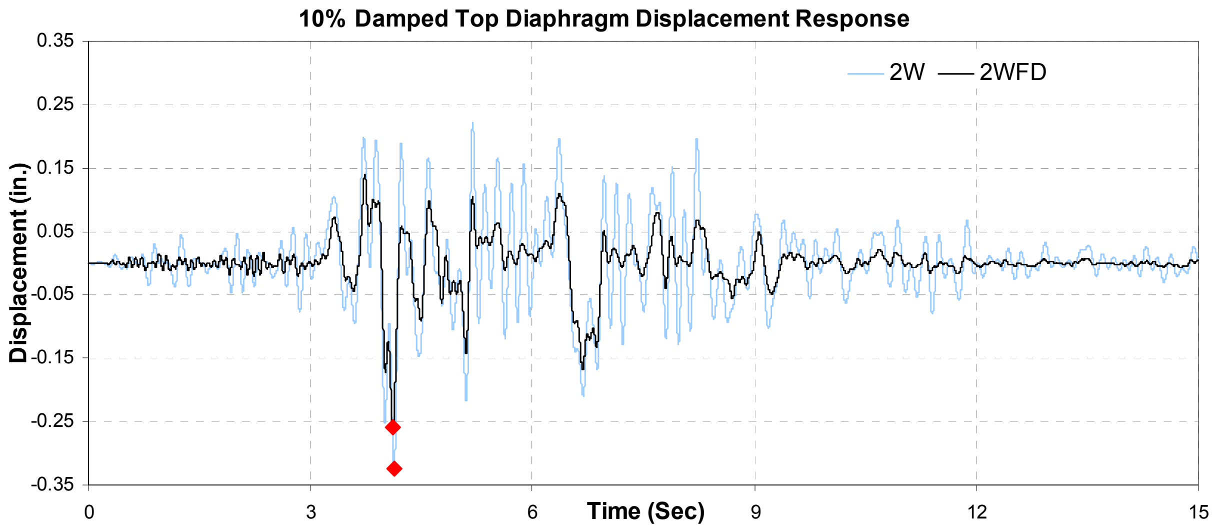

(a)

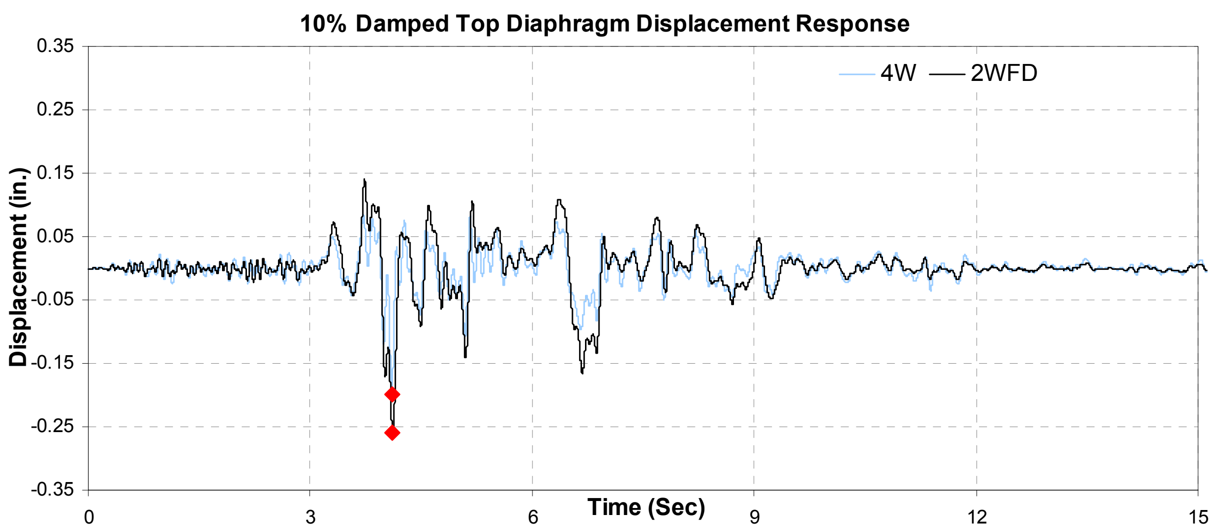

(b)

Figure 5.31: (a) Comparison of the top diaphragm disp. response 2W and 2WFD - 10% MD

(b) Comparison of the top diaphragm disp. response 4W and 2WFD - 10% MD

150% Northridge ground motion

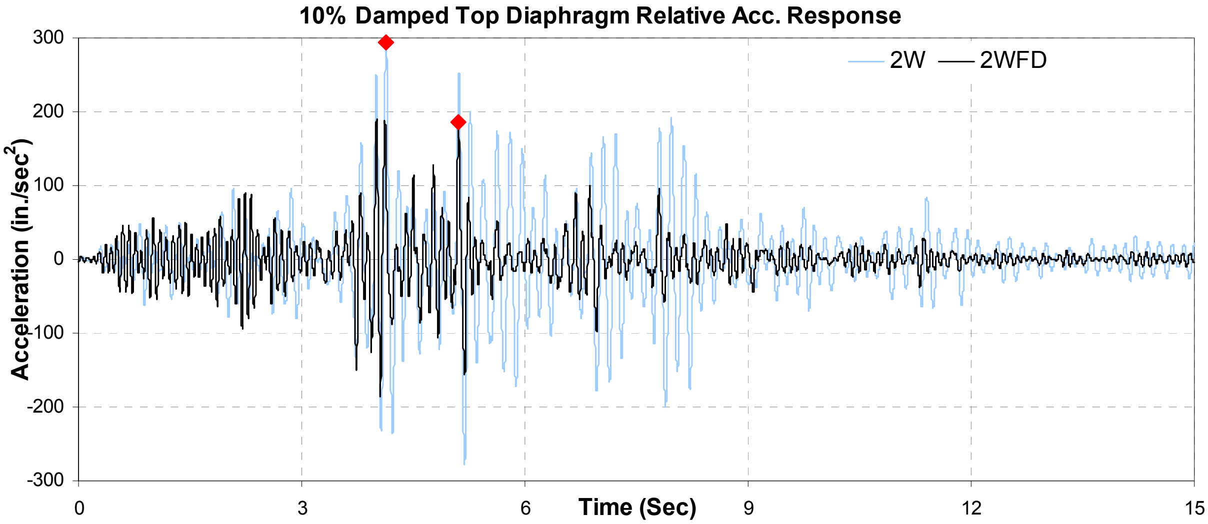

(a)

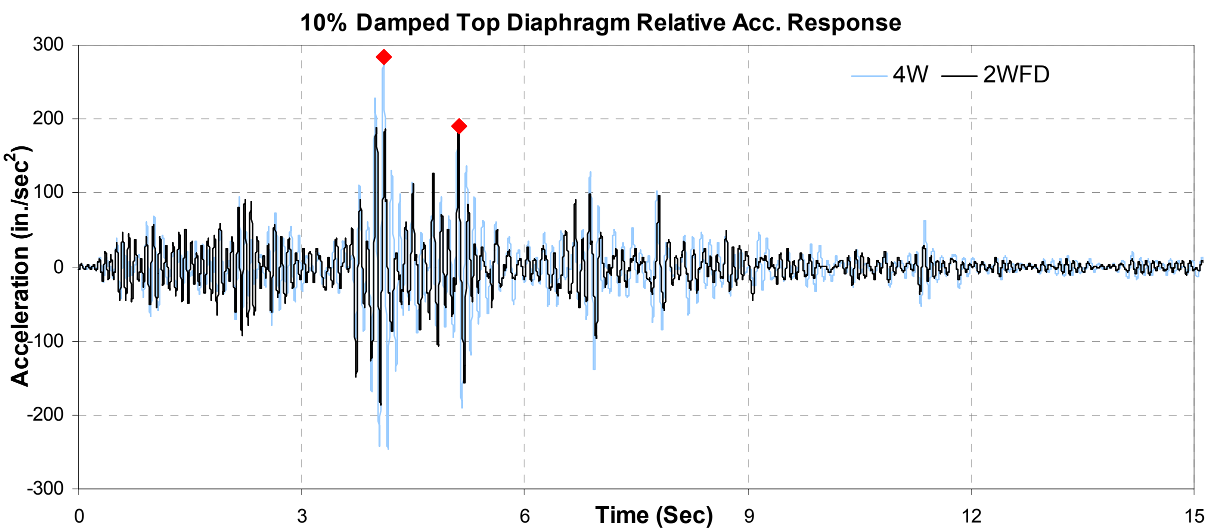

(b)

Figure 5.32: (a) Comparison of the top diaphragm relative acc. response 2W and 2WFD - 10% MD

(b) Comparison of the top diaphragm relative acc. response 4W and 2WFD - 10% MD,

150% Northridge ground motion

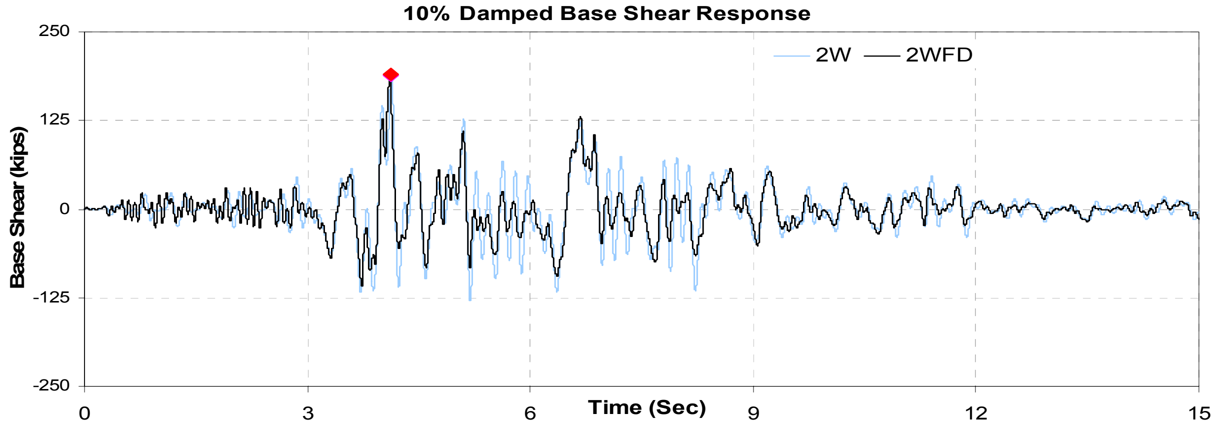

(a)

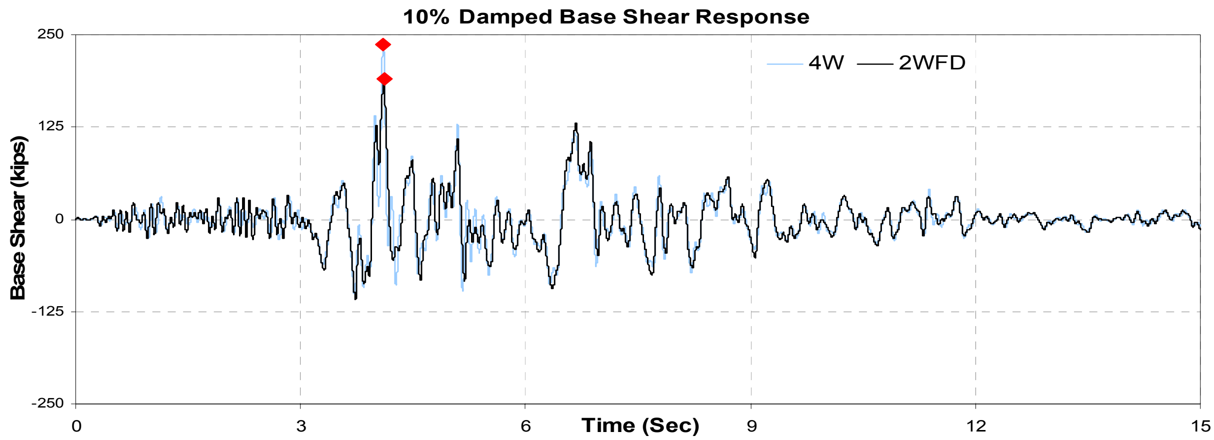

(b)

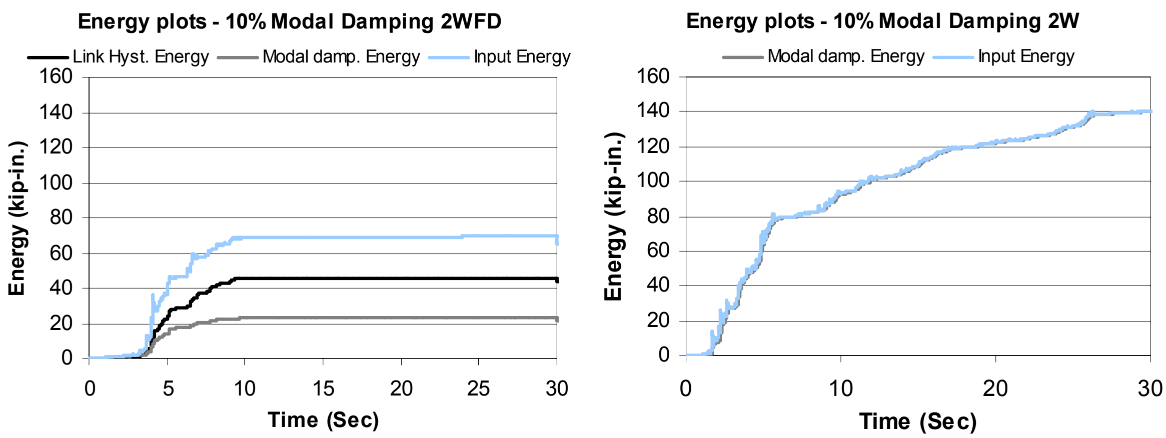

(c)

Figure 5.33: (a) Base Shear response - 2WFD and 2W structures; (b) Base Shear response - 2WFD and 4W structures; (c) Energy plots - 10% modal damping, 150 % Northridge ground motion

5.10 Slip Comparison

The amount of slip in the sliding wall dampers is compared in this section. As seen in Figure 5.34 no significant difference in displacement response for 1%, 5% and 10% modal damping is observed beyond 4 seconds. Reduction in response is observed between 1 (when slip in the wall is initiated) and 4 sec. Such behavior can be clearly understood from Figure 5.35 where the slip in one of the link elements is compared for all the three cases i.e. 1%, 5% and 10% modal damping. It is clear from Figure 5.35 that slip is initiated at 1 sec and ceases at 26 sec, beyond which no significant difference in slip is observed except for few initial cycles. The bottom part of the plot indicates the occurance of slip in the time history. The number of slip events for 1% damping is more as compared to 5% and 10% modal damping which have almost the same number of slip events. Hence, no significant difference in behavior for 5% and 10% modal damping is found except a larger amount of energy is dissipated by modal damping in the 10% damped system. This behavior warrants a change in the clamping force as well as refining the modeling technique to represent actual inherent damping capacity of the wood frame shear wall.

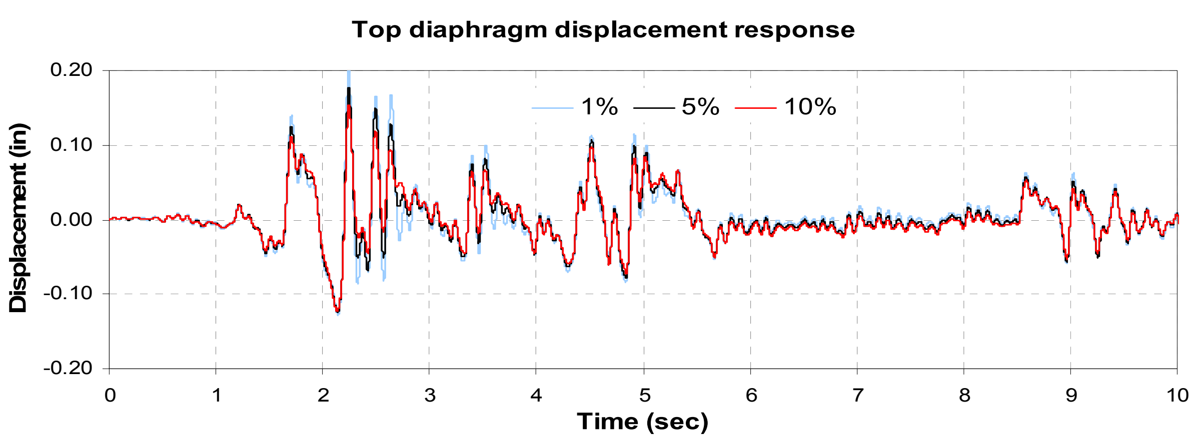

Figure 5.34: Top diaphragm displacement response – 2WFD- 150% El Centro Ground Motion

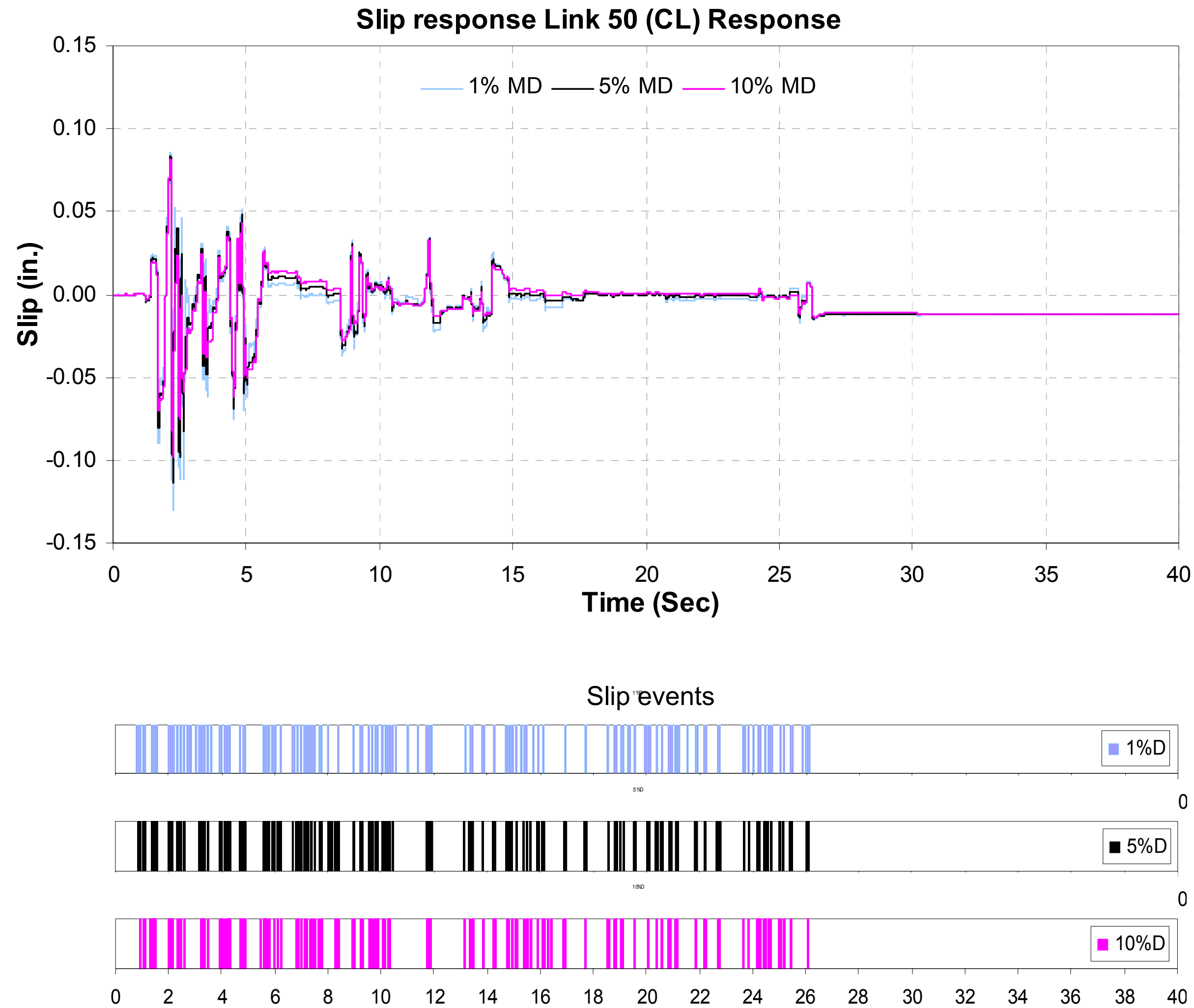

Figure 5.35: Slip comparison for 1%, 5% and 10% modal damping cases – 2WFD- 150% El Centro

5.11 Effect of Slip Resistance on Behavior of 2WFD Structure

The two-wall friction damped structure was analyzed for varying slip resistance. Figure 5.36 shows displacement response for friction damped structure for 150% El Centro ground acceleration and 1% Modal damping. X/X e.g. 10.8/10.8 indicates the clamping force in kips for bottom and top story. Note that the clamping force for both the stories is kept the same in this study. As seen in Figure 5.36 a decrease in top diaphragm displacement response was observed with increase in clamping force. Also the response for higher clamping lags behind the other lower clamping case which was anticipated due to increase in frictional (lateral) resistance. Thus, the configuration with 18 kip top and bottom slip resistance is more effective in curbing the displacement response.

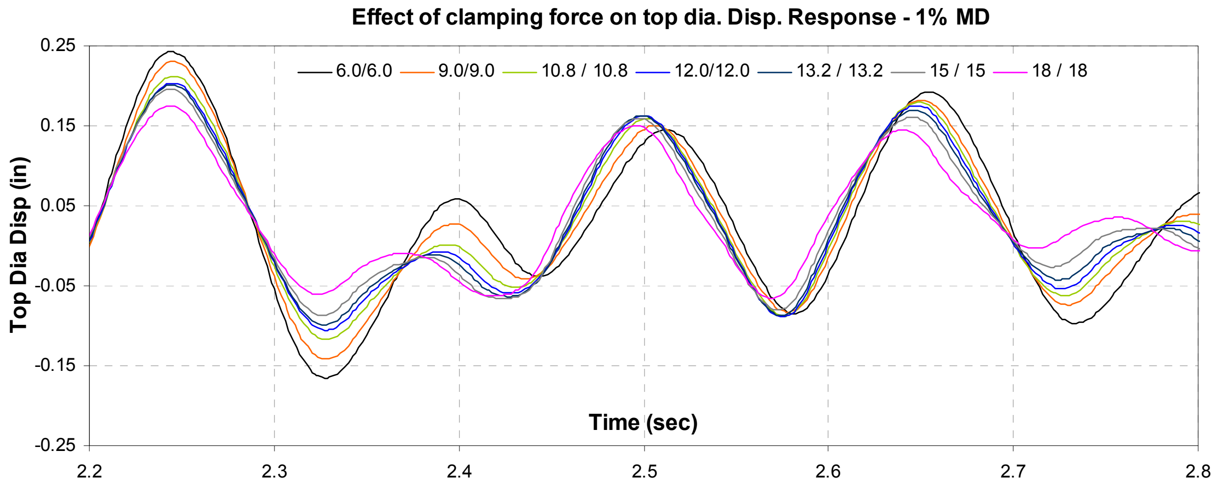

Figure 5.36: Effect of clamping force on top diaphragm displacement response – 1% MD 150% El Centro ground motion

Figure 5.37 shows force displacement hysteresis, of a typical corner NLlink element in a contact area, for different clamping forces. It is observed that no large increase in displacement occurs when the slip resistance is reduced. On the other hand almost no reduction in slip is observed with an increase in clamping force, which indicates more energy dissipation through friction damping.

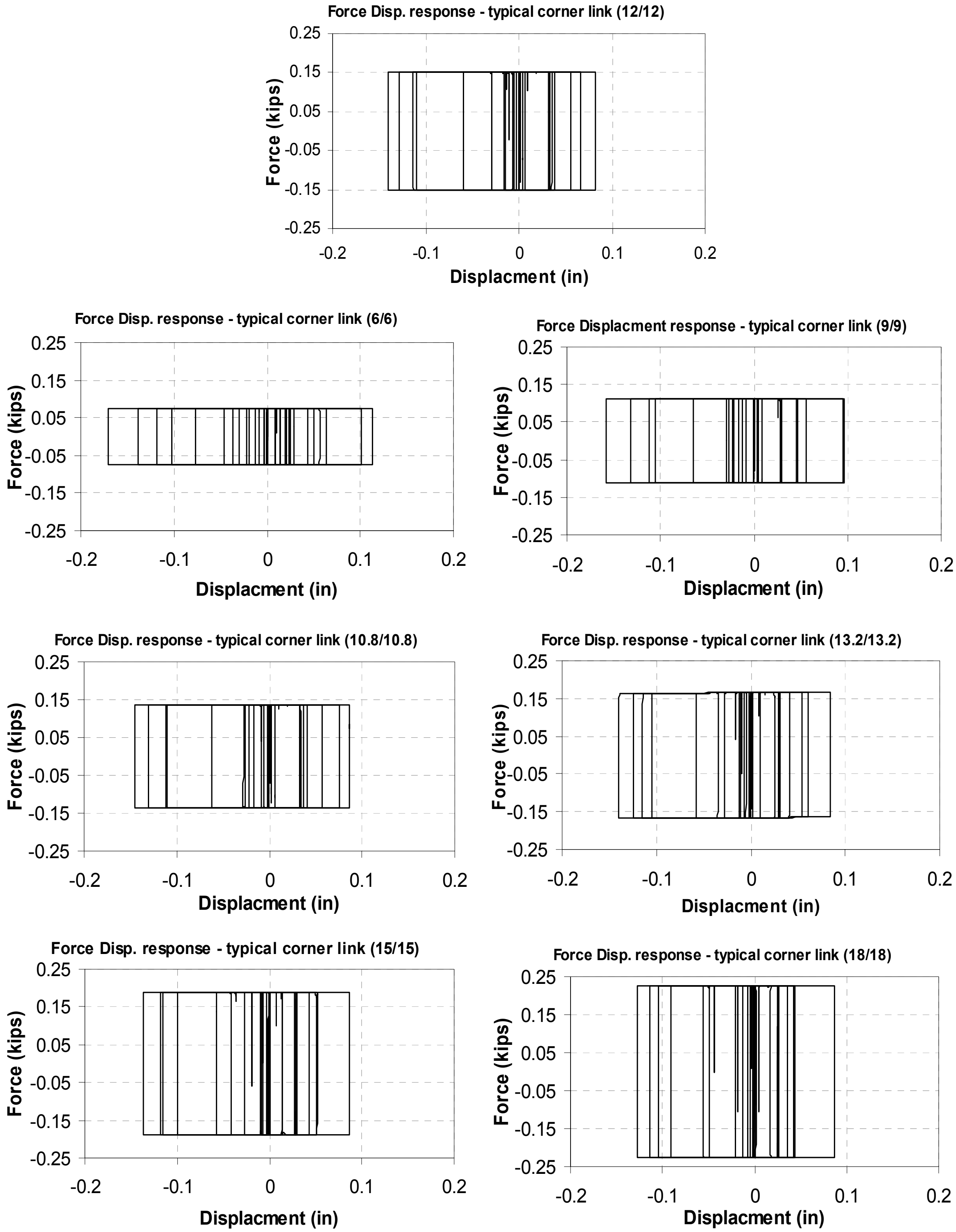

Figure 5.37: Effect of clamping force: Force displacement plots – 1% MD- 150% El Centro GM

The effect of clamping force on 5% and 10% modal damped 2WFD structure was also studied. It was observed that reducing the slip resistance for the top story by 10-25% did not affect the displacement response. Figure 5.38 shows the displacement response of the top diaphragm for the 5% modal damped 2WFD structure. Note that 18 kip and 6 kip slip resistance were selected for bottom and top story respectively in most of the analyses.

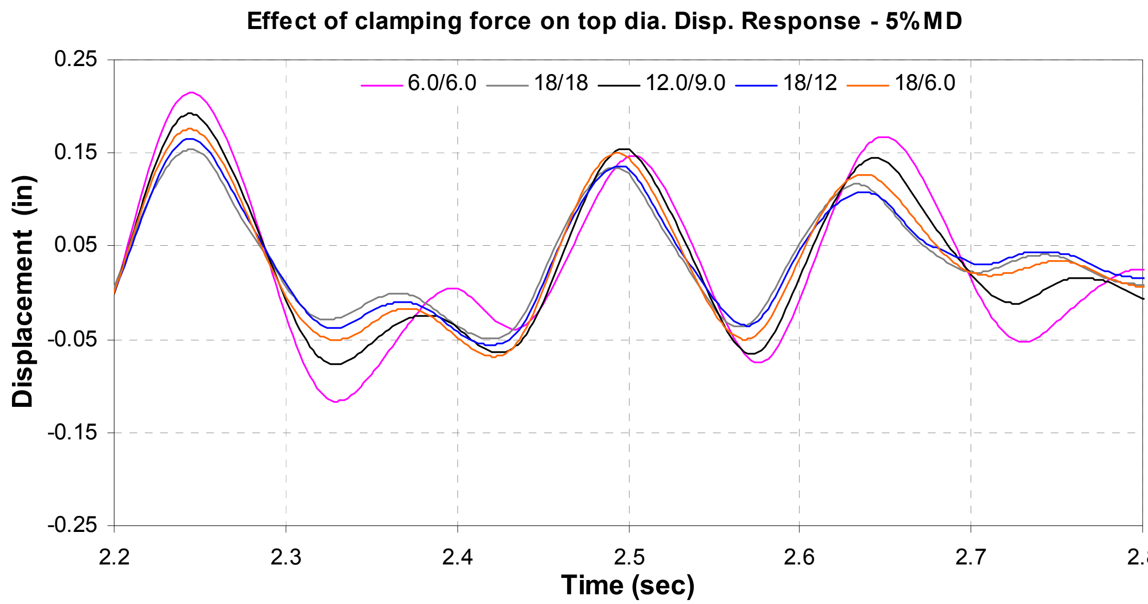

Figure 5.38: Effect of clamping force on top diaphragm displacement response – 5% MD 150% El Centro ground motion

5.12 Effect of Distribution of Mass and Force Among NLlink Elements in the Contact Area

The 2WFD model was analyzed for varying distribution of mass and slip resistance per link in a contact area. Figure 5.39 indicates that the displacement response is not sensitive to the way slip resistance and mass is distributed in the contact area. However in this study mass and slip resistance is assigned to each link element in accordance to tributary area. In Figure 5.39, UF indicates uniform distribution of slip resistance and UM indicates uniform distribution of mass respectively among the link elements. Similarly VF indicates varied slip resistance and VM indicates varied mass in accordance to the tributary area for each NLlink element. This analysis was done for 150% El Centro ground motion with slip resistance of 18 kips and 6 kips for bottom and top sliding walls respectively.

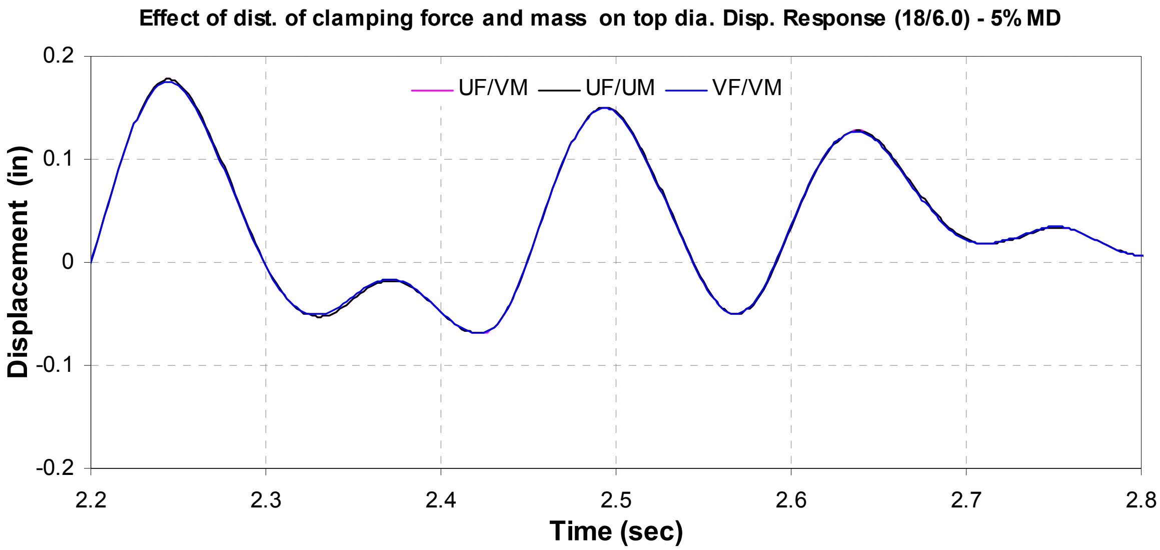

Figure 5.39: Effect of distribution of clamping force and mass – (18/6.0) 5% MD

5.13 Summary

The finite element modeling aspects and effectiveness of the proposed magnetic friction dampers were discussed in this chapter. The effects of modeling parameters such as linear effective stiffness, mass and yield exponent of the uniaxial plasticity nonlinear link elements were presented. The behavior of the friction damped structure subjected to forced and free vibrations were also discussed in this chapter. The response of the 2WFD structure subjected to 150% El Centro and Northridge ground accelerations was also studied and compared to undamped (2W) and regular (4W) structure. The slip in the friction dampers for different modal damping ratios for the 2WFD structure was also studied. Finally, the effects of slip resistance to response of friction damped structure were studied.

Chapter 6

Experimental Verification of Slip Load

6.1 General

The slip resistance of a ferrite flexible magnet with energy product 1.4 MGOe was evaluated in the laboratory. A flexible magnet sheet (FM 14) 0.06 in. thick and 24 in. wide, magnetized with 12 poles per inch (ppi), supplied by Fleximag division of Arnold Magnetic Technologies was used for this purpose. The magnetic sheet had a coating of pressure sensitive adhesive on its unmagnetized face. Static loading was applied to different contact areas so as to arrive at average slip resistance. The experimental setup and results are discussed in the following sections. All testing was carried out in the Virginia Tech structures laboratory.

6.2 Test Setup

A ¼ in.[1] thick steel plate was attached to ¾ in. thick plywood using 10 - #10 X 3/4 in. screws. As shown in Figure 6.1, 2 ft long angle section (3 in. x 3 in. x ¼ in.) was bolted to the plate and plywood using ½ in. x 1 ½ in. bolts. The so formed sheet was clamped to the bottom flange of the supporting frame girder using conventional clamps. Efforts were made to keep the plate vertical.

A 2ft x 2 ½ft piece of *FM14* was adhered to ¾ in. thick plywood sheet of 2 ½ft x 3ft. Liquid Nail ® was used to attach the magnet sheet to the plywood. Two small pieces of ¼ in. thick plates were bolted to the bottom of the plywood at point of application of pull. Such an arrangement would help prevent stress concentrations in the plywood. A ½

[1] Practically such large thickness is not needed for the magnets used. However, the availability of this size in the laboratory was the driving force for using this thickness. Magnets with higher flux density may require larger thickness to prevent saturation and thus, fully utilize the flux induced by the magnet.

in. bolt through these steel plates was used to pivot the load cell to the assembly. The load cell was calibrated in tension to measure the pulling force. The maximum capacity of the load cell was 2000 lb. The other end of the load cell was connected to the piston of the ram using a bolt. Care was taken to prevent any slip so as to measure the pull accurately. A double acting pump was used to produce the pulling force at the bottom of the assembly. The hydraulic cylinder was mounted on a piece of channel section which in turn was bolted down to the reaction floor to resist uplift produced due to hydraulic action. A displacement transducer (wire pot) was attached to the sliding plate (plate with flexible magnet) in order to observe the slip. Figures 6.1 and 6.2 show the test setup. A similar configuration without plywood backing was also tested. The strips of flexible magnet, 3 ½ in. wide were tested both with and without plywood backing. Figure 6.3 shows one such configuration. Tests were also conducted without using any additional adhesive to attach the magnetic sheet to the plywood thus, utilizing the adhesive backing of the flexible magnet sheet.

The load and the slip between the contact surfaces (flexible magnet and ferromagnetic material/steel) was recorded using the 'System 6000'[2], the data acquisition system. System 6000 has 20 channels/cards and is capable of scanning 10000 readings per second for each channel. Two types of cards, strain gauge cards and high level card, are used by System 6000 to acquire the data from any sensor. The acquired data can be processed using the 'Strain Smart'[1] software and can be stored on the hard drive in Excel or text format. The load cell was connected to the acquisition system through a strain gauge card, whereas a high level card was used for wire pot. A scanning rate of 0.001 scans/sec was used for most of the tests. The apparatus was statically loaded after zeroing all the channels in Strain Smart. Load was applied using a hand operated hydraulic pump.

---

[2] Manufactured and developed by Vishay Measurements Group, Malvern, PA.

Alternatively slip resistance was also measured manually by lifting a known weight of steel plates attached to a varying area of flexible sheet until the weight is at the verge of slipping. The slip resistance was accurately verified using this method.

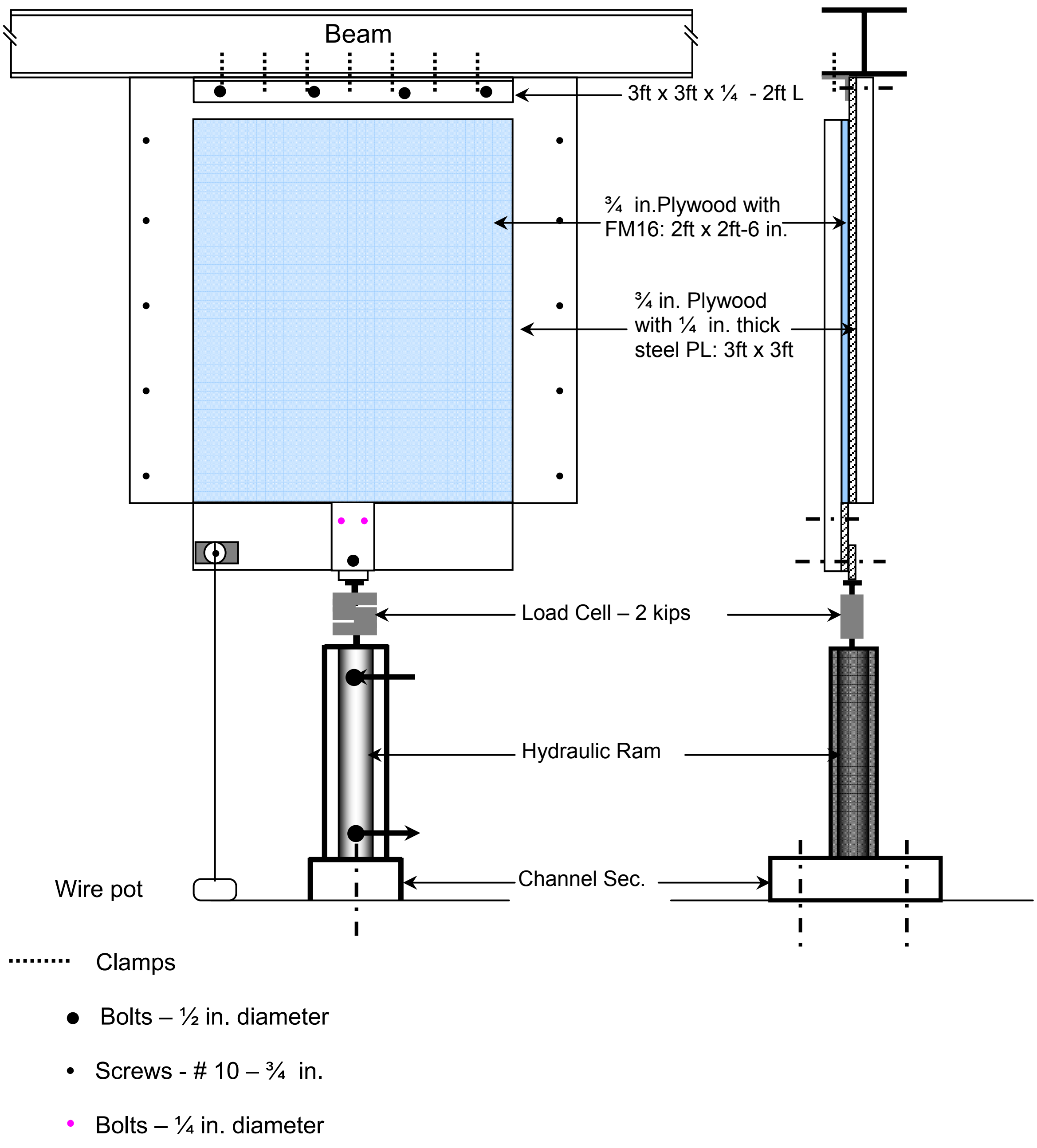

Figure 6.1: Test setup

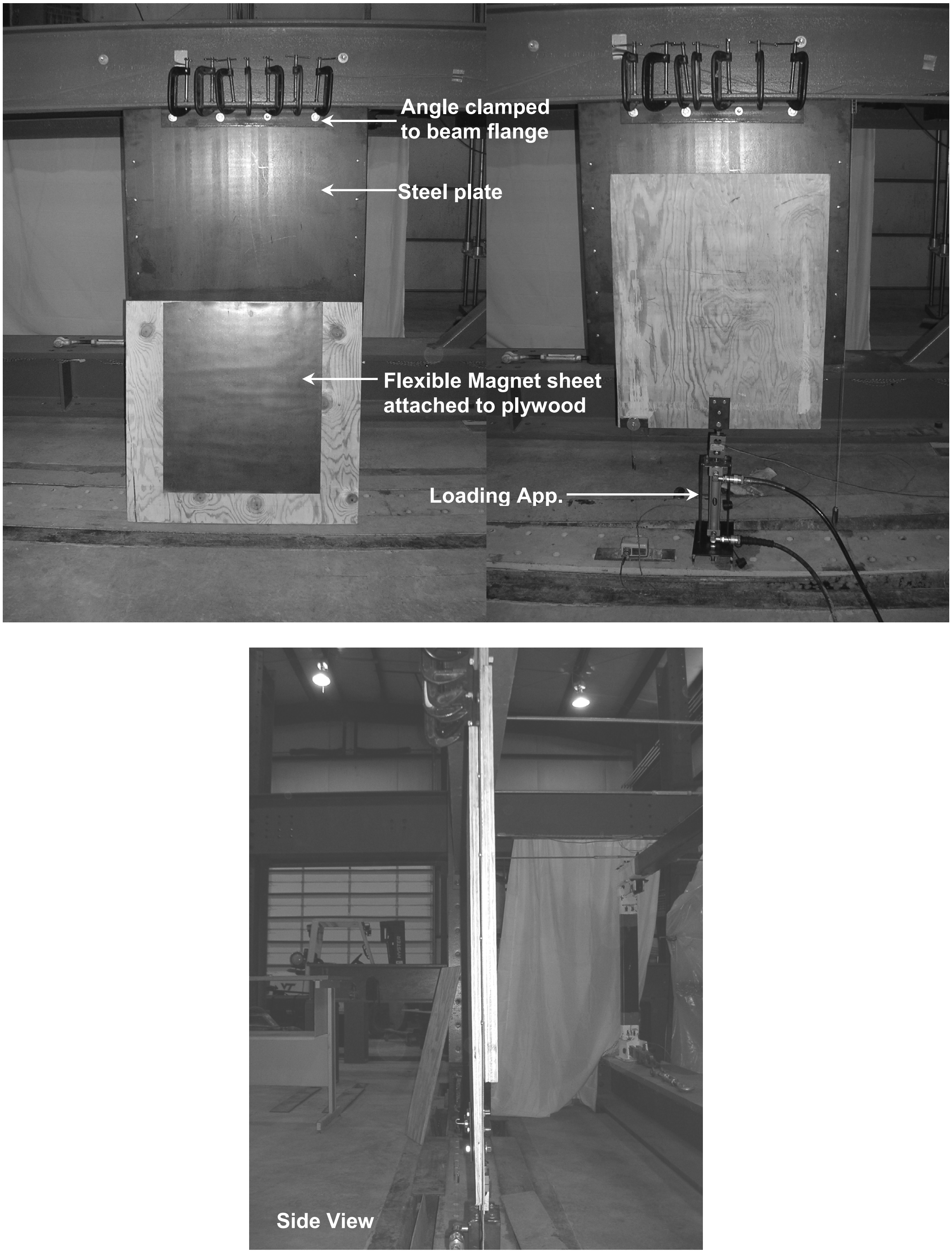

Figure 6.2: Flexible magnet attached to plywood

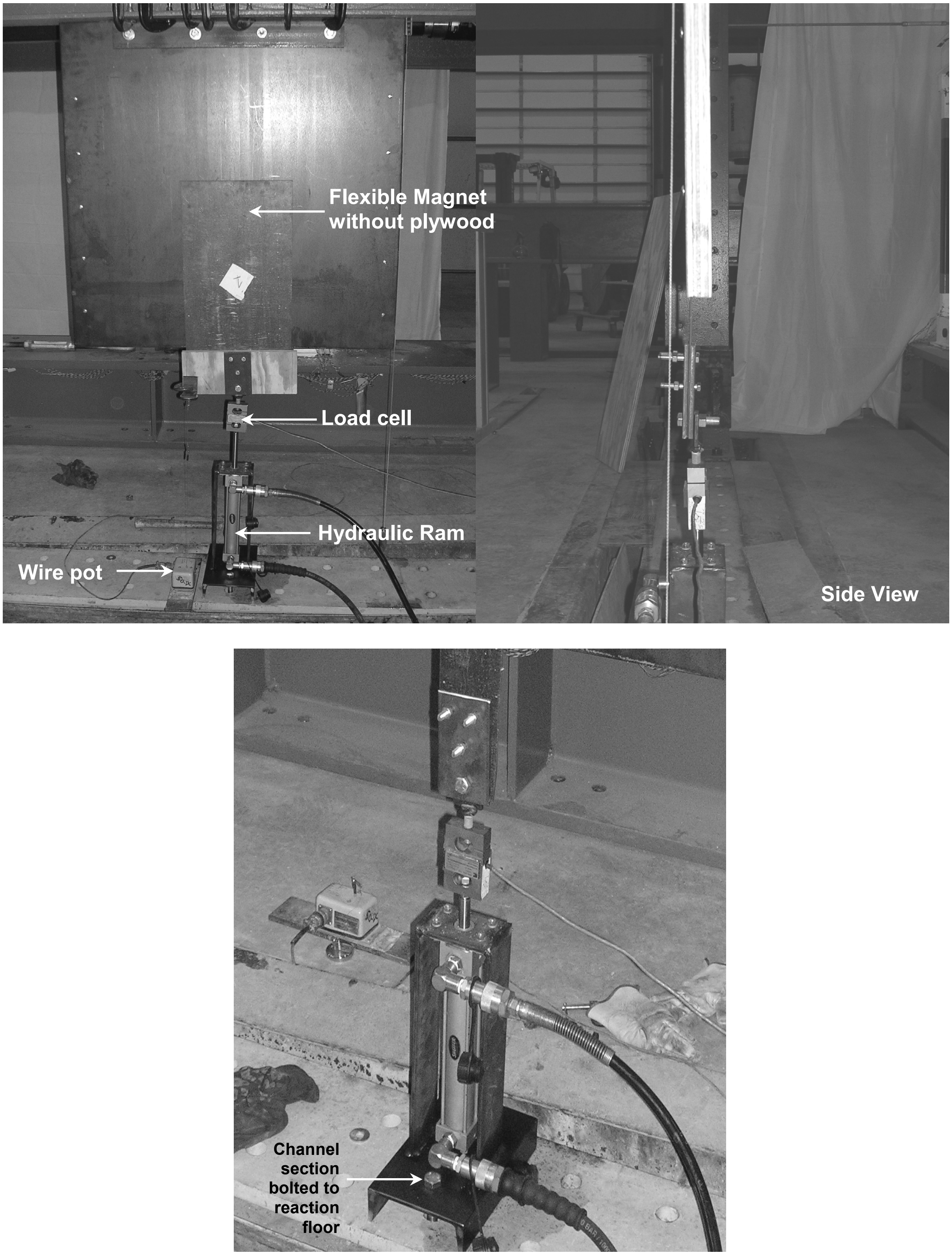

Figure 6.3: Flexible magnet without plywood and Loading apparatus

6.3 Results and Conclusion

FM14 (high energy flexible magnets) have a minimum holding force capacity of 16 oz/in^2 (144 lb/ft^2) and sliding resistance of 8 oz/in^2 (72 lb/ft^2) against smooth steel surface. The holding force which is the normal force between the ferromagnetic material and the magnet is extremely sensitive to the air-gap (distance between magnet and steel plate) even a thin layer of paint can affect the holding capacity of flexible magnets. Hence it is very important to maintain firm contact between the magnet and the steel plate. On average, the rated slip resistance for FM14 was achieved in laboratory. Deviation in the results can be attributed to the accuracy of load cell, type of steel used in the lab as compared to that used by the manufacturer and surface condition of the steel. Large deviations in slip resistance were observed for the plywood backed magnet sheets.

The slip resistance of the plywood backed plate turned out to be very low as compared to 72 lb/ft^2. This is mainly because of uneven surface conditions on the plywood resulting in undulations causing a decrease in contact area and increase in air-gap which adversely affects the holding force. Also 100% contact was not achieved as the plywood was not straight. These were the prime reasons for failure of plywood backed sheets to resist the anticipated slip. An average deviation of -12% from the rated slip resistance of 72 lb/ft^2 was observed for the specimen without plywood backing.

The coefficient of friction between the flexible magnet and steel plate ranged from 0.41-0.5. Figure 6.4 shows the force displacement relation for magnet sheet without plywood backing. A decrease in slip resistance is observed as slip between the magnet and the steel plate occurs (i.e. contact area decreases). The maximum slip resistance offered by each configuration is highlighted in the plot.

No slip was observed between the plywood and the magnetic sheet when attached without using any external adhesive (Liquid Nail ®). Thus, the strength of the pressure sensitive adhesive, on the unmagnetized face of the flexible magnet sheet was found to be adequate to resist slip between the plywood and the magnet. The results of the tests carried out are summarized in Table 6.1. Table 6.2 shows the slip resistance measured by lifting the known weight. The coefficient of friction is determined by dividing the slip resistance by the normal force of attraction. Note that the coefficient of friction for plywood backed sheets is not calculated as the results are erroneous.

Table 6.1: Results

Flexible magnet sheet no plywood backing				
Designation	**Maximum Load before slip (lb)**	**Slip resistance lb/ft^2**	**% Deviation from 72 lb/ft^2**	**Coefficient of friction (μ_s)**
S17.5 in. x 12 in.	86.25	59.14	-17.86	0.412
S18 in. x 12 in.	96.34	64.23	-10.79	0.446
S18 in. x 12 in.	98.47	65.67	-8.82	0.456
S18 in. x 12 in.	90.3	60.2	-16.39	0.418
S18.5 in. x 12 in.	112.63	73.06	1.47	0.507
S19 in. x 3.5 in.	27.5	59.54	-17.29	0.413
S19 in. x 3.5 in.	28.5	61.71	-14.28	0.429
Flexible magnet sheet with plywood backing				
Designation	**Maximum Load before slip (lb)**	**Slip resistance lb/ft^2**	**% Deviation from 72 lb/ft^2**	**Coefficient of friction (μ_s)**
P24 in. x 3.5 in.	16.11	27.61	61.64	-
P24 in. x 3.5 in.	15	25.71	64.28	-
P24 in. x 3.5 in.	16.25	27.85	61.31	-
P24 in. x 3.5 in.	31.66	54.27	24.62	-
P24 in. x 30 in.	99.72	19.94	72.3	-
P24 in. x 3.5 in.	104.72	20.94	70.91	-
P24 in. x 3.5 in.	97.36	19.47	72.95	-

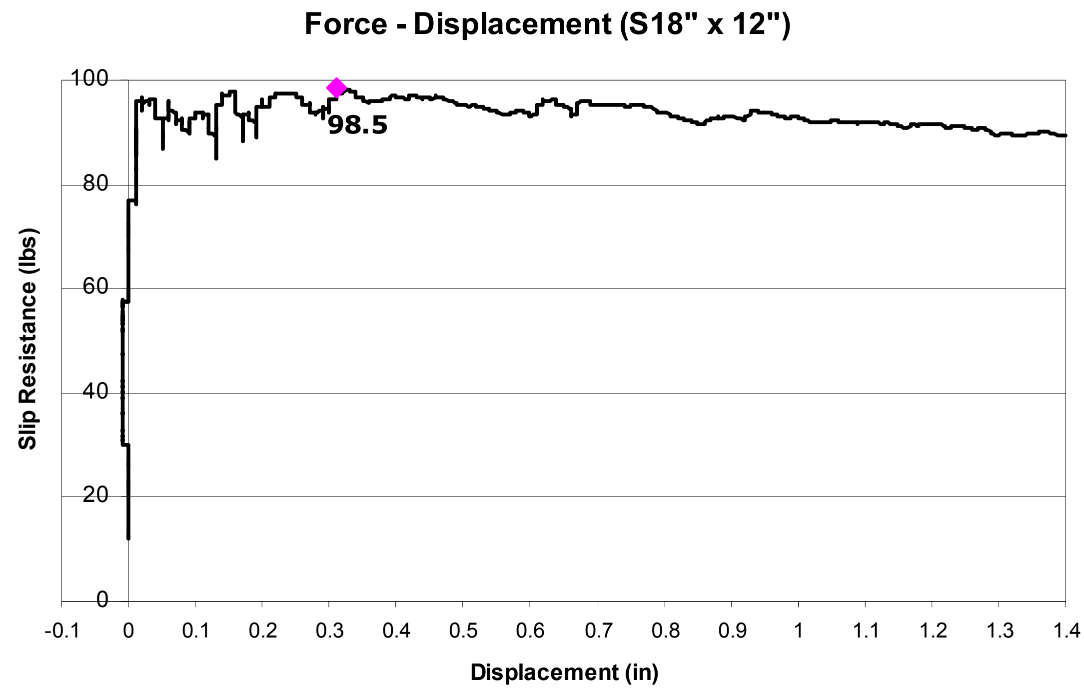

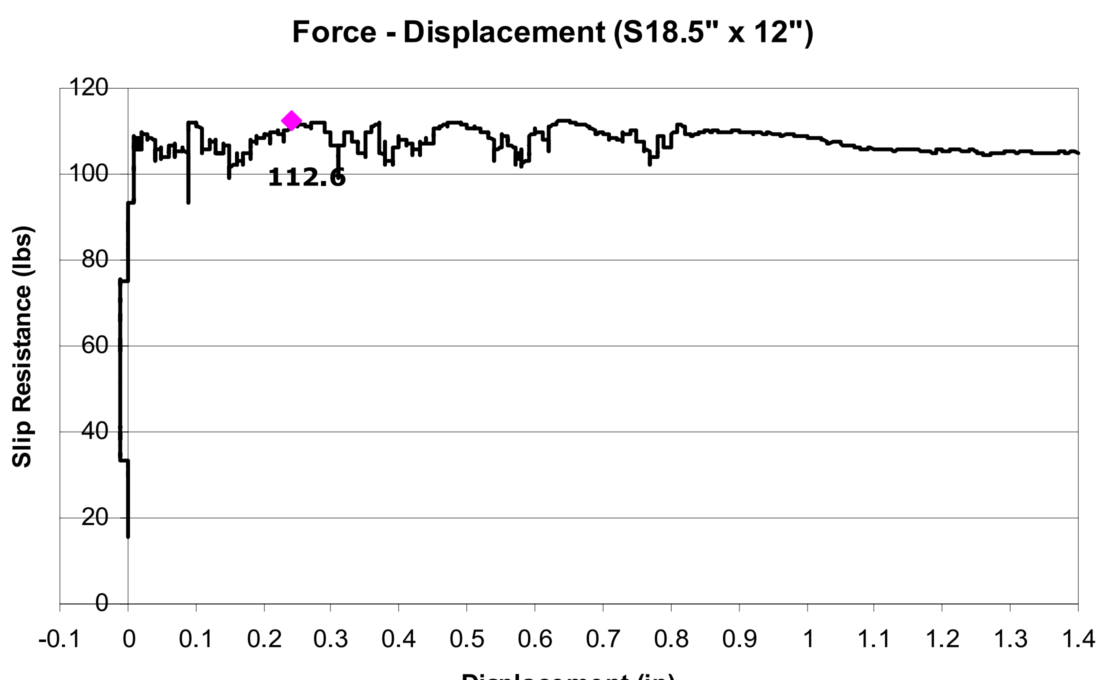

Figure 6.4: Force displacement relation for flexible magnet without plywood backing

Table 6.2 Manual verification

Area	**Load**	**Slip**	**Slip resistance lb/ft^2**
S12 in. x 3 in.	22.5	Yes	-
S12 in. x 4 in.	22.5	No	68
S12 in. x 4.5 in.	22.5	No	-
S24 in. x 1 in.	22.5	Yes	-
S24 in. x 1.5 in.	22.5	No	68
S24 in. x 2 in.	22.5	No	-
S12 in. x 6 in.	46	Yes	-
S12 in. x 7 in.	46	Yes	-
S12 in. x 8 in.	46	No	69
S24 in. x 3 in.	46	Yes	-
S24 in. x 4 in.	46	No	69

Thus, it is recommended to adhere the magnet to a thin steel plate backed by plywood so as to ensure 100% contact with minimum/no air-gap. An array of small ferrite, rare earth magnets or flexible magnets with rare earth magnetic material can also be used in lieu of ferrite flexible magnets to achieve higher slip resistance. Slip resistance of the magnets and wear due to friction should be verified before any practical use.

Chapter 7

Conclusions and Recommendations

7.1 Summary

The idea of utilizing permanent magnets to improve the seismic behavior of structures was investigated by a thorough analytical study. The properties of different types of permanent magnets available, and their effect on humans, were studied. Analytical investigation of a light frame wood structure with friction dampers composed of flexible permanent magnets was performed. Energy dissipation was achieved by friction utilizing normal force of attraction between permanent magnets and ferromagnetic material such as steel. Finite element analysis was carried out using SAP2000. The 2W, 4W and 2WFD structures were analyzed using the FNA method wherein friction was modeled using nonlinear link elements. The effect of various modeling and loading parameters on the behavior of light frame wood structures were studied. Finally the holding force for flexible magnets was verified in laboratory.

7.2 Conclusions

- A large array of permanent magnets can be utilized in different configurations to control vibration in structures.
- The proposed flexible permanent magnets can be utilized in structures without posing any health hazard to the occupants. Much stronger magnets can be utilized provided handling problems are addressed.

- Permanent magnets can retain their magnetism for long time and hence loss in clamping/slip resistance does not occur.
- Friction between contact surfaces can be effectively modeled using uniaxial plasticity nonlinear link elements in SAP2000.
- Fast Nonlinear Analysis method is very efficient in solving systems with discrete nonlinearities provided appropriate parameters are used to represent the problem.
- The response of the 2WFD structure was sensitive to effective stiffness and mass of the nonlinear link element. The effective stiffness to be used should be very low for friction dampers, since an artificially high value of stiffness is used to represent slip, to prevent huge numerical errors. The mass assigned to the nonlinear link element should correspond to the total contact area/tributary area. The distribution of mass and slip resistance do not affect the analysis results.
- The proposed permanent magnet friction device is very effective in damping the vibrations of structures with low inherent capacity to dissipate energy (as seen for 1% and 5% modal damping case – representing plywood shear wall structures, glued timber structures, timber frames and conventional wood frame shear wall structures depicting moderate inelastic behavior). About 60% to 80% of the induced energy is dissipated by friction damping in all the cases. The device curbs the peak responses for both two-wall and four-wall structure (ref. Table 5.1 – 5.6) which is a clear indication of preventing structural and non-structural losses and thus avoiding from negative economic impact.
- The friction dampers studied here do not seem to improve the displacement behavior for high modal damping (here 10% - representing high amount of inelastic behavior during lateral loading) as compared to the response of the structure in which sliding walls are replaced by regular walls. Degrading stiffness and decay of inherent damping capacity resulting due to inelastic behavior of the

connectors and loosening of the connectors/nails in the sheathing material after few initial loading cycles aggravates the response of the wood frame structure. Sliding wall friction dampers should be effective in curbing such responses. However, such behavior is not apparent from the analysis results for 10% modal damping, since the current model assumes high initial inherent damping capacity, which is achieved only for few initial loading cycles, to be constant throughout the loading event. Thus, the ineffectiveness of the proposed friction dampers for the structures with high inherent damping capacity should not be concluded as degrading stiffness and decay of inherent damping capacity of wood shear wall structures is not considered in this study.

- Displacement response and slip in the friction dampers for 5% and 10% modal damping is almost same, it appears that representing the inherent damping capacity of wood structures through modal damping is not appropriate. Instead hysteretic models for connectors should be used.
- The surfaces of the sliding wall should be flat to achieve 100% contact and thus maximum slip resistance.

7.3 Recommendations

- Effectiveness of the proposed friction dampers should be verified for high modal damping by modeling the hysteretic behavior of wood frame shear walls and degrading damping capacity. Results of the analysis performed including the inelastic behavior of the normal (regular) walls should also be studied.
- Three dimensional finite element analyses should be carried out to evaluate the proposed friction dampers.
- The analytical results should be backed by experimental investigation to prove the effectiveness of the proposed friction dampers.

- Surface coating for steel plates should be selected to prevent corrosion of the surface. Also use of material other than steel which has high magnetic permeability should be checked.
- Effect of temperature rise due to friction between the contact surfaces should also be studied.
- It is recommended to investigate the use of proposed friction dampers in light frame steel structures which have low inherent damping capacity.
- The use of the proposed sliding wall configuration to damp the vibrations induced in the upper stories of conventional steel or concrete structures, where the damping demand is comparatively less, can also be studied.
- Flexible permanent magnets (up to 0.375 in.), being composed of rubber, should be checked for energy dissipation by viscoelastic behavior before/during occurrence of slip.
- Permanent magnets should also be checked for their use in self centering dampers.

References

Aiken, I.D., Kelly, J.M., and Pall, A.S. (1988). "Seismic response of a nine-story steel frame with friction damped cross-bracing." *Report no. UCB/EERC-88/17, EERC,* University of California, Berkeley, CA.

Arima, F., Miyazaki, M., Tanaka, H., and Yamazaki, Y. (1988). "A study on building with large damping using viscous damping walls." *Proceedings 9th World Conference on Earthquake Engineering,* Tokyo-Kyoto, Japan, pp. 821-826.

Basic, D., Mesic, E. and Stojic, D. (1996). "Flexible connections as the dampers in timber frame structures." *Proceedings of International Wood Engineering Conference Vol. 1*, Edited by K. A. Gopu, New Orleans, Louisiana, October 28-32, pp. 317-322.

Bellossi, A. and Toujas, L. (1982). "The effect of a static uniform magnetic field on mice: A study of a Lewis tumor graft." *Radiation and environmental biophysics***,** Vol **20**, pp. 153-157.

Bergman, D.M. and Goel, S.C. (1987). " Evaluation of cyclic testing of steel-plate devices for added damping and stiffness." *Report UMCE 87-10,* The University of Michigan, Ann Arbor, MI.

Budinger, T.F. (1981) "Nuclear magnetic resonance (NMR) in vivo studies: known thresholds for health effects." *Journal of computer assisted tomography*, Vol. **50**, pp. 800-811.

Budinger, T.F. (1985). "Health effects of in vivo nuclear magnetic resonance*." IEEE engineering in medicine and biology magazine*, Vol. **1**, pp. 31-38.

Chandra, S. and Stefani, S. (1979). "Effect of constant and alternating magnetic fields on tumor cells in vivo and in vitro." Biological Effects of Extremely Low Frequency Electromagnetic Fields, Proceedings of the 18th Hanford Life Symposium, RD Phillips et al., Technical Information Center, U. S. DoE , pp. 436-446.

Chang, K.C., Soong, T.T., Lai, M. L. and Neilsen, E. J. (1993). "Viscoelastic dampers as energy dissipation devices for seismic applications." *Earthquake Spectra,* Vol. **9**(3), August, pp. 371-388.

Charney, F.A. (2005). "Analysis of structures with added damping and passive energy dissipation." Advanced Structural Concepts, Denver, Colorado.

Cherry, S., and Filiatrault, A. (1993). "Seismic Response Control of Buildings Using Friction Dampers." *Earthquake Spectra,* Vol. **9**(3), August, pp. 447-466.

Cho, C.G. and Kwon, M. (2004). "Development and modeling of a frictional wall damper and its applications in reinforced concrete frame structures." *Earthquake Engineering and Structural Dynamics,* Vol. **33** (7), pp. 821-838.

Chopra, A.K. (2002). *Dynamics of Structures, Theory and Applications to Earthquake Engineering*. Prentice Hall (India), New Delhi.

Computers and Structures Inc. (2002). "SAP 2000 Analysis Reference Manual".

Constantinou, M.C. and Symans, M.D. (1992). "Experimental and analytical investigation of seismic response of structures with supplemental fluid viscous dampers." *NCEER 92-0032,* National Center for Earthquake Engineering Research, Buffalo, NY.

Constantinou, M.C., Soong, T.T. and Dargush, G.F. (1998). "Passive energy dissipation systems for structural design and retrofit." Monograph Series, Multidisciplinary Center for Earthquake Engineering research, A national center of excellence in advanced technology applications.

Cullity, B.D. (1972). *Introduction to magnetic materials.* Addision-Wesley publishing company, Massachusetts.

CUREE Publication No. W-01 (1999). "Preface". *Proceedings of the Invitational Workshop on Seismic Testing, Analysis and Design of Wood frame Construction*. Edited by F.

Seible, A. Filiatrault, and C. Uang, Division of Structural Engineering. University of California, San Diego, March 5-6.

Dinehart, D. W., Joye, D. D. and Mendoza, E. (2004). "Viscoelastic Polymers Improve Cyclic Performance of Wood Connections." *Proceedings of the 8th World Conference on Timber Engineering*, Lahti, Finland.

Dinehart, D.W. and Lewicki, D.E. (2001). "Viscoelastic material as a seismic protection system for wood-framed buildings." *Proceedings of 2001 Structures Congress and Exposition*, ASCE, Edited by P. C. Chang, Washington, D.C., May.

Dinehart, D.W. and Shenton, H.W. (1998). "Application of passive energy dissipation devices to timber shear walls." *Proceedings of the SEWC Structural Engineers World Congress*, San Francisco, CA, Paper T207-5, pp. 1 – 8.

Dutil, D.A. and Symans, M.D. (2004). "Experimental investigation of seismic behavior of light-framed wood shear walls with supplemental energy dissipation." *Proceedings 13th World Conference on Earthquake Engineering*, Vancouver, Canada, August 1-6, Paper no. 3421.

Environmental Health Criteria 69 – Magnetic Fields (1987). *UN Environment Programme, International Labour Organization and World Health Organization*, WHO, Geneva.

Filiatrault, A. (1990). "Analytical predictions of the seismic response of friction damped timber shear walls." Journal of *Earthquake Engineering and Structural Dynamics.* Vol. **19**, pp. 259–273.

Filiatrault, A., Isoda, H. and Folz, B. (2003). "Hysteretic damping of wood framed buildings." *Engineering Structures.* Vol. **25**, pp. 461–471.

Grigorian, C.E., Yang, T.S., and Popov, E.P. (1993). "Slotted bolted connection energy dissipators." *Earthquake Spectra,* Vol. **9**(3), August, pp. 491-504.

Haugsdal, B., Tynes, T., Rotnes, J.S. and Griffith, G. (2001). "A single nocturnal exposure to 2-7 millitesla static magnetic fields does not inhibit the excretion of 6-sulfatoxymelatonin in healthy young men." *Bioelectromag*, Wiley – Liss, Vol. **22**, pp.1-6.

Higgins, C. (2001). "Hysteretic dampers for wood frame shear walls." *Proceedings of the 2001 Structures Congress and Exposition*, ASCE, edited by P. C. Chang, Washington, D.C., May.

Holmes, W.T. and Somers, P. (1995), "Northridge Earthquake of January 17, 1994 Reconnaissance Report, Vol. 2." *Earthquake Spectra*, Vol. **11** (supp. C), publication 95-03/2.

Hsu, S.Y. and Fafitis, A. (1992). " Seismic analysis and design of frames with viscoelastic connections." *Journal of structural engineering,* ASCE, Vol. **118**(9), pp. 2459-2474.

John, Moulder. "Static electric and magnetic fields and human health." (Electromagnetic fields and human health), [online] January 1 2004, (Accessed: May 19 2004)

Kelly, J.M. and Skinner, M.S. (1980). "The design of steel energy-absorbing restrainers and their incorporation into nuclear power plants for enhanced safety (Vol 2): Development and testing of restraints for nuclear piping systems." Report no. UCB/EERC-80/21, Earthquake Engineering Research Center, University of California, Berkeley.

Mahmoodi, P. (1969), "Structural dampers." *Journal of Structural Division,* ASCE, Vol. **95**(ST8), pp. 1661-1672.

McCaig, M. (1977). *Permanent magnets in theory and practice.* John Wiley and Sons, New York.

Miyazaki, M. and Mitsusaka, Y. (1992). "Design of a building with 20% or greater damping.", *Proceedings 10th World Conference on Earthquake Engineering,* Madrid, Spain, pp. 4143-4148.

MMPA No.0100-00 (2000). Standard specification for permanent magnets, Magnet Materials Producers Association, Chicago, Illinois.

Mur, J.M., Wild, P., Rapp, R., Vautrin, J.P. and Coulon, J.P. (1998). "Demographic evaluation of the fertility of aluminium industry workers: influence of exposure to heat and static magnetic fields." *Human Reproduction*, Vol. 13, pp. 2016-2019.

Myers, G.E., "Magnetics and the body." (Ask a scientist – Biology Archive – U.S. department of energy), [online] Updated December 2004, http://www.newton.dep.anl.gov/askasci/bio99/bio99343.htm (Accessed May 19 2004).

Nims, D.K., Richter, P.J. and Bachman, R.E. (1993). "The Use of the Energy Dissipating Restraint for Seismic Hazard Mitigation." *Earthquake Spectra,* Vol. **9**(3), August, pp. 467-489.

NISTIR 5923 (1996). "Passive Energy Dissipation Devices for Seismic Applications." Sadek, F., Mohraz, B., Taylor, A.W. and Chung, R.M., Building and Fire Research Laboratory, National Institute of Standards and Technology, Gaithersburg, Maryland

Pall, A.S. and Marsh, C. (1982). "Seismic Response of Friction Damped Braced Frames." *Journal of the Structural Division,* ASCE, Vol. **108** (ST6), pp. 1313-1323, New York.

Pathak, R. (2004). "Development of finite element modeling mesh generation and analysis software for light wood frame houses." M.S. thesis. Virginia Tech, Blacksburg, Virginia.

Pavlicek, W., Geisinger M., Castle, L., Borkowski, G.P., Meaney, T.F., Bream, B.L. and Gallagher, J.H. (1983). "The effects of nuclear magnetic resonance on patients with cardiac pacemakers." *Radiology,* Radiological Society of North America, Vol.**147,** pp.149-153.

Pinelli, J.P., Craig, J.I., Goodno, B.J. and Hsu C.C. (1993). "Passive Control of Building Response Using Energy Dissipating Cladding Connections," *Earthquake Spectra*, Vol. **9** (3), August, pp. 529-546.

Raylman, R.R., Clavo, A.C., and Wahl, R.L. (1996). "Exposure to strong static magnetic field slows the growth of human cancer cells in vitro." *Bioelectromagnetics*, Vol. **17**, pp. 358-363.

Reference and design manual (1998), Dexter Magnetic Technologies.

Sakurai, T., Shibata, K., Watanabe, S., Endoh, A., Yamada, K., Tanaka, N. and Kobayashi, H. (1992). "Application of joint damper to thermal power plant buildings." *Proceedings 10th World Conference of Earthquake Engineering,* Madrid, Spain, Vol. **7**, pp. 4149-4154.

Saunder, R.D. and Smith, H. (1984). "Safety aspects of NMR clinical imaging." *British Medical Bulletin*, Vol. **40**, pp. 148-154.

Schiffer, I.B., Schreiber, W.G., Graf, R., Schreiber, E.M., Jung, D., Rose, D.M., Manfred Hehn, M., Gebhard S., Sagemuller, J., Spieb, H.W., Oesch, F., Thelen, M. and Hengstler, J.G. (2003). "No influence of magnetic fields on cell cycle progression using conditions relevant for patients during MRI." *Bioelectromagnetics*, Vol. 24, pp. 241-250.

Symans, M.D., Cofer, W.F., Du, Y. and Fridley, K.J. (2001). "Fluid Dampers for Seismic Protection of Woodframe Structures," *Proceedings of the 2001 Structures Congress and Exposition,* ASCE, Edited by P.C. Chang, Washington, D.C., May.

Symans, M.D., Cofer, W.F., Du, Y. and Fridley, K.J. (2004). "Seismic Behavior of Wood-framed Structures with Viscous Fluid Dampers." *Earthquake Spectra,* Vol. 20(2), May, pp. 451-482.

Tenforde, T.S. and Shifrine, M. (1984). “Assessment of the immune responsiveness of mice exposed to a 1.5-Tesla stationary magnetic field.” *Bioelectromagnetics*, Vol **5**, pp. 443-446.

Tierney, K. J. (1997). “Business Impacts of the Northridge Earthquake.” *Journal of Contingencies and Crisis Management,* Vol. **5** (2), pp. 87-97.

Tsai, K.C., Chen, H.W., Hong, C.P. and Su, Y.F. (1993). “Design of steel triangular plate energy absorbers for seismic-resistant construction.” *Earthquake Spectra,* Vol. **9**(3), August, pp. 505-528.

Whittaker, A.S., Bertero, V.V., Thompson, C.L. and Alonso, L.J. (1991). “Seismic testing of steel plate energy dissipation devices.” *Earthquake Spectra,* Vol. **7**(4), November, pp. 563-604.

Wiskirchen J., Grönewäller E.F., Heinzelmann F., Kehlbach R., Rodegerdts E., Matthias Wittau, H., Rodemann, H.P, Claussen C.D., and Stephan H. Duda S.H. (2000). “Human Fetal Lung Fibroblasts: In Vitro study of repetitive magnetic field exposure at 0.2, 1.0 and 1.5 T.” *Radioilogy,* Vol. **215**, 858-862.

Yasumura, M. (1996). “Evaluation of seismic performance of timber structures.” *Proceedings of International Wood Engineering Conference Vol. 1*, Edited by K. A. Gopu, New Orleans, Louisiana, October 28-32, pp. 45-52.

Vita

Hardik Patel was born to Dineshkumar and Taramati Patel, on December 13th, 1981 in Ahmedabad, the commercial capital of the state of Gujarat (India). He completed his high school studies in March 1999 and was enrolled in the engineering program at Nirma Institute of Technology. He received his Bachelor of Engineering degree in Civil Engineering in June 2003 from Nirma Institute of Technology, Gujarat University, Ahmedabad, India. He proceeded to Virginia Tech to pursue his graduate studies in Structural Engineering. He received his Master of Science in Civil Engineering in May 2005 from Virginia Polytechnic Institute and State University, Blacksburg, Virginia. His interests lie in seismic design of structures, bridge design and rehabilitation of structures.